



Norwegian University of  
Science and Technology

# Modelling and Control of Dry and Wet Gas Compressors

**Njål Tengesdal**

Subsea Technology

Submission date: June 2017

Supervisor: Christian Holden, MTP

Norwegian University of Science and Technology  
Department of Mechanical and Industrial Engineering



**MASTER'S THESIS**  
**Spring 2017**  
**for stud.techn. Njål Tengesdal**

***Modelling and Control of Dry and Wet Gas Compressors***

An increasing challenge in gas fields on the Norwegian Continental Shelf is falling reservoir pressure. The pressure naturally drops as gas is removed from the reservoir, and if the pressure becomes too low the gas will have trouble reaching topside facilities.

One solution to this problem is to install a subsea gas compressor. At this time, worldwide, two subsea gas compressors are installed and operational, while a third is qualified for installation. Gas compressors can be either *dry* (only able to handle pure gas) or *wet* (able to handle the presence of some liquids). Both types are in use today and have their own sets of advantages and disadvantages.

There is room for improvement of the control algorithms of both dry and wet gas compressors. To study compressors, the Department of Mechanical and Industrial Engineering at NTNU is constructing a small-scale laboratory.

This work is a continuation of a specialization project titled “Wet Gas Compressors: State of the Art”. As a result of this project, two dry gas compressor models were chosen for further study as part of the master’s thesis. Suitable wet gas compressor models do not exist at this time.

In this project, the student will:

1. Establish compressor characteristics based on the compressor performance curves for the GT2252 turbocharger used in the laboratory
2. Develop a simulation model using model-based design
3. Compare the simulation performance of the two models chosen for further study in the specialization project, with the developed compressor characteristics
4. Perform a controller tuning study and implement the designed control algorithm for a compressor model
5. Investigate and test potential wet gas parameters for the dry gas compressor model
6. Contribute to the electrical wiring and documentation of the laboratory.

If time permits and the laboratory is finished, the following list of objectives will be done:

7. Establish an empirical wet gas characteristic for the turbocharger in the laboratory
8. Implement the developed controller in the laboratory and document the performance

Responsible supervisor:

Associate Professor Christian Holden

E-mail: christian.holden@ntnu.no

Telephone: +47 735 93782



## Summary

Performing gas compression subsea is an important component for future realisation of complete subsea processing facilities. Gas compressors operating with raw well fluids, categorised as wet gas, enables an increase in hydrocarbon recovery and operational efficiency together with cost reduction for extended subsea processing. The wet gas, defined with a liquid fraction up to 5%, implies challenges for existing dry gas compressor technology. To accurately predict compressor performance with wet gas and enable efficient control, research leading to first principle modelling of wet gas compressors is important. The work in this thesis expands upon the specialisation project work in the autumn of 2016. The main objectives are to establish performance characteristics of a compressor, validate dry gas compressor models through simulation and expand the models towards simulation and control with emulated wet gas flow.

Two compressor characteristics have been curve fitted to a Garrett GT2252 turbocharger compressor map. The turbocharger is stationed in the Wet Gas Compression laboratory at the Department of Mechanical and Industrial Engineering at NTNU. The map characteristics were curve fitted with two different methods in MATLAB. The least squares non-linear fit for a first principle characteristic function and with a traditional empirical 3rd-degree polynomial, commonly used in literature. The latter curve fit method produced the best fit in terms of mean absolute error. The two characteristics have been validated in simulation with two compressor models, the axial compressor model developed by Greitzer and the centrifugal compressor model developed by Gravdahl.

Through a controller tuning study, a non-linear gain scheduling controller has been developed for the normal operating region of the compressor. Two 3rd-degree polynomials, calculated offline, are used for continuously updating each controller setting in the scheduling algorithm. The performance results of the gain scheduling controller have proven to reduce the integral of absolute value of control error compared to a single linear controller for setpoint and load disturbance changes. The controller has been subject to testing with model uncertainties, by interchanging the first principle with the empirical compressor characteristic in the model.

The first principle compressor characteristic has been extended with the application of wet gas parameters. The inlet gas density, gas specific heat capacity and impeller friction loss factor are empirically calculated with changing gas volume fraction of the gas flow. Gas volume fractions of 100% to 99.90% and corresponding gas mass fractions of 100% to 54.67% are used to simulate a wet gas compressor using the gain scheduling controller. This has been performed to validate the controller robustness. The results of utilising the wet gas compressor characteristic in simulation have shown a decrease in achievable pressure ratio and an earlier saturation of the drive unit to maximum speed for the compressor.

The author has contributed to the electrical installation on the Department Wet Gas Compression laboratory. Electrical installation schematics and an operation protocol have been produced to complete the laboratory documentation. The laboratory electrical infrastructure is tested, documented and verified for operation.



## Samandrag

Utføring av gasskompresjon er ei viktig brikke i framtidig drift av komplette prosesseringsanlegg på havbotnen. Kompressorar som køyrest med ufiltrert gass frå reservoaret, kalla våtgass, gjer det mogleg å auka hydrokarbonproduksjonen og effektiviteten samt redusera kostnader for utvida havbotnanlegg. Våtgass er definert med opp til 5 % vassinnhald, som gjer det vanskeleg å nytte noverande kompressortechnologi for tørrgass. Ein modell utvikla frå fysiske lovar for ein våtgasskompressor er viktig for å kunne predikera kompressorytinga ved bruk av våtgass, samt utvikle effektive regulatoralgoritmar. Arbeidet som vart utført i denne masteroppgåva, er eit påbygg av spesialiseringsprosjektet levert hausten 2016. Hovudmåla er å utvikla kompressorkarakteristikkar for spesifikke kompressorytingslinjer, verifisera tørrgasskompressormodellar i simulering og utvida modellane for regulering med simulert våtgassflyt.

To karakteristikkar er kurvetilpassa eit kompressorkart for ein Garrett 2252 turboladar. Turboladaren står i våtgasskompresjonslaboratoriet ved Institutt for maskinteknikk og produksjon på NTNU. To kurvetilpassingsmetodar vart utført i MATLAB for å hente karakteristikane frå kartet. Ein minste kvadraters ulineær tilpassing vart brukt for ein kompressorkarakteristikk utvikla frå fysiske lovar samt ein konvensjonell 3. grads polynomkarakteristikk brukt i akademia. Den konvensjonelle empiriske metoden gav best resultat i høve utrekning av absolutt middelverdifeil for kvar karakteristik. Begge kompressorkarakteristikane er blitt validert gjennom simulering med ein aksialkompressormodel laga av Greitzer samt ein sentrifugalkompressormodell laga av Gravidahl.

Ein reguleringsteknikkstudie resulterte i utviklinga av ein ulineær gain scheduling-regulator for det normale driftsområdet for ein kompressor. Ved bruk av 3. gradstilpassning til regulatorparametraner gitt av arbeidspunktet og kontinuerleg oppdatering av desse, er det oppnådd ein lågare verdi for integralet av absoluttfel (IAE) for denne typen regulator samanlikna med ein enkel lineær regulator. IAE-verdiane er utrekna frå stegrespons og lastendringar i simuleringmodellen. Regulatoren har og vore testa med modellfeil, der karakteristikken frå Gravidahl har blitt skifta ut med den konvensjonelle 3. grads karakteristikken.

Kompressorkarakteristikken utvikla frå fysiske lovar har blitt utvida med bruk av våtgassflytparametere. Flyt-tettleiken til gassen ved innløpet, spesifikk varmekapasitet for gass og skovlhjulet sin gassfriksjonsfaktor er empirisk utrekna med endringar i volum- og massefraksjon for gassflyt. Gassvolumfraksjon frå 100 % til 99.90 % som tilsvarar ein massefraksjon frå 100 % til 54.67 %, er nytta for å simulera ein våtgasskompressorkarakteristikk ilag med gain scheduling-regulering. Dette er gjort for å verifisera ein meir robust regulator. Resultatet frå simuleringane visar at redusert gassvolumfraksjon gjer redusert differensialtrykk samt at turtallet må aukast for våtgassflyt. Det sistnemnte gjev at kompressoren går i metning for tillate turtal i modellen.

Forfattaren av oppgåva har delteke i konstruksjon av det elektriske anlegget på instituttet sitt våtgasskompressorlaboratorium. Hovud- og styrestrømstekningar samt ein driftsprotokoll for anlegget er laga denne våren, for å komplettera laboratoriet sin dokumentasjon. Det elektriske anlegget er utprøvd, dokumentert og klargjort for drift.





## Preface

This master thesis is submitted as part of the study program Subsea Technology at the Department of Mechanical and Industrial Engineering, during the spring of 2017. The thesis is a continuation of the specialisation project delivered in December 2016, with the subject *Wet Gas Compressors: State of the Art*.

The content aims towards the oil and gas sector, since the thesis subject is part of the branch *System Control* in the Subsea Production and Processing (SUBPRO) project at the Norwegian University of Science and Technology. SUBPRO is a Centre for Innovation-based Research (SFI). More information on this project is available at: <https://www.ntnu.edu/subpro>

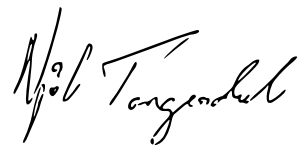
Hopefully, the research performed in this master thesis may aid as a supplement in the academic and industrial research sector of wet gas compression.

From the reader's point of view, it is required to have some knowledge of general thermodynamics and fluid dynamics along with the extensive terminology found the oil and gas sector.

## Acknowledgments

During the work performed in this thesis, guidance and valuable discussions on the topic with Professors and student colleagues at the Department have contributed to the content derived in this report. On behalf of this I would like to thank my supervisor, Associate Professor Christian Holden, along with PhD Candidate Torstein Thode Kristoffersen for guidance and constructive comments on the thesis work. I would also like to acknowledge Professor Olav Egeland for helpful comments and aid.

The support from my family have been greatly appreciated and I am grateful for my parents who have contributed to the proofreading of the content.



*Njål Tengesdal*

Trondheim, 10-06-2017



# Contents

Summary	iii
Samandrag	v
Preface	vii
Contents	ix
List of Figures	xiii
List of Tables	xv
Nomenclature	xvii
1 Introduction	1
1.1 Background	1
1.2 Small scale gas compression test laboratory	2
1.3 Limitations	3
1.4 Objectives	4
1.5 Motivation and approach	4
1.6 Information retrieval	5
1.7 Structure of the report	5
2 Theory	7
2.1 Subsea gas compression	7
2.1.1 Wet gas compression	8
2.1.2 Wet gas definitions	10
2.1.3 Performance issues with wet gas	10
2.2 Dynamic compressor fundamentals	11
2.2.1 Laboratory wet gas compressor	12
2.3 Modelling a dry gas compressor	14
2.3.1 The Greitzer compressor model	15
2.3.2 The centrifugal compressor model	16
2.4 Compressor performance and control methodology	18
2.4.1 The compressor map	18
2.4.2 Compressor losses	19

## Contents

---

2.4.3	Compressor instability . . . . .	20
2.4.4	Anti-surge control . . . . .	21
2.5	Control theory . . . . .	22
2.5.1	Non-linear control . . . . .	23
<b>3</b>	<b>Determining compressor characteristics</b>	<b>25</b>
3.1	Parameter and map evaluation for GT2252 turbocharger . . . . .	25
3.1.1	The GT2252 compressor map . . . . .	27
3.2	First principle characteristic . . . . .	28
3.2.1	Impeller losses . . . . .	30
3.2.2	Resulting characteristic function . . . . .	33
3.2.3	Discussion of the first principle characteristic . . . . .	34
3.2.4	Zero and negative mass flow region of the map . . . . .	35
3.2.5	Map curve fit of the first principle characteristic . . . . .	37
3.3	Empirically determined characteristic . . . . .	40
3.3.1	Curve fitting the compressor speed lines . . . . .	40
3.3.2	Resulting empirical pressure ratio function . . . . .	42
3.4	Comparison of characteristics . . . . .	45
<b>4</b>	<b>Simulation and control</b>	<b>47</b>
4.1	Chapter introduction and purpose . . . . .	47
4.2	Compressor system and parameters . . . . .	48
4.3	Simulation environment . . . . .	50
4.3.1	Choosing a suitable state solver . . . . .	50
4.4	Initial conditions and process dynamics . . . . .	52
4.4.1	Steady state behaviour of the Greitzer model . . . . .	53
4.4.2	Steady state behaviour of the centrifugal model . . . . .	56
4.5	Controller tuning study . . . . .	58
4.5.1	System step response and tuning parameters . . . . .	59
4.5.2	Tuning results . . . . .	61
4.6	Gain scheduling controller . . . . .	64
4.6.1	Controller performance with empirical characteristic . . . . .	70
4.7	Wet gas impact on the centrifugal compressor model . . . . .	72
4.7.1	Preliminary wet gas parameter study . . . . .	72
4.7.2	Centrifugal model wet gas characteristic . . . . .	73
4.7.3	Controller robustness . . . . .	75
4.8	Summary of chapter . . . . .	79
<b>5</b>	<b>Laboratory results</b>	<b>81</b>
5.1	System overview . . . . .	81
5.1.1	Test scenarios . . . . .	82
5.1.2	Laboratory instrumentation . . . . .	83
5.1.3	Processing equipment . . . . .	86
5.1.4	Control system . . . . .	87
5.2	Electrical circuit design . . . . .	88
5.2.1	Electrical design revisions . . . . .	89

5.3	Commissioning . . . . .	91
5.3.1	Individual functionality testing . . . . .	92
5.3.2	Protocol operation . . . . .	95
6	Discussion and conclusions	97
6.1	Discussion . . . . .	97
6.2	Conclusions . . . . .	100
6.3	Recommendations for further work . . . . .	102
	References	103
	Appendices	113
A	Measurements and calculations	115
B	WGC Laboratory - Piping and Instrumentation Diagram	117
C	WGC Laboratory - Electrical circuits	119
D	WGC Laboratory - Circuit board arrangement	123
E	WGC Laboratory - Operation protocol	125



# List of Figures

1.1	The Ormen Lange subsea field structure [80] . . . . .	1
1.2	The WGC laboratory at MTP (image courtesy: Christian Holden) . . . . .	2
2.1	Natural and boosted production curves from a subsea well [6] . . . . .	7
2.2	Early stage method of wet gas compression (Åsgard layout) [8] . . . . .	8
2.3	WGC4000 compressor installed in subsea template [81] . . . . .	9
2.4	Modern turbomachinery design . . . . .	11
2.5	The two compression stage setups . . . . .	12
2.6	Shrouded impeller [9] . . . . .	12
2.7	The WGC turbocharger [31] . . . . .	13
2.8	Common shaft turbine (left) and compressor (right) [32] . . . . .	13
2.9	The axial compressor model by Greitzer [43] . . . . .	14
2.10	The centrifugal compressor model with shaft dynamics [42] . . . . .	14
2.11	The compressor map . . . . .	18
2.12	Extended compressor map with active surge control [110] . . . . .	21
2.13	Closed loop feedback control system . . . . .	22
2.14	Gain scheduling control of non-linear process . . . . .	24
3.1	Wet gas compression application of GT2252 turbocharger . . . . .	25
3.2	Components under the discharge volute of GT2252 . . . . .	26
3.3	The compressor performance map of GT2252 [31] . . . . .	27
3.4	H-S diagram for the compression process [23] . . . . .	28
3.5	Velocity triangle for backward curved blades . . . . .	29
3.6	Inducer tip velocity triangle [23] . . . . .	31
3.7	Stagnation enthalpies for first principle characteristic . . . . .	34
3.8	First principle characteristic with 75000 rpm and corresponding GT2252 curve . . . . .	35
3.9	Result from optimal $x_n$ with first principle function $\psi_{iC}$ . . . . .	39
3.10	MATLAB <code>polyfit</code> curve fitting for characteristic lines . . . . .	41
3.11	3rd-degree polynomial curve fit of coefficients . . . . .	43
3.12	Approximated first principle and empirical characteristic to map data . . . . .	45
4.1	The laboratory layout of the compressor model simulation . . . . .	48
4.2	Simulation model of the compressor setup . . . . .	49
4.3	The GT2252 volute and discharge section . . . . .	50
4.4	Simulink block representation with subsystems . . . . .	50

## List of Figures

---

4.5	I/O of open-loop analysis . . . . .	51
4.6	The steady-state dynamics of the Greitzer model . . . . .	54
4.7	$\Delta p_c$ versus $w$ , Greitzer model . . . . .	55
4.8	Greitzer model with surge behaviour . . . . .	56
4.9	The steady-state dynamics of the centrifugal model . . . . .	57
4.10	$\Psi_c$ versus $w$ for the centrifugal model . . . . .	57
4.11	Centrifugal model with surge behaviour . . . . .	58
4.12	Input step response for the centrifugal model with an open-loop configuration . . . . .	59
4.13	Block diagram representation of the Simulink model with PI control . . . . .	62
4.14	Result of tuning the compressor PI control with four settings . . . . .	63
4.15	$K_c$ and $\tau_i$ versus GS variable $w_t$ with 3rd-degree fit . . . . .	66
4.16	System output with first stage GS control . . . . .	67
4.17	Tuned GS controller system response to setpoint and load change . . . . .	68
4.18	$K_c$ and $\tau_i$ for initial and tuned GS PI settings using 3rd-degree interpolation . . . . .	68
4.19	Process output $p_p$ for three different filter time constants $T_f$ . . . . .	69
4.20	$K_c$ , $\tau_i$ and shaft speed with and without filter on GS variable . . . . .	70
4.21	Setpoint and load step response for GS controller with empirical characteristic . . . . .	71
4.22	Control input contributions for the GS controller with empirical characteristic . . . . .	71
4.23	Empirically modelled wet gas characteristic . . . . .	74
4.24	System step response for constant GVF from 1 to 0.999 . . . . .	77
4.25	Compressor enthalpy friction loss for constant GVF values . . . . .	77
4.26	System response for ramped GVF from 100 to 99.95% . . . . .	78
5.1	WGC laboratory sections . . . . .	81
5.2	Reduced overview PFD for the WGC laboratory . . . . .	82
5.3	Siemens P200 and Lutron PT100 transmitter in the high temperature side . . . . .	84
5.4	Impeller blades and rpm sensor port . . . . .	84
5.5	WGC laboratory control valves . . . . .	85
5.6	Laboratory vertical separator [10] . . . . .	86
5.7	A section of the WGC control system front panel (courtesy of Daniel Nedregård) . . . . .	87
5.8	Tab view of the control system (courtesy of Daniel Nedregård) . . . . .	88
5.9	WGC laboratory control cabinet and circuit board . . . . .	89
5.10	A section of the 400/230 VAC circuit drawing . . . . .	90
5.11	FAT test markings on the 24 VDC schematic . . . . .	92
5.12	WGC laboratory turbocharger installation . . . . .	93
5.13	A section of the 24 VDC control circuit drawing . . . . .	95
A.1	Measuring the inducer blade angle $\beta_{1b}$ on the impeller . . . . .	115
B.1	P&ID for WGC laboratory, turbocharger section . . . . .	117
B.2	WGC laboratory P&ID . . . . .	118
C.1	24 VDC control circuit CAD layout . . . . .	120
C.2	400/230 VAC main circuit CAD layout . . . . .	121
D.1	Circuit board arrangement schematic . . . . .	124



# List of Tables

3.1	Design parameters for GT2252 . . . . .	26
3.2	Numerical values for the characteristic parameters . . . . .	34
3.3	MATLAB LSQ curve fit parameters . . . . .	38
3.4	Fit error using <code>lsqcurvefit</code> in MATLAB on $\Psi_c$ . . . . .	39
3.5	Comparing the accuracy of curve fit for different polynomials . . . . .	41
3.6	Fit error for the empirical characteristic function . . . . .	44
4.1	System setup parameters . . . . .	49
4.2	Initial simulation model parameters . . . . .	52
4.3	Initial simulation parameters, Greitzer model . . . . .	54
4.4	Tuning parameters for the compressor PI controller . . . . .	62
4.5	Tuning parameters for the compressor PI-controller . . . . .	63
4.6	GS variable, process gain and time constant and linear process transfer function . . . . .	65
4.7	Initial PI settings for each scheduling point with $\tau_c = \tau_1$ and $\theta = 0$ . . . . .	66
4.8	Tuned PI settings for each scheduling point with $\tau_c = 0.002$ and $\theta = 0.0005$ . . . . .	67
4.9	Comparing three GS controller options to single PI controller . . . . .	70
4.10	GVF and GMF values used in the simulation of wet gas . . . . .	74
4.11	Initial conditions for wet gas performance test . . . . .	75
4.12	IAE for plenum control with wet gas . . . . .	79
5.1	Volume and GVF specifications for the laboratory . . . . .	83
5.2	Wet gas laboratory process measurements and control . . . . .	83
A.1	Measured angles on impeller inducer and exit blade for GT2252 . . . . .	116
A.2	WGC laboratory process values . . . . .	116
A.3	Zero-mass flow values for each speed line, GT2252 . . . . .	116



# Nomenclature

Symbol	Description	SI Units
<b>Uppercase</b>		
<i>A</i>	Area	$m^2$
<i>B</i>	Greitzer parameter	-
<i>C</i>	Velocity	$ms^{-1}$
<i>C<sub>h</sub></i>	Surface friction loss coefficient	-
<i>D</i>	Diameter	m
<i>J</i>	Inertia	$kgm^2$
<i>K</i>	Process gain	-
<i>K<sub>c</sub></i>	Proportional gain	-
<i>L</i>	Length	m
<i>N</i>	Revolutions per minute	$rmin^{-1}$
<i>M</i>	Vector length	-
<i>N<sub>s</sub></i>	Rotor revolutions pre-stall cell formation	-
<i>R<sub>s</sub></i>	Rotor mean radius	m
<i>Re</i>	Reynold's number	-
<i>T</i>	Temperature	K
<i>U</i>	Tangential velocity	$ms^{-1}$
<i>V</i>	Volume	$m^3$
<i>W</i>	Relative velocity	$Jkg^{-1}$
<b>Lower case</b>		
<i>a</i>	Speed of sound	$ms^{-1}$
<i>c<sub>p</sub></i>	Specific heat at constant pressure	$Jkg^{-1}K^{-1}$
<i>c<sub>v</sub></i>	Specific heat at constant volume	$Jkg^{-1}K^{-1}$
<i>e</i>	Error	-
<i>h</i>	Specific enthalpy	$Jkg^{-1}$
<i>f</i>	friction factor	-
<i>k<sub>t</sub></i>	Throttle gain	-
<i>l</i>	Mean channel length	m
<i>m</i>	Mass	kg
<i>n</i>	Number of impeller blades	-
<i>p</i>	Pressure	Pa
<i>Δp<sub>c</sub></i>	Pressure rise (Greitzer)	-

## Nomenclature

---

$\Delta p$	Pressure difference	Pa
$q$	Volumetric flow rate	$\text{m}^3 \text{s}^{-1}$
$r$	Radius	m
$s$	Specific entropy	$\text{J kg}^{-1}$
$t$	Time	s
$u$	Input	-
$w$	Mass flow	$\text{kg s}^{-1}$
$x$	State variable	-
$y$	Output variable	-

### Greek Letters

$\alpha$	Incidence angle coefficient, inducer	rad
$\beta$	Blade angle	rad
$\eta$	Efficiency	-
$\kappa$	Ratio of specific heats	-
$\lambda$	Eigenvalue	-
$\mu$	Energy transfer coefficient	-
$\omega$	Angular velocity	$\text{rad s}^{-1}$
$\omega_i$	Measurement deviation frequency	-
$\omega_H$	Helmholtz frequency	$\text{rad s}^{-1}$
$\phi$	Flow coefficient	-
$\Psi$	Pressure ratio	-
$\rho$	Density	$\text{kg m}^{-3}$
$\tau$	Torque	Nm
$\tau_1$	Process time constant	s
$\tau_c$	Closed-loop response time	s
$\tau_i$	Integral time	-
$\tau_D$	Derivative time	-
$\theta$	Dead time	s

### Subscript

Subscript	Description
$a$	Actual
Amp	Amplitude
$b$	Blade
$c$	Compressor
emp	Empirical
$g$	Gas
$f$	Friction
$h$	Homogeneous
$l$	Liquid
$m$	Measured
$p$	Plenum
$s$	Isentropic
$t$	Throttle
$0i$	Stagnation state number

---

<b>Abbreviations</b>	<b>Description</b>
AC	Alternating Current
DC	Direct Current
DAQ	Data Acquisition Unit
FAT	Factory Acceptance Test
GMF	Gas Mass Fraction
GVF	Gas Volume Fraction
GS	Gain Scheduling
IAE	Integral of Absolute value of control Error
IO	Input-Output
HPHT	High Pressure High Temperature
LPV	Linear Parameter Varying
LPLT	Low Pressure Low Temperature
MW	Megawatt
NCS	Norwegian Continental Shelf
NORSOK	Norwegian shelf Competition Position
PFD	Process Flow Diagram
PID	Proportional Integral Derivative
P&ID	Piping and Instrumentation Diagram
PV	Process Value
RPM	Revolutions Per Minute
SAT	Site Acceptance Test
SGCS	Subsea Gas Compression Station
LSQ	Least Squares
SIMC	Skogestad Internal Model Control
SUBPRO	Subsea Processing and Production
WGC	Wet Gas Compression



# Chapter 1

## Introduction

This chapter includes the thesis background, the thesis scope along with the objectives to be fulfilled during the spring.

### 1.1 Background

Subsea processing is a field of technology in growth. In waters with large depth, long step-out distances between production wells, harsh weather conditions and non-feasible rig or floating vessel production, subsea solutions are efficient [101]. An example of a subsea installation is the Ormen Lange field illustrated in Figure 1.1. The field is located on the Norwegian Continental Shelf (NCS) and has a 140 km production pipeline tie-back to onshore infrastructure [93]. However, due to the large capacity equipment installed at the seabed, an update of the existing solutions for efficient use of the available power is critical. Therefore, reducing the required equipment to perform processing of hydrocarbons subsea is a step towards the total reduction in economic expenses and prolonging the production of oil and gas on the shelf [6, Ch. 2], [78].

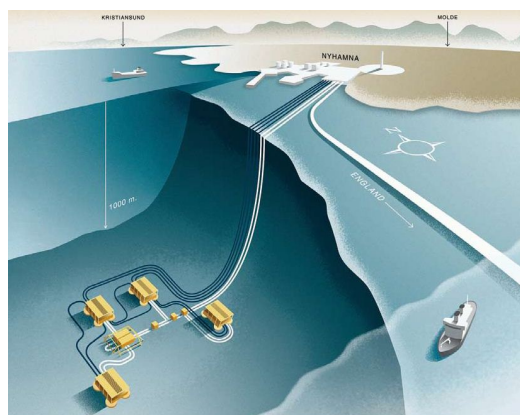


Figure 1.1: The Ormen Lange subsea field structure [80]

## 1. Introduction

---

At the Department of Mechanical and Industrial Engineering (MTP), two laboratories are in the construction phase, simulating a processing facility located on the seabed. These two are part of *Subsea Process Control Laboratory* named *Compact Separation Laboratory* and *Wet Gas Compression Laboratory* [103]. In this thesis, the scope is built around the latter one where experiments on a down-scaled compressor will be performed to analyse the performance with single- and multiphase fluids. The first phase of the laboratory was designed by [10] and have been continued during the autumn of 2016 and this spring.

Subsea compressors handling direct well stream fluids without separation is a subject that contributes to reducing the complexity of integrated template structure at the seabed and reduce cost [8]. However, multiphase flow in gas compressors intended for single phase dry gas flow has shown through experiments to increase power consumption and lead to thermodynamic behaviour difficult to define properly [79]. The research at MTP on direct well stream compression is on the topic of extending existing compressor models to adapt to wet gas characteristics. This is to establish models for efficient subsea system controls [104]. Since most of the established physical phenomena around wet gas in compressors is built around experiments, it is valuable for the research that a facility is constructed enabling testing and analysis.

The previous project work by the author [106] in the autumn of 2016 was about state of the art on wet gas compressors with a literature review of existing mathematical modelling approaches to dry gas compressors. The work presented in this thesis builds on the findings and recommendations from the previous project work.

### 1.2 Small scale gas compression test laboratory

During the work on this master thesis, a collaboration with Daniel Nedregård on developing the Wet Gas Compression (WGC) laboratory at MTP has been performed. The WGC laboratory is seen in Figure 1.2.



Figure 1.2: The WGC laboratory at MTP (image courtesy: Christian Holden)



The following list describes the status for the rig in the start of January 2017:

- Process loop is completed, with installed instrumentation<sup>1</sup>
- Electrical wiring towards each field instrument is finished
- Electrical wiring of control cabinet is not complete
- Control system software has not been developed
- Testing of the rig has not been done.

The finished facility will be used in research and lecturing purposes at the department. The author will contribute to revising the electrical schematics for the control circuits, the Piping and Instrumentation Diagram (P&ID) and the physical wiring of the control cabinet (including the high voltage supply side). To complete the process loop, performing work on piping and loop setup is also considered part of the contribution.

The wet gas compressor is the part of the laboratory that is in focus during this project. The test scenario with direct inlet wet gas to the laboratory turbocharger GT2252 is the scenario considered in the work on this thesis.

## Problem Formulation

The wet gas compressor as a dynamic first principle or empirical model is still not well developed. To predict compressor performance with a wet gas flow and developing optimal control on this subject, a mathematical model describing the physical phenomena must be established. Due to the increased installation of fields with subsea equipment, efficiency must increase to benefit economically in extracting fossil fuels. Wet gas compressors handling direct inlet flow from the well is a topic of interest in the academic sector and for R&D in oil and gas sector to increase production and reduce cost.

### 1.3 Limitations

The main limitation of the thesis work is that there exist no mathematical dynamic state model for a wet gas compressor. The work of deriving one is an undergoing research field for the PhD candidate Torstein T. Kristoffersen at MTP. This limits the model analysis to two existing dry gas compressor models:

1. The centrifugal compressor model by [40]
2. The Greitzer model, for an axial compression system by [43].

The models were selected on behalf of the literature review performed in the specialisation project. These two models will be described in Chapter 2.

To validate the effect of wet gas in existing dry gas compressor models, the model findings is limited to the wet gas experiments in current performed research. The actual testing with dry and wet gas for the laboratory turbocharger is limited to the date when the laboratory is operational.

---

<sup>1</sup>The design might change during the spring of 2017, to incorporate more equipment or instruments. Changes due to test results might also be applied.

### 1.4 Objectives

In order to finish the thesis work and contributing to the research in effects of compressors exposed to wet gas, the following objectives have been defined:

1. Establishing compressor characteristics based on the compressor performance curves for the GT2252 turbocharger in the WGC laboratory at MTP
2. Develop a simulation model using model-based design
3. Compare the simulation performance of the two models chosen for further study in [106], with the developed compressor characteristics
4. Perform a controller tuning study and implement the designed control algorithm for a compressor model
5. Investigate and test potential wet gas parameters for the dry gas compressor model
6. Contribute to the electrical wiring and documentation of the WGC laboratory.

If time permits and the wet gas laboratory is finished, the following list of objectives will be done:

7. Establish an empirical wet gas characteristic for the turbocharger in the WGC laboratory
8. Implement the developed controller in 4. in the WGC laboratory and document the performance.

### 1.5 Motivation and approach

The motivation for working on the thesis subject is the ground work made in the specialisation project and the ability to contribute to the field of research on wet gas compression. The further work includes more hands-on practical work and development in computer simulation tools with the use of previously acquired knowledge from the master program. The privilege to be able to contribute to a small-scale subsea gas compression laboratory is also a contributing factor.

The approach taken for the continued phase on the subject is to use model-based design software to investigate the first principle compressor models. This will be done with MATLAB R2016b, Simulink.

On the subject of modelling wet gas compressors with the physical phenomena obtained by experiments, the work in [28, 45, 63] gives an extensive testing of the physical aspects of wet gas in centrifugal dry gas compressors. Both [28, 45] has conducted experiments on the Wet Gas Compressor and Multiphase Boosting Test Facility at NTNU.

Previous thesis work on the subject of control design for Subsea Gas Compression Stations (SGCS) is commonly performed in the simulation software Aspen Hysys Dynamics, used by industry for simulation of oil and gas processes (see for example [88]). For wet gas compressor control with varying Gas Volume Fraction (GVF) at the separator gas outlet, [2] used a set of linear controllers. Using two different correction methods for wet gas compression in Hysys, a set of linear controllers were able to adjust to the changing dynamics when the fluid properties changed.

In terms of the WGC laboratory startup phase, a practical approach to the controller design may be adequate, as it simplifies the transfer to the actual laboratory control system program.

### 1.6 Information retrieval

During the work on the master thesis, relevant literature has been searched for and evaluated. The sources to the theoretical content and material from other relevant authors are retrieved from academic search engines. The primary source for literature is the online university library Oria (Bibsys). The database extensions SCOPUS (Elsevier) and Science Direct (<http://www.sciencedirect.com/science/article>) have been chosen as the most relevant source for technology and science articles. The advantage of using the academically oriented search engines is to attain peer-reviewed articles which focus on the subject of matter. The search engines are found in <https://www.ntnu.no/ub>, with all the available databases.

### 1.7 Structure of the report

The rest of the report is structured as follows. Chapter 2 gives the reader the necessary background in relevant theory on subsea gas compression, compressor performance and control theory. Chapter 3 contains the work on establishing compressor characteristics for GT2252 for further use in simulation. Chapter 4 includes the simulation of the compressor models, and the developed control algorithm being subject to testing of stability and robustness. The centrifugal model compressor characteristic is corrected for wet gas flow and is used as a measure to test the controller robustness. Chapter 5 introduces the reader to the WGC laboratory at MTP with relevant background on the components. The author's contribution in the facility is included in this chapter. Chapter 6 includes the discussion from the author's point of view, conclusions from the thesis work along with recommendations for further work on the topic of wet gas compression control.



# Chapter 2

## Theory

This chapter is intended to give an overview of the existing methods of subsea gas compression, the approaches currently made to predict compressor behaviour with wet gas and theory concerning the thesis subject.

### 2.1 Subsea gas compression

Subsea gas compression is still under further development to effectively accelerate the hydrocarbon production. Challenges associated with ageing reservoirs and remote fields with hydrocarbon potential is the decline in natural reservoir pressure and large step-out distances. On behalf of the challenges, the gas compressor is proficient [78], [82].

The subsea gas compressor is installed close to the production well (upstream of production vessel or rig) and increases the differential pressure between the reservoir natural pressure and the downstream system resistance. This resistance origins from pressure drop due to friction, bends and large piping lengths, valves and other processing equipment. Utilising gas compression the well flow is boosted to a higher pressure, resulting in a longer plateau on the production curve and an increased accumulative production of gas [101]. In Figure 2.1, a typical pressure profile of the production well is presented.

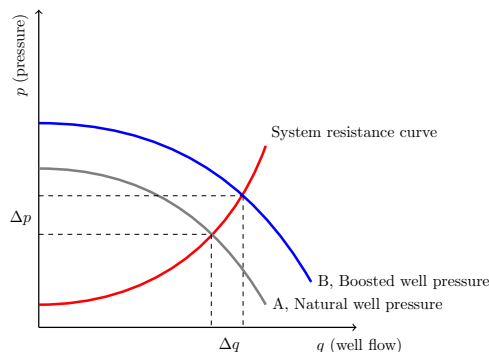


Figure 2.1: Natural and boosted production curves from a subsea well [6]

## 2. Theory

Utilising gas boosting, the new well pressure curve (B) seeks a new equilibrium point with a larger well flow and differential pressure. However, a natural gas reservoir fluid contains a mixture of liquid and gas. The gas-liquid mixture is defined as *wet gas* if it has a liquid fraction of up to 5% for offshore reservoirs on the NCS. Existing dry gas compressor technology is not compatible with large liquid content in the gas flow, and requires a separator upstream of the compressor [79], [62].

### 2.1.1 Wet gas compression

According to [61] there exist two methods of performing wet gas compression. The first and most common is to use a vertical gas-liquid separator (scrubber) on the reservoir gas to separate the liquid particles, enabling the use of common dry gas compressor technology. The second method implies no separation of the gas and directs the raw well stream directly to the wet gas compressor [8].

A successful implementation of the first method is located at the Åsgard field on the NCS. The compressor station is developed and built by Aker Solutions, where the compressor module is delivered by MAN Turbo & Diesel [87]. The SGCS, installed by Statoil, is intended to increase the production by 306 million barrels of oil equivalents (BOE)<sup>1</sup>. A process flow diagram (PFD) for a SGCS is seen in Figure 2.2.

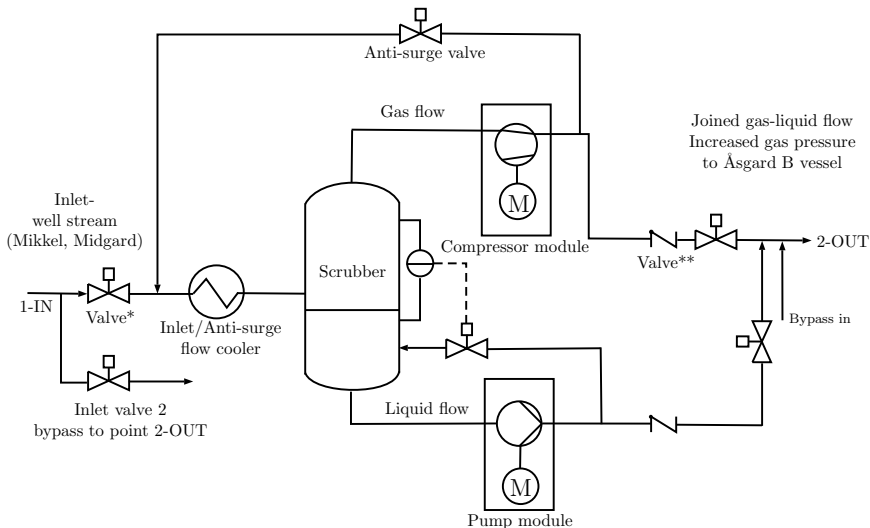


Figure 2.2: Early stage method of wet gas compression (Åsgard layout) [8]. (\* - Subsea control valve, \*\* - One way valve).

The extraction from the gas and condensate deposits, Midgard and the satellite wells at Mikkel, is directed through a manifold to the inlet of the SGCS. The gas is cooled by a heat exchanger before entering the separator (scrubber). The gas and liquid are separated and the gas flow is directed to a 10 megawatt (MW) compressor module, increasing the gas pressure. The liquid flow is pumped and joined with the high pressurised gas at the outlet

<sup>1</sup> 1 standard BOE is equal to 1000 standard cubic meters of natural gas [51]

of the compression station. Before startup and at minimum flow conditions the recycle anti-surge valve opens and the flow is directed back to the heat exchanger. Increasing the gas pressure also implies a temperature increase, making it necessary to cool the recycle flow before separation [26].

In 2015, a subsea wet gas compressor unit called WGC4000, built by Onesubsea, capable of handling a multiphase flow of gas and liquid were ready for installation [16]. The scrubber and liquid pump units are discarded, where the well stream is cooled ensuring that the temperature does not exceed the limits of the machinery. The flow enters then a mixing unit before compression. The WGC4000 unit, installed into an integrated template structure is seen in Figure 2.3.

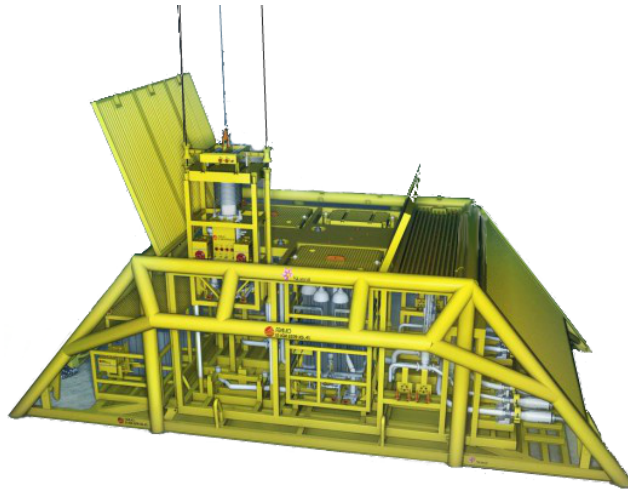


Figure 2.3: WGC4000 compressor installed in subsea template [81]

The WGC4000 compressor is driven by two 5 MW electrical motors and accelerates the multiphase flow with contra-rotating impellers capable of processing a flow with 0 to 100% liquid content. This enables the compressor to operate without a control system for anti-surge protection [61]. The wet gas compressor unit was installed at Gullfaks Sør field by Statoil and associated operating companies in June 2015. The wet gas compressor unit receives its power through an umbilical tie-in from the Gullfaks C platform, where the control system and hydraulic power unit are located [87].

Compression of natural gas and gas condensate directly from the well bore without separation is in its infancy. Due to the limited amount of projects implemented on behalf of this topic. It is of interest from the industry and the academic sector to be able to predict the compressor behaviour operating with wet gas. Predicting the dynamic behaviour enables the development of effective control algorithms, optimising the process through simulation before installing the equipment subsea. The Kårstø facility in Rogaland, Norway, are one of the locations used extensively for research and testing procedures, also known as the K-lab. The facility receives the gas and condensate from fields on the NCS through the Statpipe-pipeline. At the K-lab, a subsea compressor can be tested with identical hydrocarbon flow and conditions similar to what the machinery will experience on the NCS [90], [91].

## 2. Theory

---

### 2.1.2 Wet gas definitions

The scope of wet gas is large and in this section, a short description of the common definitions are included which are useful for the continued work. In this thesis, the definitions from [62] are used for the wet gas GVF. This is a common measure of the volumetric rate of gas to the total volumetric rate of all the fluids at the measured point of the pipeline. The GVF is given as

$$\text{GVF} = \frac{q_g}{q_g + q_l} \quad (2.1)$$

where  $q_g$  is the gas volumetric flow and  $q_l$  is the liquid volumetric flow. If the gas mass flow is monitored, the Gas Mass Fraction (GMF) can be calculated according to [45] as

$$\text{GMF} = \frac{w_g}{w_g + w_l} = \frac{\rho_g \text{GVF}}{\rho_g \text{GVF} + (1 - \text{GVF})\rho_l} \quad (2.2)$$

where  $w_g$  is the gas mass flow rate and  $w_l$  is the liquid mass flow rate.

Well stream with both liquid and gas present (natural gas, condensate etc.) can be characterised with a specific flow pattern according to the turbulence of the flow, defined by phase flow velocity and the flow Reynolds number [54], [50]. In the transportation and processing of hydrocarbons in the oil & gas industry, the pipe flow Reynolds number is typically large and in the turbulent end of the spectre [50]. For wet gas flow, the homogeneous flow model is used to describe the characteristics of wet gas. This treats the two-phase flow as single fluid flow where a mixture density is used and according to [47] it is defined as

$$\rho_h = \rho_g \text{GVF} + (1 - \text{GVF})\rho_l \quad (2.3)$$

where  $\rho_h$  is the homogeneous density,  $\rho_g$  is the gas density, GVF is the flow GVF and  $\rho_l$  is the liquid density. However, the flow patten internally in the compressor channels is annular [45]. This is due to the large value of GVF and high gas flow velocity. The core gas flow is centred and the liquid film is concentrated along the walls or edges of the channel.

### 2.1.3 Performance issues with wet gas

The projects introduced in Section 2.1.1 are subject to extensive research of wet gas effects in existing dry gas compressor technology. The work of [62] and [63] on wet gas compression (WGC) is often referred to in literature. The latter article is the result of both an analysis on existing compressor performance calculation procedures (ASME PTC-10 [4]) and a test on a single stage centrifugal dry gas compressor at K-lab. In terms of WGC experiments, the centrifugal compressor has played a large role due to its use as a pipeline compressor in process facilities on offshore rigs and onshore [14]. See for example [63] and [13]. In these experiments some of the following observations are made for wet gas in centrifugal dry gas compressors:

1. Evaporation or condensation of the liquid phase inside the compressor. This led to a temperature drop of the gas inside the compressor, decreasing its density and reducing the flow rate [62]



2. A drop in compressor pressure ratio for decreasing GVF. However, the individual impeller showed an increasing pressure ratio with wet gas revealing that the pressure ratio drop most likely occurred in the following section of the compressor discharge path [46]
3. Increase in frictional losses and other internal losses of the compressor. The result of these conditions ultimately leads to a reduced efficiency of the dry compressor dealing with wet gas [36]
4. The compressor drive increases the power consumption, due to increase in internal losses when compressing wet gas compared to ordinary pre-separation and dry-gas compression [79], [13].

These observations make some of the fundamental knowledge in dynamics of wet gas compression.

## 2.2 Dynamic compressor fundamentals

In the offshore oil and gas sector, the axial and the centrifugal flow compressor are commonly used due to their versatile operation envelope and process flow tolerance with high speed operation [11], [14]. The two types are presented in Figure 2.4a and 2.4b. The compressor category is named *turbomachinery* since the gas flow receives its energy by the dynamic action of the components on the rotor shaft [21].

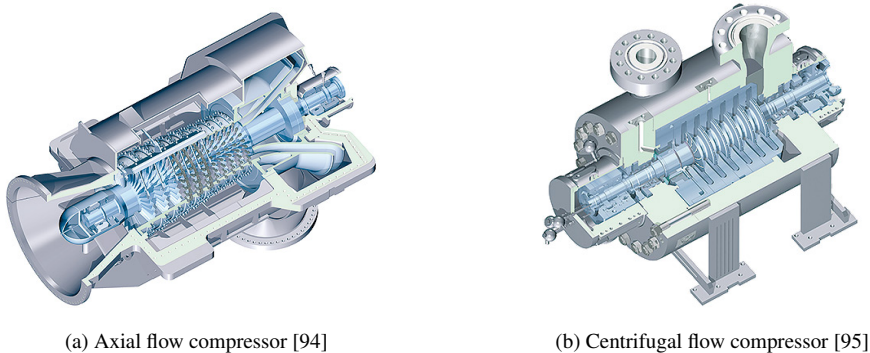


Figure 2.4: Modern turbomachinery design

In the axial compressor, the gas flow travels in the axial direction, through rotor blade rows increasing the gas kinetic energy. The following stator row converts this kinetic energy to static pressure due to the diffusion of the gas molecules. The specific axial compressor stage is seen in Figure 2.5a. Common use for axial compressors is in gas turbines, for power generation such as at the Snøhvit field onshore process facility and in aviation industry [33]. The gas flow in the centrifugal flow compressor is drawn either perpendicular or axially into the inlet depending on the design. Axial inlet flow is seen in Figure 2.5b.

The impeller is the main component of the centrifugal compressor that transfer energy from the rotor to gas through the blades, seen in the centre of Figure 2.5b. The kinetic energy

## 2. Theory

---

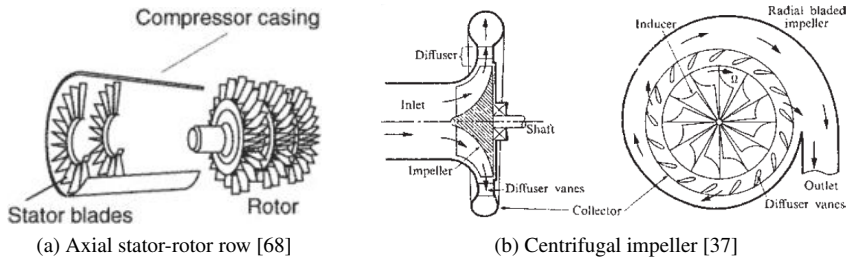


Figure 2.5: The two compression stage setups

of the gas is increased flowing through the impeller and then converted to pressure energy when the gas is slowed down in the stationary diffuser section. The diffuser section can either be vaned (seen to the right in Figure 2.5b) or vaneless implying an exit surface with no blades after the impeller. Furthermore, the gas flow enters a collector chamber called the volute, before being discharged into the downstream piping. The difference from the axial design is the radial exit of the gas flow in the impeller section [37], [84].

The centrifugal compressor impeller design is also divided into a shrouded or unshrouded design. The front end of the impeller is often referred to as the shroud and the back end as the disc. The unshrouded design offer high-pressure ratios per stage, and offer high blade tip speed with lower blade stresses [55]. Furthermore, the common standard in centrifugal compressors comprises of a shrouded impeller where large flow capacity is favoured [9, Ch. 11]. Figure 2.6 presents the shroud impeller design.



Figure 2.6: Shrouded impeller [9]

The shrouded design offers higher efficiency at larger speed than the unshrouded design. This is due to the lower frontal gas flow leakage [30].

### 2.2.1 Laboratory wet gas compressor

The wet gas compressor at the MTP laboratory is a turbine-driven compressor on a common shaft. This equipment will be referred to as the *turbocharger*. The relevant use of this turbocharger is in the automobile industry, and it was selected by the previous project group working on the laboratory after evaluating the required process conditions [10]. The turbocharger is shown in Figure 2.7.



Figure 2.7: The WGC turbocharger [31]

The turbocharger is driven by pressurised air fed into the turbine side seen at the top in Figure 2.7, converting the kinetic energy of the air flow through the turbine impeller to the shaft. The shaft rotates the compressor impeller and increases the gas kinetic energy. The absent factor is the high-temperature an exhaust gas in a vehicle holds when entering the turbine chamber. The high temperature gas is converted to kinetic energy in the turbine volute from gas expansion and the impeller converts this energy to mechanic energy, rotating the shaft [55], [27].

The common shaft connects the turbine impeller and the compressor impeller, presented in detail in Figure 2.8. The shaft spins the compressor impeller, creating a suction pressure which draws gas into the inlet. The gas is then discharged with a higher pressure. Furthermore, speed control is achieved by controlling the inlet air flow to the turbine. The impeller type is unshrouded, with high-speed operation (up to 195000 revolutions per minute (RPM) according to the data sheet).

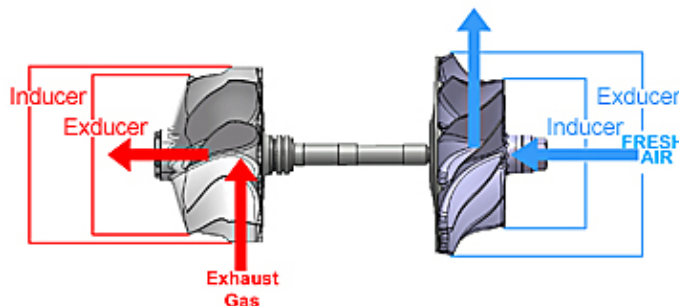


Figure 2.8: Common shaft turbine (left) and compressor (right) [32]

### 2.3 Modelling a dry gas compressor

To continue the work on adapting the dynamics of wet gas in the compressor modelling arena, a preliminary study on how gas dynamics behave in dry gas compressors must be performed. The modelling and simulation which will be done in this thesis have its basis from the recommendations proposed in the specialisation project [106]. This section will introduce the compressor models being important for the work on wet gas modelling and control. The two dynamic models selected for further study is the Greitzer's axial compressor model in [43] seen in Figure 2.9, and the centrifugal compressor model derived in [40]. The material in this section, Section 2.3.1 and 2.3.2 are drawn from the above-mentioned literature. The axial compressor model will be referred to as the *Greitzer model*, and the compressor model with a centrifugal configuration as the *centrifugal model*.

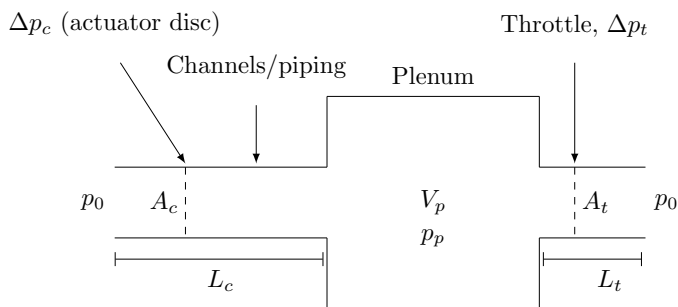


Figure 2.9: The axial compressor model by Greitzer [43]

The model representation is more or less the same in these two in the view of how the sections are established. The Greitzer model does not include shaft dynamics and represents the compressor and throttle by actuator discs<sup>2</sup>. The extension by [40] was to include a variable for rotational speed, enabling the control of the shaft torque shown in Figure 2.10. The centrifugal model is divided into three sections, with the motor drive unit extension.

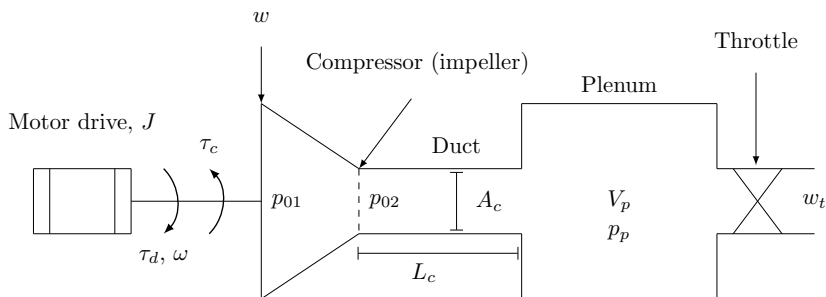


Figure 2.10: The centrifugal compressor model with shaft dynamics [42]

<sup>2</sup>The actuator disc representation is for an axial compressor model of a blade row including the rotor and stator. In the low-order models confined in this thesis, it represents the pressure rise across the compressor and pressure drop across the throttle. This theory originates from the derivation in [59] to model the flow across a consecutive blade row in an axial compressor [108].

The compressor model itself consist of a section to model the pressure increase by the impeller connected to a duct with a constant area, a plenum accounting for the compression process and an exit duct with a discharge throttle. The motor drive supplies the torque to the common drive shaft. This is where the speed variable  $\omega$  is included in the derivation of the model equations.

Regarding the model assumptions, it is important to understand what physical and theoretical interpretation the researchers have made to establish the dynamic equations for predicting operating behaviour.

### 2.3.1 The Greitzer compressor model

The Greitzer model is drawn from [43] and [44] where the latter article describes the dynamic model in relation to actual experiments on an axial compressor. With reference towards Figure 2.9, the model assumptions as made by the author is:

1. The model is constrained to small inlet Mach numbers and inlet pressure rise compared to the surrounding ambient pressure. Moreover, the inlet suction pressure is assumed to be atmospheric. However, no restrictions are set to the oscillations that occur during operation when comparing the values to the steady-state conditions
2. The gas flow in the compressor duct are assumed to be one-dimensional and incompressible. Incompressibility is assumed due to small inlet Mach numbers, neglecting compressibility effects due to shock waves
3. The plenum is modelled as a Helmholtz resonator, and the oscillations in the plenum represents the potential energy of the compressed gas. The kinetic energy of the oscillations are associated with the motion of the gas in the compressor and throttle duct
4. The compression of the gas in the plenum is assumed to be isentropic. This implies that the process is reversible and that there are no heat transfer, as well as constant entropy.

Compressible flow are addressed for Mach numbers above 0.3 in industrial applications [21], [20]. Furthermore, Greitzer assumed that the model ducts leads to the same unsteady pressure difference and change in mass flow for an actual compressor duct. On behalf of this, a lumped parameter analysis of the compressor sections leads to a constant area duct representation [3]. The dimensional equations are established by analysing the momentum balance in the duct, both for the compressor and the throttle, along with deriving the mass balance for the plenum. The compressor mass flow  $w_c$  is given in terms of the pressure difference across the duct as

$$\frac{L_c}{A_c} \dot{w}_c = \Delta p_c - \Delta p \quad (2.4)$$

where  $L_c$  is the effective duct length,  $A_c$  is the compressor flow-through area,  $\Delta p_c$  is the compressor pressure ratio (the gas pressure rise across the compressor stator blade row) and  $\Delta p$  is the plenum pressure difference from ambient pressure  $p_p - p_0$ . The throttle mass flow dynamics is given as

$$\frac{L_t}{A_t} \dot{w}_t = \Delta p - \Delta p_t \quad (2.5)$$

## 2. Theory

---

where  $L_t$  is the effective throttle duct length,  $A_t$  is the flow through area of the throttle and  $\Delta p_t$  is the pressure drop across the throttle. The plenum mass balance is derived as

$$\frac{V_p}{\kappa} \frac{\rho_p}{p_p} \dot{p}_p = w_c - w_t \quad (2.6)$$

where  $V_p$  is the plenum volume,  $\kappa$  is the ratio of specific heats ( $\kappa = c_v/c_p$ ),  $\rho_p$  is the gas density in the plenum and  $p_p$  is the plenum pressure. A first-order transient equation is used to model the dynamic behaviour before the onset of an instability in the compressor. This was first done by Greitzer, considering a non-quasi steady operation of the compressor with transient changes in the mass flow. Therefore, the introduction of the time-lag dependence on the number of rotor revolutions to form a compressor stall was used [60]. The dynamic behaviour of the gas pressure rise is given by

$$\Delta \dot{p}_c = \frac{1}{t_c} (\Delta p_{c,ss} - \Delta p_c) \quad (2.7)$$

where  $\Delta p_{c,ss}$  is the steady-state pressure ratio over the compressor and  $t_c$  is the compressor time constant. The non-dimensional Greitzer parameter,  $B$  appears from scaling the physical quantities to non-dimensional quantities. It can be described with physical parameters as

$$B = \frac{U}{2a} \sqrt{\frac{V_p}{A_c L_c}} \quad (2.8)$$

where  $a$  is the sonic velocity of the gas in the plenum. The plenum is modelled as a Helmholtz resonator. The Helmholtz frequency occurring in the plenum chamber is derived as

$$\omega_H = a \sqrt{\frac{A_c}{V_p L_c}} \quad (2.9)$$

The dynamic model in terms of physical dimensions is given by (2.4) - (2.7).

### 2.3.2 The centrifugal compressor model

Since the representation of the centrifugal model is based on the Greitzer model the assumptions are seen to be similar, with an extension towards the application of centrifugal compressor properties. The model assumptions applied to the centrifugal compressor system are listed below:

1. The compressor duct in series with the plenum is modelled as a Helmholtz resonator and the oscillations in the compressor is analogous with those occurring in a resonator system
2. The compression is isentropic modelled in series with an isobaric process. The latter process will then account for the compressor losses due to increasing entropy
3. Isentropic reduction for the gas velocity in the diffuser. If the gas velocity is reduced close to zero in the diffuser, the static outlet pressure at the diffuser is assumed equal to the stagnation pressure at the outlet of the impeller
4. Impeller blade geometry is backwards curved, to incorporate the energy transfer from the blades to the gas flow

5. No pre-whirl of the gas into the impeller inlet. This implies that the inlet gas flow enters axially into the inducer blades.

Assumption 1 leads to an incompressible duct flow with constant velocity and density. Furthermore, the compressibility effect is restricted to the plenum section of the resonator model, where pressure varies with time. The notable difference from the Greitzer model is that compressor shaft speed  $\omega$  is included as a state variable. The compressor shaft speed is modelled by the torque balance between the motor drive  $\tau_d$ , and the compressor torque implied on the shaft  $\tau_c$  given as

$$J_m \dot{\omega} = \tau_d - w\mu(\phi)r_2^2\omega \quad (2.10)$$

where  $J_m$  is the motor drive inertia,  $\omega$  is the shaft speed,  $\tau_d$  is the motor drive torque and  $\tau_c$ , the compressor torque in opposite direction of the drive torque. It is given as  $\tau_c = w\mu(\phi)r_2^2\omega$ , where  $\mu$  is the energy transfer coefficient dependent on the flow coefficient and  $r_2$  is the outer radius of the impeller. The momentum balance for the duct is in terms of the duct mass flow and assumption 3 given as

$$L_c \dot{w} = A_c (p_{02}(w, \omega) - p_p) \quad (2.11)$$

where  $L_c$  is the effective length of the compressor internal channels,  $A_c$  is the compressor flow-through area,  $p_{02}$  is the outlet stagnation pressure of the impeller and  $p_p$  is the plenum pressure. The outlet pressure is derived through a thermodynamic process analysis of the isentropic compression with the isobaric loss modelling. This leads to a relation between the inlet and outlet pressure, a pressure ratio known as the compressor characteristic, defining the pressure ratio the compressor is capable of achieving. The characteristic is defined as

$$\Psi_c = \frac{p_{02}}{p_{01}} \quad (2.12)$$

where  $\Psi_c$  is the compressor characteristic and  $p_{01}$  is the inlet stagnation pressure at the inducer. The characteristic is modelled with a stagnation enthalpy balance for the compression process including friction and incidence losses in the compressor. The resulting duct equation is according to [40], derived as

$$L_c \dot{w} = A_c \left( \left[ 1 + \frac{\mu(\phi)r_2^2\omega^2 - \frac{r_1^2}{2}(\omega - \alpha\omega)^2 - k_f w^2}{c_p T_{01}} \right]^{\left(\frac{\kappa}{\kappa-1}\right)} p_{01} - p_p \right) \quad (2.13)$$

where  $r_1$  is the radius of the inlet to the impeller (the inducer),  $\alpha$  is the incidence loss parameter,  $k_f$  is the friction loss coefficient for the impeller gas flow,  $c_p$  is the specific heat at constant pressure and  $T_{01}$  is the inlet stagnation temperature. The plenum mass balance, assuming isentropic gas flow is derived in terms of the plenum pressure as

$$\dot{p}_p = \frac{a_p^2}{V_p} (w - w_t(p_p)) \quad (2.14)$$

where  $a_p$  is the speed of sound of the gas in the plenum,  $V_p$  is the plenum volume and  $w_t$  is the mass flow through the throttle.

## 2.4 Compressor performance and control methodology

This section will give an overview of the compressor performance topics necessary for further work on the thesis subject. An overview of common methods of controlling a compressor is given. The content in this section is drawn from [27], [55, ch. 4] and [75, ch. 2].

### 2.4.1 The compressor map

The compressor map characterises the performance of a specific compressor rig [69]. Parameters such as inlet and discharge pressure and temperature, mass flow and the compression efficiency are important when describing the performance. These factors are directly dependent on the rotational speed of the machinery and fluid properties. The dimensionless pressure ratio is given in terms of the parameters according to [37] as

$$\frac{p_{02}}{p_{01}} = f\left(\frac{T_{02}}{T_{01}}, w \frac{\sqrt{T_{01}}}{p_{01}}, \frac{N}{\sqrt{T_{01}}}\right) \quad (2.15)$$

where  $p_{02}/p_{01}$  is the pressure ratio (discharge to inlet),  $T_{01}$  and  $T_{02}$  is inlet and discharge temperature,  $w$  is the compressor mass flow and  $N$  is the rotational speed (commonly in revolutions per minute (rpm)). These quantities are corrected in terms of the gas properties the compressor is operating with, such as molecular weight and density. The resulting pressure ratio from (2.15) is plotted in a compressor map for one specific machinery [30]. A general compressor map is presented in Figure 2.11.

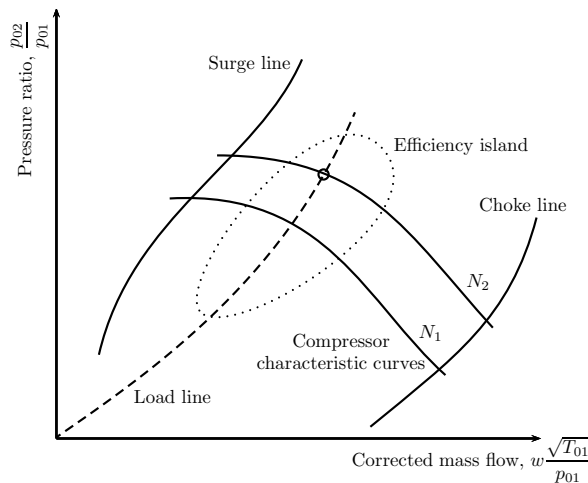


Figure 2.11: The compressor map

The map notation and quantities are:

1. The compressor characteristic curves, defined for one constant speed  $N$ . In a specific map, there may be plotted several lines where the top most are indicating maximum operational speed of the compressor.



2. The surge line<sup>3</sup> indicating the left most operating point before reaching the unstable area of the compressor operation. The compressor map usually indicates the negative slope characteristics of the compressor, where a increase in flow results in a decrease pressure ratio. The instabilities are said to occur when the slope of the characteristic curve is zero [75], [109, Ch. 3]
3. The choke line<sup>4</sup> where the compressor mass flow is not further increased. Looking at  $N_2$  in Figure 2.11, the gas flow chokes when passing the choke line. The pressure drops and the mass flow must be decreased to shift the operating point into the stable area [27, Ch. 8].

Commonly in a compressor map is also to represent the constant efficiency islands. In this area, the compressor is operating according to a defined efficiency the manufacturer has specified. The efficiency for a turbomachine such as a compressor is defined for the thermodynamic process it is calculated from [30]. According to [21], the adiabatic compressor efficiency is defined as

$$\eta_c = \frac{\text{Ideal energy input to rotor}}{\text{Actual energy input to rotor}} \quad (2.16)$$

where  $\eta_c$  is the compressor efficiency, the nominator is the calculated ideal energy (isentropic process with constant entropy) input and the denominator represent the actual energy input. These are commonly expressed as specific enthalpies for the process [21].

The load line represents the demand from downstream equipment. This can be pipelines and installed processing equipment such as separators. All of this will influence the system resistance in terms of pressure increase, drop or demands on gas flow. The operating point for the compressor (marked with a circle in Figure 2.11) is where the load demand curve intersects the characteristic curve [75]. If the load demand is too high, the operating point might be shifted to the left on the characteristic bringing the compressor into the unstable operating area.

### 2.4.2 Compressor losses

A compressor stationed at a processing facility, subsea or in a refinery are never likely to operate with ideal gases where assumptions to isentropic process conditions and ideal energy transfer from the impeller to the gas are valid. However, when designing the geometry of internal piping and the specific impeller for a compression stage, the goal is to reduce the generation of entropy in the system and achieve high-efficiency [23]. The entropy in a compressor is equal to the amount of lost compression work [21]. The quantity increases due to the fact that the process is irreversible and the fluid properties change due to friction and heat transfer [64]. Therefore, an accurate modelling of the process must consider the thermodynamic properties of the off-design conditions for the compressor operation.

---

<sup>3</sup>There exist different names for this line, and commonly used is the stall or surge line [75].

<sup>4</sup>Also referred to as the stone wall line in literature

## 2. Theory

---

Off-design is defined as a mismatch between the design parameters and the gas flow at a specified section of the compressor. This can be for example mismatch from optimal inlet gas flow, discharge at the impeller outlet due to the angle of gas flow in the blade passages [64], [55]. Common losses associated with a centrifugal compressor can be divided into three major categories according to [11]:

1. External losses
  - Loss of flow capacity in leakage points between mechanical components
  - Rotating disc frictional losses at the impeller
2. Rotor losses
  - Specific losses for the impeller section
  - Shock losses at the impeller inlet due to high Mach numbers
  - Incidence loss due to mismatch between inlet gas flow angle and fixed inducer blade angle
  - Diffusion loss in impeller passages and friction losses
3. Stator losses
  - Losses occurring in the diffuser section of the compressor.

### 2.4.3 Compressor instability

The instabilities associated with the region to the left for the surge line is *rotating stall* and *surge* phenomena [110]. The scope of compressor instability is wide, and this section will give a short introduction on the subject. Reference is given towards literature such as [19] and [110] on this subject.

#### Rotating stall

If the flow oscillates around a local point on the rotor, either if the operation point has passed the surge line or in the steady-state operation envelope, the instability is distinguished as rotating stall [75]. Rotating stall is characterised by the development of stall-cells in the circumferential flow pattern in the compressor. The cells will have a reduced or stalled flow, travelling around the annulus<sup>5</sup> of the compressor at slower rotational speed [102]. For an axial compressor, a rotational stall is considered to occur in the rotating blade passages on the stator-rotor configuration. In centrifugal compressors rotating stall is harder to distinguish [29]. The phenomena can be initiated at different stages such as the impeller or diffuser section. In either case, the stall will give a reduced performance for the compressor with a limited mass flow and pressure ratio and may apply large stresses on the compressor rotor blades due to vibrations [21].

#### Surge

Operating in stall, or the compressor operation point is rapidly shifted to the left of the surge line the compressor may initiate surge [75]. Surge is dependent on the properties of the compressor characteristic and also the system which the compressor is connected to (discharge

---

<sup>5</sup>The term annulus refers to the flow area, between rotor and compressor casing

pipeline and downstream equipment). A sudden increase in system pressure, defined by the load line may initiate surge as the demand in gas flow decreases. The phenomena is characterised with large fluctuations of the flow with time, resulting in oscillations in the gas flow and pressure [37], [19].

The consequences of surge is more severe than for rotating stall, where the compressor internal components (such as bearings and sealings in the rotor) may be damaged [48]. A direct effect of surge in the compressor system is large noise due to vibrations and temperature rise. If flow reversal is present, the temperature of the gas increases leading to increased temperature in the compressor.

In literature, several different surge categories exist. To limit the scope, two well-defined types are the classic and deep surge category. The difference of these two is in the oscillating frequency of the pressure and mass flow and also the occurrence of flow reversal inside the compressor [19]. According to [11], the frequency of surge can be from a few cycles per minute (deep surge) to 20 or more cycles per second. Increased surge frequency is associated with classic surge where no flow reversal is said to occur and low frequency with deep surge.

### 2.4.4 Anti-surge control

Anti-surge control is the measure to mitigate or stabilize the instability of surge in a compressor. The most common approach in industry towards mitigation of compressor instabilities is *surge avoidance control*. This is performed in terms of ratio-control between the adjustable parameters, mass flow and suction or discharge pressure. A recycle line is opened to ensure a minimum flow to the compressor inlet, to avoid the compressor operating point shifting to the left of the surge line. However, by introducing margins to the operating area, peak efficiency may not be reached for the compressor since the maximum efficiency are usually close to the surge margin [39]. Point A in Figure 2.12 may illustrate the highest achievable pressure ratio of the compressor at the current constant speed line (dotted line). If utilising surge ratio control, the operating point A might not be a part of the operating area since the controller will limit the compressor to the defined area [30], [75].

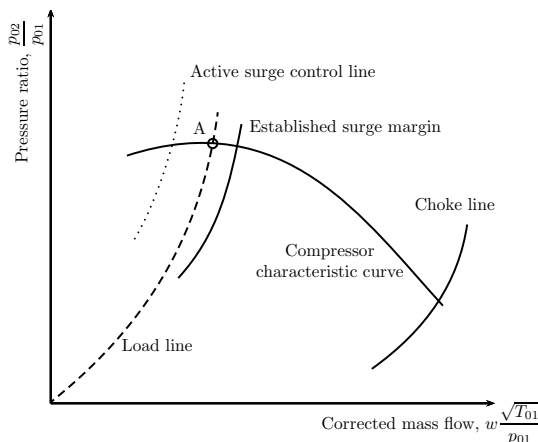


Figure 2.12: Extended compressor map with active surge control [110]

## 2. Theory

---

Active surge control is another method of compressor instability control, to ensure steady operation close to or beyond the surge line. The difference from the ratio control setup is that an active controller adjusts directly on the compressor actuators [110]. Using feedback from the state variables (pressure, mass flow etc.) in the process, predictions on the input to the controller can be made. The control algorithm adjusts the actuators such as the drive shaft speed or throttle valves to actively stabilise the machine in the unstable area of the map. This is illustrated in Figure 2.12, where the load line is the system resistance curve (increase in back pressure of the process loop due to the closing of valves for example), and the dashed line left of the load line resembles the limit towards active surge control [19], [75].

### 2.5 Control theory

This section is intended to present control algorithms topics being important for the work on the WGC turbocharger. The definitions and subjects are drawn from [67, ch.1 & 3] for the proportional integral derivative controller section, [57] and [89] for adaptive non-linear control.

To control a process installation, the implemented controller is dependent on feedback from the process variable. A schematic overview of a closed-loop feedback system where a controller is adjusting the input to the process is seen in Figure 2.13. The control output is  $u(t)$ , the outer disturbance on the process is  $v(t)$  and the measured output is  $y_m(t)$  with is routed through a measurement device and subtracted from the chosen setpoint  $y_{SP}$ .

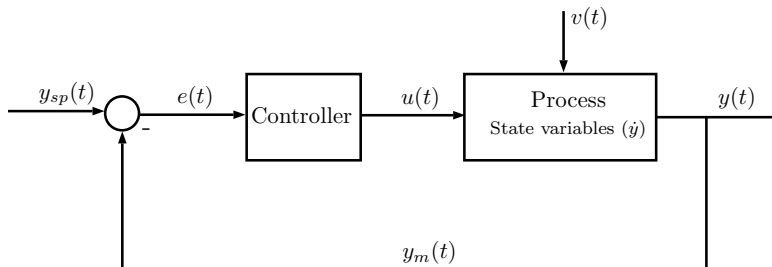


Figure 2.13: Closed loop feedback control system

For compression system control, the control loops maintaining stable operating conditions consists commonly of industrial standard Proportional-Integral-Derivative (PID) or PI-controllers [34]. However, according to [77], for surge avoidance the stand-alone PI controller is not sufficiently fast-acting enough for compressor control. This is due to rapidly acting dynamics of surge when crossing the surge line.

The acronym describes the control output in the form of three states dependent on the control error. A time-domain PID controller output, with the notation used in [98], is given as

$$u(t) = K_c \left( e(t) + \frac{1}{\tau_i} \int_{t_0}^t e(\tau) d\tau + \tau_D \frac{de(t)}{dt} \right) \quad (2.17)$$

where  $K_c$  is the proportional gain,  $\tau_i$  is the integral time,  $\tau_D$  is the derivative time and  $e$  is the control error. The control error  $e(t)$  is the deviation from the chosen reference value known as the *process setpoint* defined as

$$e = y_{SP} - y_m \quad (2.18)$$

where  $y_{SP}$  is the setpoint, and  $y_m$  is the measured process output. In the WGC laboratory, the preliminary control design is rooted in a PID algorithm for the individual control loops on:

- Mixing pressure control (choke valve control)
- Turbocharger speed control
- Turbocharger inlet suction pressure control.

### 2.5.1 Non-linear control

The PID controller is a linear controller which is optimal for control of strict linear processes such as a tank model. If the dynamics are non-linear, the process gain might vary for different operating points influencing the stability of the system. In these cases, adaptive control to varying operating conditions is mostly preferred [53]. A form of non-linear control is called Gain Scheduling (GS) control and this method will be the topic of this section.

A GS controller switches between linear controller settings, either PID or other optimal design control algorithms for specified operating points of the system using linear approximation [7]. These operating points are representing the overall dynamic response of the non-linear model. The controller settings are adjusted according to a specified gain scheduling variable which is measurable [67]. A generic non-linear system can be described as

$$\begin{aligned} \dot{\underline{x}} &= \underline{f}(\underline{x}, \underline{u}, t) \\ \underline{y} &= \underline{h}(\underline{x}, \underline{u}, t) \end{aligned} \quad (2.19)$$

where  $\underline{x}$  is the vector of state variables,  $\underline{u}$  is the vector of input signals and  $\underline{y}$  is the output vector. According to [89], a gain scheduling procedure for continuously varying a linear controller to a non-linear process model consists of:

1. Linearization of the non-linear process model in (2.19) to a Linear Parameter Varying (LPV) model (in the form of a state-space model)
2. Determination of a scheduling variable for the process
  - A common approach is to linearize the model at different equilibrium operating points, switching the controller gain between fixed values of the scheduling variable. An example is in [92] for automotive cruise control where the model is linearized for different operating points of the throttle

## 2. Theory

---

3. Design a linear controller for the LPV model found in 1
4. Implementation of the controller and a method of switching between settings, adjusting the gain(s) according to the varying scheduling variable.

To efficiently enable fast response of the controller, it is important that the scheduling variable reflects the process dynamics when operating points change. A block diagram representation of the GS algorithm is presented in Figure 2.14.

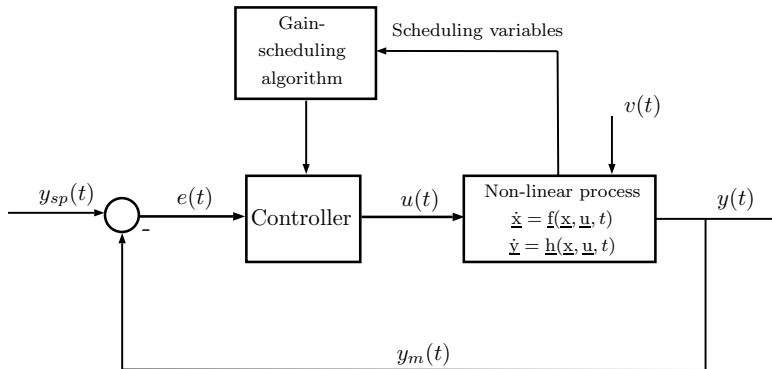


Figure 2.14: Gain scheduling control of non-linear process

The algorithm can for example adjust the linear PID controller parameters  $K_c$ ,  $\tau_i$ ,  $\tau_D$  according to a time-varying process variable.

## Chapter 3

### Establishing the compressor characteristic

This chapter includes the parameter definition for the GT2252 turbocharger used in the WGC laboratory and the first principle and empirical characteristic for later use in the simulation environment. The MATLAB program scripts for the material produced in this chapter are included in the electronic appendix file for this thesis.

#### 3.1 Parameter and map evaluation for GT2252 turbocharger

The turbocharger located in the wet gas compression laboratory at MTP is the source of information to establish the characteristic functions in MATLAB. These functions are key to compare the differences from the empirical and first principle characteristics in Simulink simulation. The turbocharger setup in the laboratory (without inlet and discharge hoses connected) is shown in Figure 3.1a and 3.1b. From the data sheet, the dimensions on inlet and outlet areas, impeller dimensions and geometry ratios are obtained.

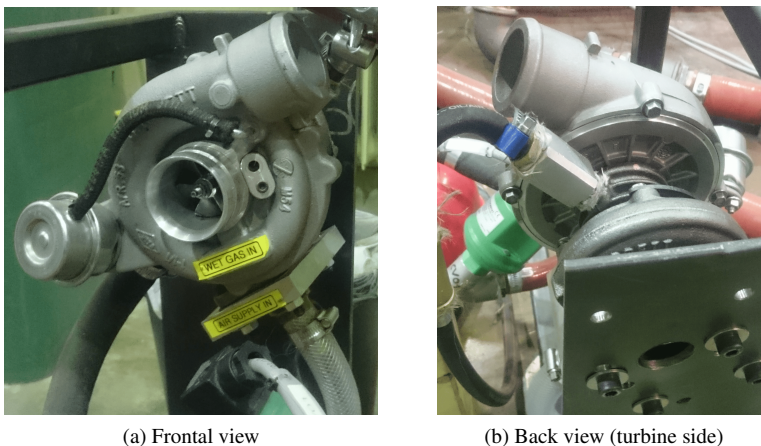


Figure 3.1: Wet gas compression application of GT2252 turbocharger

### 3. Determining compressor characteristics

The inlet and discharge hose on the turbocharger are disconnected to expose the eye of the impeller and show the turbine air outlet (the hole seen in Figure 3.1b). A summary of the parameters for the Garrett GT2252 turbocharger is presented in Table 3.1. The angles of the impeller blades (gas entry and exit) are approximated by manual measurements. The GT2252 impeller consists of 12 blades, where six of these are splitter blades.

Table 3.1: Design parameters for GT2252

Parameters	Value
Inlet area, compressor	$2.83 \cdot 10^{-3} \text{ m}^2$
Outlet area, -	$1.96 \cdot 10^{-3} \text{ m}^2$
Impeller specifications:	
- Type	Unshrouded
- Blade geometry	Backward curved
- Number of blades	12 (6 splitter)
- Inducer diameter	40.2 mm
- Exducer diam.	52.0 mm
- Inducer blade angle, ( $\tilde{\beta}_{1b}$ )	$21.4^\circ$ Measured
- Exit blade angle, ( $\tilde{\beta}_{2b}$ )	$54.1^\circ$ Measured
Diffuser type:	Vaneless to volute

An average of five measurements gave the result shown in Table 3.1 where the angles are given the tilde notation to differ it from the exact in the first principle characteristic. The full data set for the measurements are included in Appendix A.

In the design phase of a compressor, the desired optimal operation envelope is decided. This includes calculation of internal gas flow and optimising impeller blade angles for the designed gas velocities. The splitter blades is used to reduce the chance of flow blockage at the impeller periphery and create a larger suction pressure on the inlet of the compressor. This is done by increasing the number of blades, where the splitters are not extended fully towards the inlet hub [1]. Figure 3.2 indicates where the measurements are taken on the centrifugal impeller for the turbocharger.

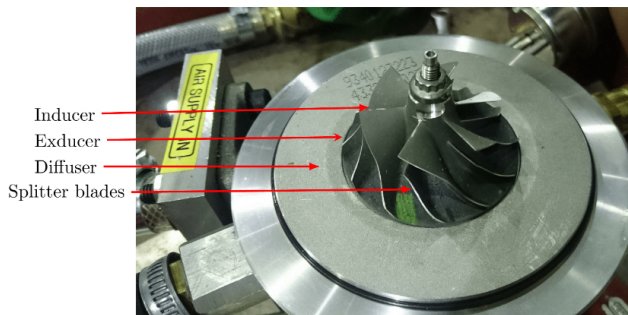


Figure 3.2: Components under the discharge volute of GT2252

The impeller exit blade angle influences the gas velocity when entering the diffuser section. According to [30],  $\beta_{2b}$ , the fixed blade exit angle lies between  $40$  to  $50^\circ$  to produce an effective increase in pressure ratio. The



## 3.1.1 The GT2252 compressor map

The turbocharger comes with a datasheet including the compressor performance map. From the preliminary theory in Chapter 1, the performance map is key to evaluate the compressor in terms of the process it is intended to operate in. The map for the GT2252 is calculated with pure air flow and is shown in Figure 3.3.

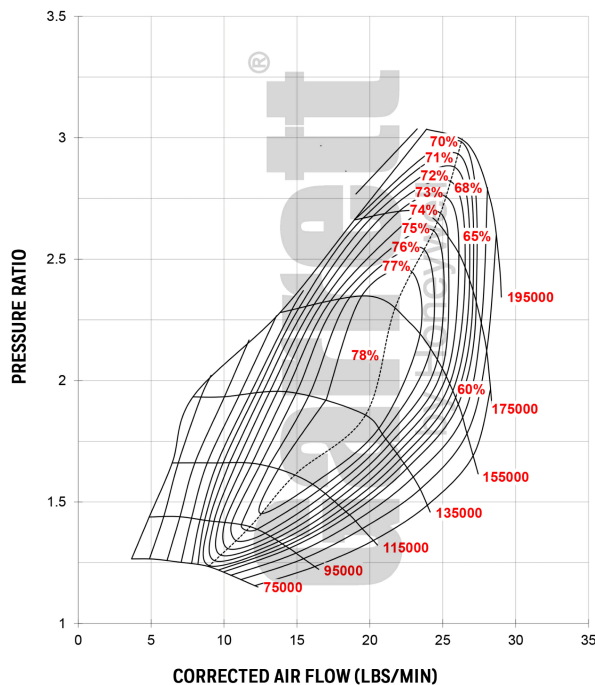


Figure 3.3: The compressor performance map of GT2252 [31]. Gas mass flow rate in  $\text{lbmin}^{-1}$  along the x-axis, speed lines in rpm, efficiency islands in % and the y-axis represents the dimensionless pressure ratio

The work on developing an empirical characteristic for simulation purposes are dependent on the information collected from this map. The resulting pressure ratio, denoted  $\Psi_c$ , is decided by both the rpm and the mass flow through the compressor. Therefore, to enable control of the compressor a function that predicts the pressure ratio given the mass flow rate and speed is required. The compressor map data (characteristic curves, surge line etc.) is sampled by discrete sampling points to adopt the map to the software. This is done with the GRABIT script developed by [22] for MATLAB. The map axis are set in GRABIT according to the actual map, and then each data point are picked from the figure. Furthermore, the map mass flow rate (x-axis) are converted to the SI-unit  $\text{kg s}^{-1}$  since all the other units are in SI.

#### 3.2 First principle characteristic

The first approach to adapt the characteristic curves from Figure 3.3 is to fit the first principle characteristic in the model developed by [40]. The content of this section is included to evaluate the important parameters that define the pressure ratio function  $\Psi_c$  in (2.12). The analysis is drawn from [40] and [23, Ch. 13], presenting the important equations for the continued work on simulation and control. On the subject of wet gas flow in a compressor, the topics presented in Section 2.1.3 stated that the friction losses increased. Since this is a factor included in the derivation of the first principle characteristic, it will be described more thoroughly.

A first principle analysis of the thermo- and fluid dynamics of the compressor is the basis for developing a complete mathematical model. Instead of using an empirically determined characteristic to evaluate the pressure ratio, the characteristic based on compressor energy transfer derived in [40] is presented in this section.

The factor that increase the energy of the gas is the impeller. The drive shaft torque transfers energy to the impeller, increasing the kinetic energy of the gas [21]. The pressure ratio is derived by the momentum balance in the duct given by (2.11). The produced compressor pressure ratio is assumed to be an isentropic process. The pressure  $p_{02}$  is derived from the isentropic relation, and according to [100] it is given as

$$\frac{p_{02}}{p_{01}} = \left( \frac{T_{02}}{T_{01}} \right)^{\left( \frac{\kappa}{\kappa-1} \right)} \quad (3.1)$$

where  $p_{01}$  is the inlet stagnation pressure to the impeller inducer,  $T_{02}$  and  $T_{01}$  is the stagnation temperature at the outlet and inlet of impeller and  $\kappa$  is the ratio of specific heats. However, the pressure increase from inlet to discharge is not ideally an isentropic process and the derivation in [40] accounts for this by modelling the thermodynamic states during compression with an isentropic in series with an isobaric process. The latter accounts for the entropy increase, generating losses in the compressor. The isentropic pressure increase implies an increase in stagnation enthalpy of the gas through the impeller. The complete process is presented with a enthalpy-entropy diagram (h-s diagram) in Figure 3.4. The figure shows the isentropic pressure increase from point 01 to 02s, then the isobaric process with heat transfer from 02s to 02.

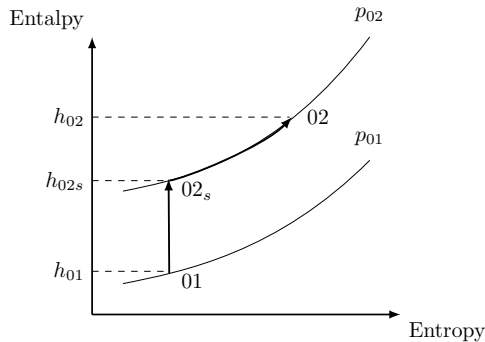


Figure 3.4: H-S diagram for the compression process [23]

In the figure,  $\Delta h_{02s}$  is the change in stagnation enthalpy during the pressure increase from  $h_{01}$  to  $h_{02s}$ . This is the enthalpy change for the gas flowing through the impeller. The total increase of specific stagnation enthalpy from 01 to 02 is then

$$\Delta h_{02} = \Delta h_{02s} + \text{losses} \quad (3.2)$$

where the losses are generated in the states 02s to 02. In Figure 3.4, the lines show the stagnation conditions and therefore the notation  $0i$ . Stagnation enthalpy are derived as  $h_{0i} = h_i + \frac{C^2}{2}$ , where  $h_i$  is the static enthalpy, showing that the static enthalpy is a offset in vertical distance in the  $h$ - $s$ -diagram. This is due to the definition of stagnation enthalpy as an isentropic process with no entropy change ( $ds = 0$ ) [64].

The enthalpy  $\Delta h_{02}$  is the energy transfer from the compressor impeller to the gas flow. The impeller is unable to store the produced energy and all of the energy is transferred to the gas. The energy transfer in terms of enthalpy is given as

$$\Delta h_{02} = \frac{\tau_c \omega}{w} \quad (3.3)$$

where  $\tau_c$  is the compressor torque acting in the opposite direction of the drive torque,  $\omega$  is the shaft speed and  $w$  is the compressor mass flow. Referring to Figure 2.10, the rate of change of angular momentum on the spool is given by the torque balance on the common shaft (drive and compressor) derived in (2.10). Applying control volume analysis of the gas flow in the rotor, the compressor torque is given as

$$\tau_c = w (r_2 C_{\theta 2} - r_1 C_{\theta 1}) \quad (3.4)$$

where  $r_1$  and  $r_2$  is the inducer and exducer radius respectively and  $C_{\theta 1}$  and  $C_{\theta 2}$  is the tangential velocity vector of the gas at the inlet and outlet of the impeller respectively. The velocity vector is dependent on the design of the impeller blades and defines the velocity of gas flowing through the blade passages. The impeller blades are curved in the opposite direction of rotation, as shown in Figure 3.5.

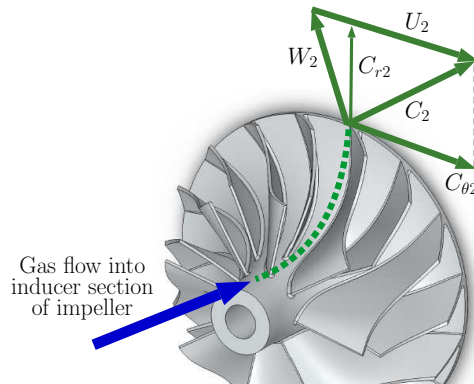


Figure 3.5: Velocity triangle for backward curved blades

### 3. Determining compressor characteristics

---

The total velocity triangle for this type of design is also presented in the figure. The assumption made in [40], is that there exist no gas flow pre-whirl made by inlet guide vanes into the impeller inducer section. This allows for an independent analysis of the exducer section since  $C_{\theta 1}$  is zero. In the figure,  $C_2$  is the absolute gas flow velocity vector,  $C_{r2}$  is the radial component,  $W_2$  is the relative component and  $U_2$  is the blade tip linear velocity.

The gas flow tangential velocity at impeller blade outlet  $C_{\theta 2}$  is found from the geometrical properties and is derived as

$$C_{\theta 2} = (1 - \phi \cot(\beta_{2b}))U_2 \quad (3.5)$$

where  $\mu$  is the energy transfer coefficient from the blade to the gas and  $\phi$  is the flow coefficient. For backward curve blades, the angle  $\beta_{2b}$  is less than  $90^\circ$  and the energy transfer coefficient is given as

$$\mu(\phi) = \sigma (1 - \phi \cot(\beta_{2b})) \quad (3.6)$$

where  $\sigma$  is the *Stanitz slip factor*. The slip factor is dependent on the number of blades on the impeller and is incorporated into the energy transfer since the gas flow is in reality not perfectly aligned with the angle of the blades ( $\beta_{2b}$ ) [64]. The slip factor is defined as  $\sigma = 1 - \frac{2}{n}$  where  $n$  is the number of blades. The flow coefficient  $\phi$  is determined from the relationship of the radial gas flow to the tangential blade tip velocity in

$$\phi = \frac{C_{r2}}{U_2} = \frac{\frac{w}{\rho A}}{r_2 \omega} = \frac{w}{\rho_1 A r_2 \omega} \quad (3.7)$$

where  $\rho_1$  is the gas density,  $A$  is the compressor reference outlet area and  $r_2$  is the exducer radius. For backward curved blades the fixed blade angle  $\beta_{2b}$  is less than  $90^\circ$ .

Inserting (3.5) into the compressor torque in (3.4) and applying the assumption of an inlet gas tangential velocity  $C_{\theta 1} = 0$  (no pre-whirl of the gas flow at impeller entry) yields

$$\tau_c = w r_2 \mu(\phi) U_2 \quad (3.8)$$

Inserting (3.8) into (3.3) and using  $U_2 = \omega r_2$  gives

$$\Delta h_{02} = r_2^2 \omega^2 \mu(\phi) \quad (3.9)$$

where  $\mu(\phi)$  is given by (3.6) and (3.7). The increase in specific stagnation enthalpy is given by (3.9). Furthermore, the enthalpy sum in (3.2) also incorporate the losses. According to [40] and [17] the two important losses to consider in the centrifugal compressor model design is the friction and incidence losses. These were presented in 2 from Section 2.4.2. However, the losses are limited to the impeller region of the compressor according the derivation by [40].

#### 3.2.1 Impeller losses

The incidence loss origins from the mismatch in gas entry angle to the inducer blade [17]. The inducer velocity triangle can be drawn as shown in Figure 3.6.

The incidence angle is defined as  $\beta_i = \beta_{1b} - \beta_1$ . It is associated with a kinetic energy reduction of the gas with the lost tangential velocity  $W_{\theta 1}$ . This velocity is the result of

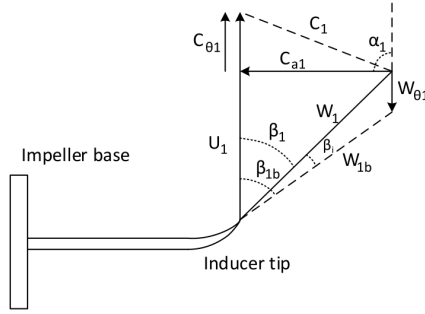


Figure 3.6: Inducer tip velocity triangle [23]

reducing the gas relative velocity  $W_1$  to  $W_{1b}$ . From the derivation in [40], the incidence loss is described in terms of the change in specific enthalpy according to the NASA shock loss theory model. The fixed blade, with an angle  $\beta_{1b}$ , changes the relative inlet gas flow velocity to  $W_{1b}$ . This will generate the vector  $W_{\theta 1}$  [17]. The specific enthalpy of the incidence loss is given as

$$\Delta h_i = \frac{1}{2} W_{\theta 1}^2 \quad (3.10)$$

From the velocity triangle at the inducer tip, the lost velocity component due to gas flow mismatch (with  $C_{\theta 1} = 0$ ) is given as

$$W_{\theta 1} = U_1 - \cot(\beta_{1b}) C_{a1} \quad (3.11)$$

Inserting (3.11) into (3.10) and using the continuity relation  $C_{a1} = w / \rho_1 A_1$ , then the incidence loss is derived as

$$\Delta h_i = \frac{1}{2} \left( U_1 - C_{\theta 1} - \cot(\beta_{1b}) \frac{w}{\rho_1 A_1} \right)^2 \quad (3.12)$$

where  $\rho_1$  is the density of the gas at the blade inlet,  $A_1$  is the inlet area and  $w$  is the inlet mass flow. Extracting the inlet radius  $r_1$ , the final expression for the incidence loss can be derived as

$$\Delta h_i = \frac{r_1^2}{2} (\omega - \alpha w)^2 \quad (3.13)$$

where  $\alpha = \cot(\beta_{1b}) \frac{1}{A_1 r_1 \rho_1}$  and  $U_1 = r_1 \omega$ . The incidence loss  $\Delta h_i$  is given by the inducer blade geometry giving rise to the loss at off-design conditions in the compressor inlet. The design goal will then be to optimize  $\beta_{1b}$  to minimize the sum  $\omega - \alpha w$ .

The gas flow through an impeller blade passage will be influenced by the friction towards the surface of the blades. To model the friction loss occurring in the impeller, a common approach is use the well established turbulent pipe flow model [27]. According to [40], the friction loss in a blade passage can be derived as

### 3. Determining compressor characteristics

---

$$\Delta h_f = C_h \frac{l W_{1b}^2}{2D} \quad (3.14)$$

where  $\Delta h_f$  is the specific enthalpy for friction loss,  $C_h$  is the surface friction loss coefficient,  $l$  is the mean channel length,  $D$  is the mean hydraulic diameter and  $W_{1b}$  is the relative velocity of the gas flow to the fixed blade angle  $\beta_{1b}$  at impeller inlet. This is the velocity the gas is assumed to have in the blade passage.

Since an impeller blade passage (for actual image see Figure 3.2) is not a straight pipeline with constant area, the mean is taken along the blade passage. The diameter  $D$  is measured perpendicular to the blade edge and averaged along the passage. The length  $l$  is also estimated through the impeller blade passage.

In an impeller, several factors increases the friction loss. According to [109], it is difficult to separate these factors experimentally and therefore the friction loss contributions are commonly grouped in an overall surface friction loss coefficient  $C_h$ . This approach is used by [40], where  $C_h = 4f$  and  $f$  is the friction factor dependent on the Reynolds number of the gas flow. In literature (see for example [49]), numerous friction factor relations has been defined, depending on the Reynolds number for the flow. This quantity is defined as

$$Re = \frac{\rho \bar{C} D}{\mu} \quad (3.15)$$

where  $\rho$  is the gas density,  $\bar{C}$  is the mean gas velocity,  $D$  is the mean hydraulic diameter for the gas flow and  $\mu$  is the viscosity of the gas. According to [70], the flow is commonly turbulent in compressor applications. This is due to the gas being accelerated in the pipelines and laminar flow may only occur along the blade edges on the impeller.

The *Blasius* relation is used for the friction factor  $f$  in [40]. This relation is valid for Reynolds numbers  $4000 < Re < 80000$  [49]. The factor is defined as

$$f = \frac{0.3164}{Re^{0.25}} \quad (3.16)$$

where 0.3164 and 0.25 are empirically determined through experiments. However, the exact measurement and estimation of the hydraulic diameter and length for the gas flow in the impeller blade passage channel can be ambiguous. In this work to establish the parameters for the GT2252 impeller, an estimate is done by measurements. The compressor axial inlet mass flow is defined as

$$w = \rho_1 A_1 C_{a1} = \rho_1 A_1 \sin(\beta_{1b}) W_{1b} \quad (3.17)$$

where  $\rho_1$  is the gas inlet density and  $A_1$  is the inlet area. Solving for the relative gas velocity  $W_{1b}$  and inserting the result into (3.14) it gives

$$\Delta h_f = \frac{C_h l}{2D \rho_1^2 A_1^2 \sin(\beta_{1b})} w^2 \quad (3.18)$$

where  $\beta_{1b}$  is the fixed inducer blade angle. All the constant parameters is drawn to a friction coefficient  $k_f$  altering (3.18) as

$$\Delta h_f = k_f w^2 \quad (3.19)$$

### 3.2.2 Resulting characteristic function

The result from Section 3.2.1 are part of the total stagnation enthalpy increase from (3.2). The energy transfer is the change in enthalpy from inlet to outlet, derived as the total change in specific stagnation enthalpy  $\Delta h_{02s}$ . This is the unknown quantity and is drawn from (3.2) as

$$\Delta h_{02s} = \Delta h_{02} - \Delta h_i - \Delta h_f \quad (3.20)$$

where  $\Delta h_{02}$  is the actual energy increase in enthalpy from Section 3.2,  $\Delta h_i$  is the incidence loss and  $\Delta h_f$  is the modelled friction loss in the impeller blade passage. The pressure ratio from (3.1) is calculated from the temperature ratio from inlet to discharge in the compressor. According to [23], the pressure ratio can be represented by the compressor enthalpy. The isentropic compression process from state 01 to 02s in the hs-diagram from Figure 3.4 is derived as

$$\frac{p_{02}}{p_{01}} = \left( \frac{h_{02s}}{h_{01}} \right)^{\frac{\kappa}{\kappa-1}} \quad (3.21)$$

where  $h_{02s}$  is the specific enthalpy of the gas at discharge of the impeller and  $h_{01}$  is the initial specific enthalpy. The enthalpy at stage 02s is, according to Figure 3.4  $h_{02s} = \Delta h_{02s} + h_{01}$ . Inserting this into (3.21) gives

$$\frac{p_{02}}{p_{01}} = \left( \frac{\Delta h_{02s} + h_{01}}{h_{01}} \right)^{\frac{\kappa}{\kappa-1}} \quad (3.22)$$

and defining the specific enthalpy  $h_{01} = c_p T_{01}$  the pressure ratio is derived as

$$\frac{p_{02}}{p_{01}} = \left( 1 + \frac{\Delta h_{02s}}{c_p T_{01}} \right)^{\frac{\kappa}{\kappa-1}} \quad (3.23)$$

where  $c_p$  is the heat capacity at constant pressure and  $T_{01}$  is the inlet stagnation temperature. Using the derived expression for the total change in stagnation enthalpy from (3.20) gives

$$\frac{p_{02}}{p_{01}} = \left( 1 + \frac{\Delta h_{02} - \Delta h_i - \Delta h_f}{c_p T_{01}} \right)^{\frac{\kappa}{\kappa-1}} \quad (3.24)$$

and inserting for each of the specific enthalpy quantities gives the resulting pressure ratio

$$\frac{p_{02}}{p_{01}} = \underbrace{\left( 1 + \frac{r_2^2 \omega^2 \mu(\phi) - \frac{r_1^2}{2} (\omega - \alpha \omega)^2 - k_f \omega^2}{c_p T_{01}} \right)^{\frac{\kappa}{\kappa-1}}}_{= \Psi_c(w, \omega)} \quad (3.25)$$

The right hand side of (3.25) is defined as the first principle compressor characteristic  $\Psi_c$  and represents the pressure increase from inlet to discharge. The resulting momentum balance for the duct in (2.11) is used with  $\Psi_c$  from (3.25).

### 3. Determining compressor characteristics

#### 3.2.3 Discussion of the first principle characteristic

The characteristic represents the numerical result of one of the compressor map characteristic curves. Therefore, it is necessary to validate how good the theoretical approximation is compared to the data. This is done in MATLAB, with the process parameters assumed to be in the WGC laboratory at operational conditions and the GT2252 internal parameters. The parameters governing the equations shown in the previous sections are summarised in Table 3.2.

Table 3.2: Numerical values for the characteristic parameters

Parameters	Value
rpm, rotational speed	75000
$A_1$ , inlet area	$2.83 \cdot 10^{-3} \text{ m}^2$
$n$ , number of blades	12
$r_1$ , inducer hub-tip radius	$20.1 \cdot 10^{-3} \text{ m}$
$r_2$ , exducer hub-tip radius	$52.0 \cdot 10^{-3} \text{ m}$
$\beta_{1b}$ , inducer blade angle	$21.4^\circ$
$\beta_{2b}$ , exducer exit blade angle,	$54.1^\circ$
$c_p$ , specific heat constant pressure	$1004.6 \text{ J kg}^{-1} \text{ K}^{-1}$
$\kappa$ , ratio of specific heats	1.4
$\rho_1$ , gas density at inlet ( $20^\circ\text{C}$ )	$1.205 \text{ kg m}^{-3}$
$f$ , friction factor ( $\text{Re} = 80\,000$ )	0.0188
$C_h$ , surface friction loss coeff.	0.0753
$D$ , mean hydraulic diameter	$3.75 \cdot 10^{-3} \text{ m}$
$l$ , mean channel length	0.04 m

The total change in stagnation enthalpy  $\Delta h_{02s}$  and the ideal energy transfer  $\Delta h_{02}$  is plotted versus the mass flow in Figure 3.7. Seen from the figure, the total change in stagnation enthalpy decreases around  $w = 0.1$  since the losses increases in the compressor.

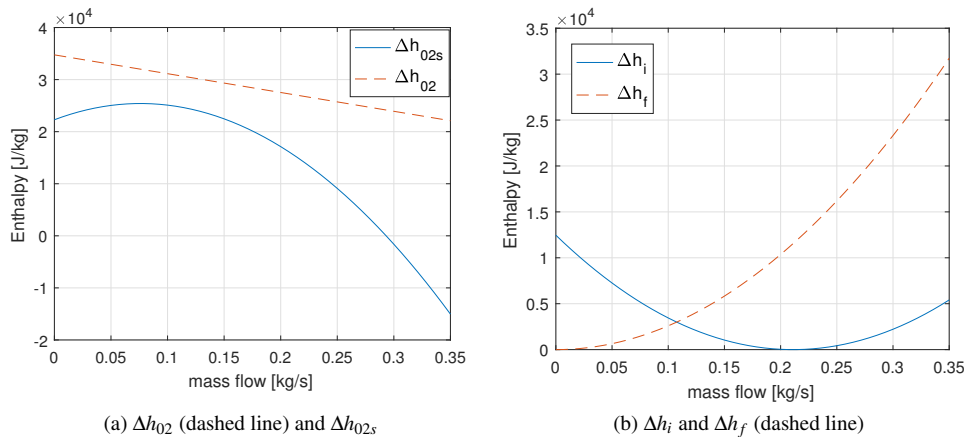


Figure 3.7: Stagnation enthalpies for first principle characteristic



The resulting characteristic curve at a constant speed of 75000 rpm is seen in Figure 3.8. The curve flats out after  $w \approx 0.28$  for the numerical value of  $\Psi_c$ . The function is not valid for this area, where the sum between the brackets in (3.25) is negative (there exist no imaginary pressure ratio). Seen from the plot of  $\Delta h_{02s}$ , the value is negative after  $w \approx 0.28$  since the incidence and friction loss has become larger than the ideal enthalpy increase  $\Delta h_{02}$ .

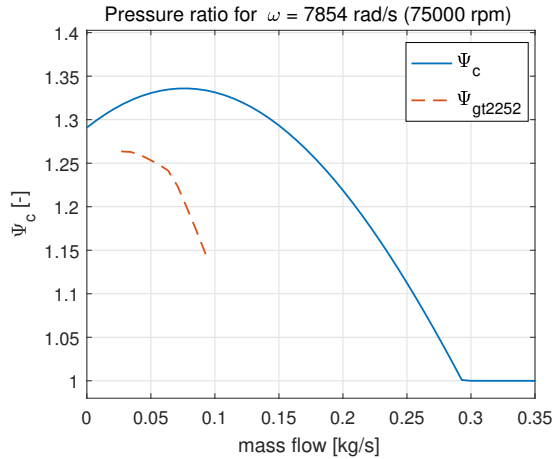


Figure 3.8: First principle characteristic with 75000 rpm and corresponding GT2252 curve

The next step is to compare the curve in Figure 3.8 to the compressor map in Figure 3.3 for the 75000 rpm line. The map characteristic curve is shown from approximately 3.5 to 12.3  $\text{lbmin}^{-1}$ , which is approximately 0.026 to 0.093  $\text{kg s}^{-1}$  with the maximum  $\Psi_c \approx 1.26$ . In the curve for the first principle function with the GT2252 parameters,  $\Psi_c$  generates a larger pressure ratio. The reason for this may be that the parameters in Table 3.2 for the process flow in this numerical example are different from the process conditions when generating the GT2252 map. However, this will be the topic in Section 3.2.5 where the parameters from Table 3.2 will be related to the required parameters to fit this first principle curve to the actual characteristic lines in GT2252 compressor map.

### 3.2.4 Zero and negative mass flow region of the map

The region towards zero and negative mass flow in the compressor map is usually not defined by the data sheet delivered for the specific compressor. This region does imply unstable operation of the machinery and is most likely not interesting for the consumer since it is part of the efficient operation area. However, for simulation purposes and active control of processes with compressors, estimating this area may be favourable to predict the behaviour and design efficient algorithms to avoid instabilities.

The method of estimating the negative flow region might in most cases only produce an approximate result of the compressor operation. An experiment with negative (reversed) compressor gas flow was done by [56]. To estimate the branch of the curve not found in the map, gas (dry air) were fed into the discharge nozzle of the compressor and driven towards the inlet. The measured data were fit to a parabolic curve.

### 3. Determining compressor characteristics

---

Due to a non-operative WGC laboratory at this stage of the thesis work, the practical approach of determining the zero and negative flow branch is unavailable. However, the approach of using the first principle characteristic is preferable for an initial estimate. The estimate will be compared when testing the laboratory turbocharger. This section will first show the derivation of the zero mass flow from the first principle characteristic and then the approximated negative branch of the curve.

The compressor discharge pressure delivered is dependent on the system load (also referred to as system resistance) imposed downstream of compressor. This load is a combination of the piping, valves and equipment in the system [9].

#### Deriving the zero mass flow characteristic

The derivation presented in this section is drawn from [23, Ch. 13], and the article in [42]. According to [42], the compressor produces a pressure increase when the gas is brought to rest in the impeller and internal chambers. This is due to the centrifugal forces acted upon the gas by the impeller. At rest, the condition is referred to as zero mass flow. However, it is important to know what pressure conditions occurs at zero mass flow as the state quantities are in stagnation condition since the gas is not flowing [64]. When the gas is slowed down isentropically, the stagnation states for enthalpy,  $h_{0i}$  and pressure  $p_{0i}$  changes. To derive the zero-mass flow pressure ratio, [42] utilise the first principle characteristic. The total change stagnation enthalpy  $\Delta h_{02s}$  for the gas at the outlet of the impeller is given by the isentropic increase in stagnation enthalpy and the isobaric modelled losses in the compressor. The rest of the derivation follows the assumption of isentropic gas conditions. The compressor torque in (3.4) is altered with  $r = U\omega$  given as

$$\tau_c \omega = w(U_2 C_{\theta 2} - U_1 C_{\theta 1}) \quad (3.26)$$

where  $U_2$  is the radial velocity of the impeller outlet,  $U_1$  is the radial velocity of the impeller inlet (inducer),  $C_{\theta 1}$  and  $C_{\theta 2}$  is the gas flow tangential velocity at impeller inlet and outlet (see for reference Figure 3.5 and 3.6). The ideal energy transfer in (3.3) can be derived with (3.26) as

$$\Delta h_{02} = (U_2 C_{\theta 2} - U_1 C_{\theta 1}) \quad (3.27)$$

The result in (3.27) shows that the increase in stagnation enthalpy is independent on the mass flow. An assumption to the zero-mass flow is that these losses are neglected with  $w = 0$ . As the mass flow is slowed down to zero, the tangential velocity can be assumed equal to the tangential velocity of the impeller blade,  $C_{\theta 1} = U_1$  and  $C_{\theta 2} = U_2$ . Then, (3.27) is derived as

$$\Delta h_{02} = (U_2^2 - U_1^2) \quad (3.28)$$

and with  $U = \omega r$  the stagnation enthalpy increase is

$$\Delta h_{02} = ((\omega r_2)^2 - (\omega r_1)^2) \quad (3.29)$$

where  $r_1$  is the inducer radius and  $r_2$  is the outer radius of the impeller. With no losses and inserting (3.29) into the pressure ratio from (3.24), the zero mass flow characteristic is derived as

$$\Psi_c(0, N) = \left( 1 + \frac{\omega^2(r_2^2 - r_1^2)}{c_p T_{01}} \right)^{\frac{\kappa}{\kappa - 1}} \quad (3.30)$$

To relate the speed and geometric quantities to the compressor chart, the conversion of (3.30) represented by the impeller diameter at inducer and outlet together with speed in rpm is appropriate. With  $\omega = \frac{N2\pi}{60}$  to convert<sup>1</sup> the angular velocity in  $\text{rad s}^{-1}$  to rpm, the compressor characteristic at zero-mass flow is derived as

$$\Psi_c(0, N) = \left( 1 + \frac{N^2 \pi^2 (D_2^2 - D_1^2)}{60^2 c_p T_{01}} \right)^{\frac{\kappa}{\kappa - 1}} \quad (3.31)$$

where  $N$  is the rotational speed in revolutions per minute,  $D_1$  is the inducer diameter and  $D_2$  is the outer diameter of the impeller,  $c_p$  is the specific heat in  $\text{J kg}^{-1} \text{K}^{-1}$  and  $T_{01}$  is the inlet temperature. The final result in (3.31) is valid under the assumption of isentropic pressure ratio over the compressor and steady adiabatic flow, as it builds on the *Euler work equation* in (3.27). The calculated zero-mass flow points is included in Appendix A, Table A.3.

The negative flow portion of the map is estimated by one point for each speed line. To avoid intersection of each individual speed line at the negative map area, the distance between the two points are chosen with equal spacing. This is done according to the procedure in [23, Ch. 13].

### 3.2.5 Map curve fit of the first principle characteristic

To be able to compare the validity in simulation of both the first principle characteristic and an empirical characteristic, the first principle needs to be curve fitted to the GT2252 compressor map. The first step is to develop a function in MATLAB from (3.25). This function will be evaluated by the non-linear Least Squares (LSQ) procedure in MATLAB, `lsqcurvefit`. The procedure evaluates a user defined function, finding the optimal parameters in the function to represent the best fit to the data [72]. The objective function to minimise in order to obtain the function parameters, is the quadratic problem defined as

$$x_{\min} = \sum (f(\theta, x_d) - y_d)^2 \quad (3.32)$$

where  $\theta$  is the parameters in the first principle function being curve fitted,  $x_d$  is the data set with mass flow and rpm values and  $y_d$  is the corresponding pressure ratios from the map. The parameters such as the impeller inducer and outer radius  $r_1$  and  $r_2$  and the process conditions  $c_p$  and  $T_{01}$ , is known. However, the products such as  $c_p T_{01}$  can not be distinguished as separated variable by MATLAB. Merging parameters in the function defined by products it will allow LSQ curve fit more freedom in determining the best fit.

<sup>1</sup>In the derivation by [23], the conversion from  $\text{rad s}^{-1}$  to rpm is done with  $N = 2\pi\omega$ . However, it results in wrong units ( $\frac{\text{rad}^2}{\text{s rev}}$ ) and will give an incorrect value for the pressure ratio.

### 3. Determining compressor characteristics

---

Using LSQ curve fit, all the data for the individual speed lines are merged forming a data vector to use as input to the MATLAB function. A short part of the total script is shown in pseudocode in Algorithm 1.

---

#### Algorithm 1 Pseudocode for lsqcurvefit of $\Psi_c$

---

```

1: procedure FIRSTPRINCIPLECURVEFIT(xdata, ydata, bounds, init)
2:    $l_b = \text{bounds}(1)$  ▷ Set lower bounds for LSQ fit
3:    $u_b = \text{bounds}(2)$  ▷ Set upper bounds for LSQ fit
4:   ▷ xdata - [mass flow data, rpm data]
5:   ▷ ydata - [pressure ratio data]
6:    $x_0 = \text{init}$  ▷ init - Initial guess vector for first iteration
Ensure: LSQoptions= true ▷ Set LSQ algorithm and tolerances
Require: Trust Region Reflective algorithm if bounds  $\neq 0$ 
7:   function LSQCURVEFIT( $\Psi_c(\cdot)$ ,  $x_0$ , [xdata ydata],  $l_b$ ,  $u_b$ )
8:     while Convergence $\neq$ true do ▷ Stop algorithm when LSQ converge
9:       Produce fit with initial coefficients  $x_0$ 
10:      Adjust  $x_n$  and evaluate new fit
11:      Continue to step 10, until convergence limit is met
12:     end while
13:     return  $x_n$  ▷ The optimal  $\Psi_c$  parameters are returned in  $x_n$ 
14:   end function
15: end procedure

```

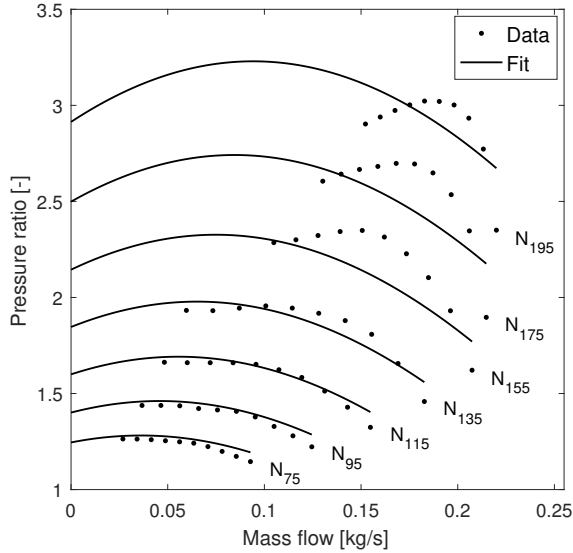
---

The result for evaluating the first principle characteristic function with constraints on the  $\Psi_c$  parameters is shown in Table 3.3. The parameters can be recognised from (3.25). The initial guess vector  $x_0$  holds the parameter products which have been estimated with the values from Table 3.2 in Section 3.2.

Table 3.3: MATLAB LSQ curve fit parameters

Parameters	$x_0$	$x_n$
$\sigma r_2^2$	0.00054	0.00038
$\cot(\beta_{2b})/\rho_1 A_1 r_2$	8200	9100
$r_1^2/2$	0.0002	0.00025
$\alpha$	37000	19000
$k_f$	$2.5 \cdot 10^5$	$6.4 \cdot 10^5$
$1/c_p T_{01}$	$3.5 \cdot 10^{-6}$	$2.5 \cdot 10^{-5}$
$\kappa/(\kappa - 1)$	3.5	1.4

The optimised parameters  $x_n$ , giving the local minimum for (3.32) is not exceeding the lower and upper bounds, but can be seen to deviated from the initial. The value for  $\kappa$  is approximately 1.4 for air at 20°C. Evaluating the result  $\kappa/(\kappa - 1) = 1.4$  gives  $\kappa = 3.5$ . The same yields for the geometric turbocharger parameters. However, this is the best fit, with the optimised parameters given by lsqcurvefit. The resulting function psiC developed in MATLAB is presented with the data from the original map in Figure 3.9.


 Figure 3.9: Result from optimal  $x_n$  with first principle function  $\text{psiC}$ 

The estimated negative data point series is excluded, since the function would not comply with a 3rd degree polynomial curve making the fit difficult. However, according to [40], the negative region of the curve can be estimated by assuming a symmetrical pressure ratio in mass flow. This is shown as  $\Psi_c(w, \omega) = \Psi_c(-w, \omega)$  giving the same maximum for  $\Psi_{c,max}(w) = \Psi_{c,max}(-w)$ . This curve resembles the pressure increase achieved in the compressor due to instability of surge and rotating stall.

The error from the achieved fit can be calculated in terms of the mean absolute error of the function value to the actual pressure ratio from the data set. The error is given by

$$e = \frac{1}{M} \sum_{i=1}^M |f(w) - y_d| \quad (3.33)$$

where  $M$  is the length of the data vector for the chosen rpm line,  $f(w)$  is the estimated function value from the curve fit and  $y_d$  is the corresponding pressure ratio point on the compressor map. For the constant speed lines, the error is calculated at the first data-point of the sampled data to the end. The result is presented in Table 3.4.

 Table 3.4: Fit error using `lsqcurvefit` in MATLAB on  $\Psi_c$ 

rpm	$e$
75000	0.0268
95000	0.0278
115000	0.0250
135000	0.0503
155000	0.1324
175000	0.1565
195000	0.1270

## 3.3 Empirically determined characteristic

The empirical method of determining the compressor characteristic curve departs from the approach in Section 3.2 by relying on known data points from the actual compressor performance map. The actual compressor is the one intended to be used, or the machine that has already been performed test and experiments on. The data used to determine the empirical characteristic compressor function needs to be collected from a data-sheet for the specific compressor. A curve fit approach to describe the properties of the characteristic curves on a data sheet is used. The fit is then based on a function (polynomial, spline etc.) which better fits the data points.

### 3.3.1 Curve fitting the compressor speed lines

The first stage in building the polynomial for each speed line is to approximate each individual speed line with a function. The function can be for example linear, 2nd or 3rd degree. In literature, the 3rd degree polynomials are commonly used to represent the characteristic curve (see for example [42, 44, 56]). However, this is the general approach and must be discussed in regards to what properties the researcher want to predict from the compressor map. This can be either the operational accuracy, where performance margins are not exceeded (maximum pressure ratio and mass flow) or to achieve the best fit towards the surge line aiding the accuracy of predicting instabilities. The latter will also give a better accuracy when establishing active surge control for the model.

To establish a 3rd degree polynomial, the MATLAB function `polyfit` can be used. The fit is obtained by least-squares calculation and requires the x and y-axis data along with the chosen degree. The limitation is that the data vector for the x-axis is constrained to a single vector with mass flow data. An excerpt of the pseudocode to establish the characteristic curves is shown in Algorithm 2.

---

**Algorithm 2** Pseudocode for `polyfit` of pressure ratio with mass flow data

---

```
1: procedure EMPIRICALFIT(xdata, ydata)
2:   num = 7                                ▷ Number of compressor speed lines
3:   deg = 3                                ▷ Set polynomial degree for curve fit
4:   for i=num do
5:     x(:,i) = xdata(:,i)                  ▷ Set mass flow data for specific rpm interval
6:     y(:,i) = ydata(:,i)                  ▷ Set corresponding pressure ratio data
7:     p(:,i) = polyFitCreate([x(:,i), y(:,i)], deg);    ▷ Call function script
8:   end for
9:   function POLYFITCREATE([x(:,i), y(:,i)], deg)
10:    Obtain the selected polynomial degree
11:    Define the data set x and y vector
12:    Run MATLAB function polyfit and polyval
13:    Obtain the best least squares fit for the speed line coefficients
14:    return coefficients for  $p$ , evaluated function values and error
15:   end function
16: end procedure
```

---

The MATLAB function `polyval` evaluates the polynomial with coefficients obtained from `polyfit`. The error fit can be found by evaluating the polynomial for each corresponding data point of mass flow. A selective comparison around the maximum pressure ratio for the 155000 rpm line is chosen to illustrate the deviation from 1st to 3rd and 4th degree. This error is calculated with the same procedure as in Section 3.2.5. The result is presented in Table 3.5. This is in the region of  $0.12 - 0.21 \text{ kg s}^{-1}$ .

Table 3.5: Comparing the accuracy of curve fit for different polynomials

	Polynomial degree		
	1st	3rd	4th
$e$	0.1504	0.0456	0.0100

The error shows that the characteristic curve of a compressor is better suitable fit for a 3rd degree function, or a polynomial of higher degree than three.

The intermediate result of using `polyfit` to establish the pressure ratio function with dependency to mass flow rate, is shown in Figure 3.10a. The optimised fit is shown in Figure 3.10b. Each polynomial is then representing an individual speed line from 75000 to 195000 rpm with a 20000 rpm interval.

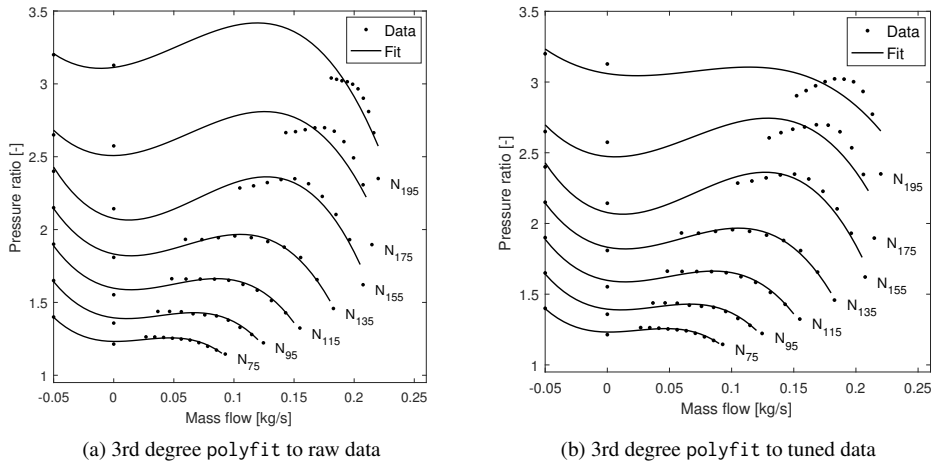


Figure 3.10: MATLAB polyfit curve fitting for characteristic lines

The curve for 195000 rpm in Figure 3.10a overshoots by approximately 0.5 in pressure ratio. This is due to the limited number of data points which `polyfit` adjusts the curve to. It gives an unrealistic view of how the compressor performance is, since it is exceeding the maximum pressure ratio for this characteristic curve. For the 175000 and 195000 rpm curves, 4 additional interpolated data points are added to force the curve fit not to over estimate the pressure ratio for the compressor.

### 3. Determining compressor characteristics

---

The tuned characteristic lines used for further research is shown in Figure 3.10b. The third degree polynomial is given by

$$\Psi_{\text{emp}} = p(4) + p(3)w + p(2)w^2 + p(1)w^3 \quad (3.34)$$

where  $\Psi_{\text{emp}}$  is the empirical pressure ratio vector,  $p(i)$  is the vector of coefficients produced by Polyfit in MATLAB and  $w$  is the mass flow variable. The coefficient vectors is given as

$$p(4) = \begin{bmatrix} 1.2 \\ 1.4 \\ 1.6 \\ 1.8 \\ 2.1 \\ 2.5 \\ 3.1 \end{bmatrix}, p(3) = (-1) \cdot \begin{bmatrix} 0.12 \\ 1.0 \\ 1.6 \\ 1.8 \\ 1.9 \\ 0.73 \\ 1.3 \end{bmatrix}, p(2) = \begin{bmatrix} 38.0 \\ 55.0 \\ 64.0 \\ 70.0 \\ 83.0 \\ 60.0 \\ 34.0 \end{bmatrix}, p(1) = (-1) \cdot \begin{bmatrix} 522.0 \\ 477.0 \\ 433.0 \\ 399.0 \\ 400.0 \\ 300.0 \\ 177.0 \end{bmatrix} \quad (3.35)$$

The resulting speed lines determined by polyfit has  $w$  as dependent variable to give the pressure ratio  $\Psi_{\text{emp}}$ . This is however only for a given speed. Furthermore, the pressure ratio is determined by both mass flow and speed which is the next step to interpolate in the vertical direction on the map.

#### 3.3.2 Resulting empirical pressure ratio function

Based on the result in the previous section, the next step is to be able to represent the pressure ratio as a function of both rotational speed,  $N$  and the corresponding mass flow. A common approach is to connect the output for both y-axis values and x-axis values, resulting in a connection of two polynomials. In [42], the 3rd degree polynomial used to evaluate the compressor characteristic is determined by

$$\Psi_{\text{emp}}(w, N) = c_0(N) + c_1(N)w + c_2(N)w^2 + c_3(N)w^3 \quad (3.36)$$

where  $\Psi_{\text{emp}}$  is the compressor characteristic given by the mass flow  $w$  and the rotational speed  $N$  in rpm. The coefficients  $c_i$  is determined by the polynomial evaluation of each curve, with increasing rotational speed. Furthermore, these coefficients are continuous in rpm, determined by

$$c_i(N) = c_{i0} + c_{i1}N + c_{i2}N^2 + c_{i3}N^3 \quad (3.37)$$

where  $N$  is the rpm variable. The expression in (3.37) is the interconnection between each characteristic curve in the vertical direction, allowing a prediction of the pressure ratio in between each of the GT2252 map constant speed lines. The data, determining  $c_i$  in (3.37) is given by the polynomial speed line coefficients,  $p(i)$  in (3.35) from Section 3.3.1. The code snippet that stacks the vectors from (3.35) and again calls polyfit to determine the speed dependent coefficients is presented in Algorithm 3.



**Algorithm 3** Pseudocode for continued curve fit of coefficients  $c_i$  with rpm data

```

1: procedure EMPIRICALCOEFFICIENTFIT( $p_{1-4}$ )      ▷ Input polynomial fit coefficients
2:   deg = 3                                       ▷ Set polynomial degree for curve fit
3:   for j=4 do                                  ▷ 4 speed coefficients
4:     ndata = zeros vector with 4 columns
5:     ndata(j) = [75, 95, ..., 195]·103      ▷ Set ndata vector row with rpm data
6:   end for
7:   for i=4 do
8:      $x(:, i) = \text{ndata}(:, i)$                   ▷ Set rpm data for
9:      $y(:, i) = p(:, i)$                         ▷ Set corresponding speed line coefficient data
10:     $C(:, i) = \text{polyFitCreate}([x(:, i), p(:, i)], \text{deg});$   ▷ Call function script
11:  end for
12:  function POLYFITCREATE( $[x(:, i), p(:, i)], \text{deg}$ )
13:    Obtain the selected polynomial degree
14:    Define the data set x and y vector
15:    Run MATLAB function polyfit and polyval
16:    Obtain the best least squares fit for the rpm coefficients
17:    return coefficients for C, evaluated function values, error
18:  end function
19: end procedure

```

Each coefficient in (3.36), continuous in rotational speed, is shown in Figure 3.11 along with the 3rd degree polyfit result.

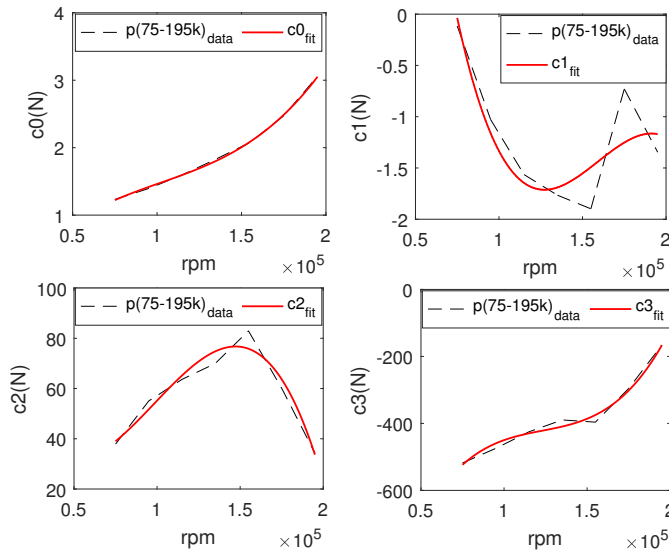


Figure 3.11: 3rd degree polynomial curve fit of coefficients. The coefficient curve fit is the solid lines, and the dotted lines originates from the produced coefficient values in (3.35)

### 3. Determining compressor characteristics

---

The coefficients obtained in Algorithm 3 are saved to a ".mat" in MATLAB being initialized in the simulation file. The parameters are used to connect the two functions in (3.36) and (3.37). Both are implemented in the resulting empirical MATLAB function `empiricalPsi`.

The mean absolute error is calculated for the final empirical function from (3.33). The result is presented in Table 3.6. The 3rd degree fit, without using a predefined function is seen from the error to present a better fit.

Table 3.6: Fit error for the empirical characteristic function

rpm	$e$
75000	0.0084
95000	0.0103
115000	0.0151
135000	0.0237
155000	0.0518
175000	0.1037
195000	0.1181

### 3.4 Comparison of characteristics

The resulting compressor characteristic functions  $\psi_{cI}$  and  $\text{empiricalPsi}$  are plotted together in Figure 3.12 to compare the outcome of curve fitting. Furthermore, the compressor mass flow limitation in the process, maximum rotational speed and the compressors rated minimum and maximum pressure increase must be included when using the function in simulation. This is to be as accurate as possible when predicting the performance. Too high rotational speed may in reality cause mechanical damage to the equipment [27].

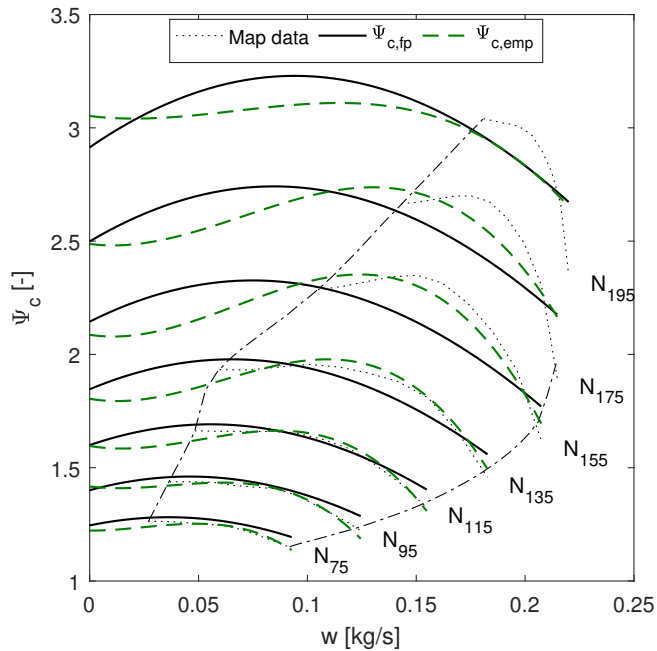


Figure 3.12: Approximated first principle and empirical characteristic to map data

As seen in the plot and comparing the error from Table 3.4 and 3.6 for the 155000 rpm line, the most accurate in the compressor map region is the empirical characteristic. However, as mentioned previously, the accuracy of the fit also depends on what phenomena the researcher decides to model.

The best fit for both functions is in the optimal region of the map, in the area of 100 to 155 thousand rpm. The first principle function parameters is optimised with a lower and upper bound, to not evaluate it with "unreal" values. However, the bounds are approximate, due to the uncertainty when determining parameters such as mean hydraulic diameter of the impeller blade passage  $D_h$  in the function. Since this is the area of operation which is wanted, the curve fit from Section 3.2 can also be considered a good estimate for the continued work.



# Chapter 4

## Compressor model simulation and control

This chapter presents the implementation of the compressor characteristic functions, simulation of the models and extension towards effective control algorithms. The material produced in this chapter, including MATLAB Simulink models and program scripts to run the simulation are included in electronic appendix file for this thesis.

### 4.1 Chapter introduction and purpose

The purpose of using the characteristic functions from Chapter 3 is to be able to predict the behaviour of the compressor system. The systems must be simulated with throttle adjustments to simulate a change in the back pressure of the system, to initiate surge and verify the response.

The Gretizer and the centrifugal model are purposely developed to predict compressor behaviour in surge, occurring for various tested system conditions (plenum volume size, throttle adjustments). The development of effective control algorithms for active surge control is a wide research field in the academic sector. According to the review in [110], the linear proportional feedback is extensively used to prove active surge control of compressors. For example, active surge control using downstream throttle valve as the actuator with proportional feedback control was performed by [85]. In [40], the centrifugal compressor model were included in series with a valve upstream of the plenum section. The valve pressure drop were used to control the compressor at the left of the surge line altering the compressor characteristic. The surge control law for the valve were joined with a PI control algorithm for the compressor speed. A backstepping control law was also developed in [41] for the centrifugal model.

Since the compressor system is subject to many constraints, efficient control strategies have been developed. The previously mentioned control loops in a compressor system can be replaced Model Predictive Control algorithms (see for example [18, 99]). However, these type of algorithms are not further elaborated in this thesis.

The topics presented in this section are based on extensive research on the dynamics of surge in a compressor system. This work deviates from the surge aspect of compressor control, but will adapt some of the control algorithm approaches to construct an efficient and robust controller. The practical aspect is more weighted in this thesis, since WGC laboratory

## 4. Simulation and control

---

is the eminent place to implement the controller. The focus is directed to development of a controller capable of operating the non-linear compressor model with setpoint and load disturbance changes in the normal operating region of the GT2252 compressor map.

The further procedure is to study the impact of wet gas, analogous to what the controller can experience in the WGC laboratory. A preliminary study will be done on the simulation model. However, more specific work must be undertaken by testing in the laboratory.

### 4.2 Compressor system and parameters

The simulation model will be based on an altered setup of the turbocharger in the WGC laboratory, seen in Figure 4.1. The simulation model will be based on the open-loop configuration with inlet suction pressure close to the atmospheric pressure in the laboratory. This setup is drawn from the research done by [44] and [29], and the open-loop test rig described in [45]. The length of piping between the compressor and the manual ball-valve (addressed as the throttle valve) is the extension of the compressor plenum volume, capturing the dynamics of compressed gas and oscillations associated with surge behaviour [105].



Figure 4.1: The laboratory layout of the compressor model simulation. The turbocharger is located in the upper left corner and throttle valve in the lower right corner. The red tank in the center is the oil lubrication-loop reservoir

In the computer simulated model, the gas flow downstream of the ball-valve is out to atmospheric pressure. The inlet suction pressure is drawn from the atmospheric conditions and the discharge after throttling the gas flow is out again to atmospheric conditions. The suction pressure for a turbocharger is normally from atmospheric conditions [27]. However, a larger suction pressure is the normal operating conditions for GT2252 in the finished WGC laboratory. The proposed scenario for simulation and control is schematically presented in Figure 4.2.

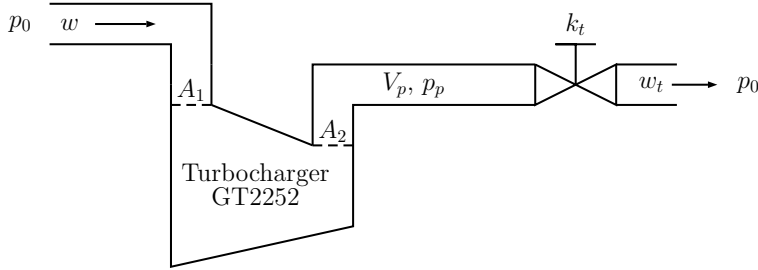


Figure 4.2: Simulation model of the compressor setup. The variables are:  $p_0$  is the atmospheric pressure,  $w$  is the compressor mass flow,  $w_t$  is the throttle mass flow,  $A_1$  and  $A_2$  are the inlet and outlet area of the compressor section,  $V_p$  is the plenum volume and  $k_t$  is the throttle valve gain

The overall measures for the compressor system are included in Table 4.1. The specific parameters for the impeller configuration are drawn from Table 3.1. The setup is used both for simulating the performance of the Greitzer model and the centrifugal model. However, the compressor characteristic used for the Greitzer model is the empirical one, drawn directly from the map for GT2252.

Table 4.1: System setup parameters

Description	Notation	Value
<b>Compressor:</b>		
Inlet area	$A_1$	0.0028 m <sup>2</sup>
Outlet area	$A_2$	0.0019 m <sup>2</sup>
Effective duct length	$L_c$	0.500m
Cross sectional flow through area	$A_c$	0.0024 m <sup>2</sup>
Plenum volume	$V_p$	0.0025 m <sup>3</sup>
<b>Throttle:</b>		
Cross sectional flow through area	$A_t$	0.002 m <sup>2</sup>
Effective length	$L_t$	0.05 m
Opening control parameter	$k_t$	variable

The approximated plenum volume of the compressor is the internal piping and the extension of piping towards the throttling valve installed downstream. This measure is estimated through the actual component discharge volute towards the outlet at the top and the dimensions of the downstream pipeline. The GT2252 discharge volute is shown in Figure 4.3, where the numerical values are taken.

## 4. Simulation and control

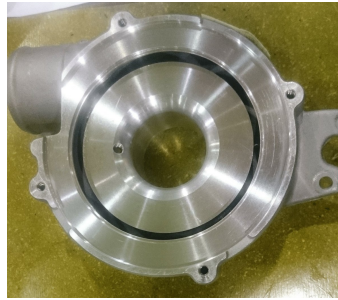


Figure 4.3: The GT2252 volute and discharge section

### 4.3 Simulation environment

The simulations are done with the MATLAB model-based simulation tool named Simulink. The state models are developed using block diagrams, with integrator blocks, mathematical tools and a set of solvers to simulate the designed dynamic system [73]. An example from the preliminary Greitzer simulation model design is shown in Figure 4.4. This model is dependent on the empirical designed characteristic from Section 3.3, implemented as a MATLAB function block incorporating script code to be run during simulation.

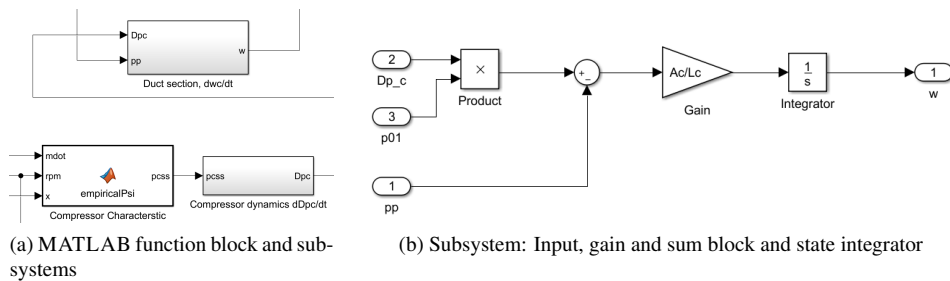


Figure 4.4: Simulink block representation with subsystems

The state equations in physical dimensions for the Greitzer and the centrifugal model were introduced in Section 2.3, and these are implemented in two different scripts. For a representative method of simulating the models, all the parameters are set in the script, allowing total control and easy saving of the specific variable values from one simulation to another.

#### 4.3.1 Choosing a suitable state solver

The accuracy of simulating the continuous state equations for each model depends on the chosen solver. In Simulink, there exist both fixed-step and variable-step size solvers for both explicit and implicit solving of the continuous states. Choosing a solver for the simulation models in this work is based on two selected criteria:

1. The sample time must be available



2. The solver must keep the error tolerances set by the user (variable-step solvers)

The first criteria leads to a fixed step solver. This is appropriate for computations such as the Integral of Absolute value of control Error (IAE), a measure of controller performance being used in this chapter. However, the downside of using a fixed step is that the computation might be slower [74]. The second criteria leads to a variable-step solver. However, since the accuracy also depends on the step size, by decreasing this, the more accurate numerical results for each state is achieved. On the basis of this discussion, a fixed-step solver will be used. Furthermore, a choice of explicit and implicit solvers must also be discussed.

To select between an explicit or implicit solver, the system dynamics must be evaluated. The linearised system eigenvalues describe the stability of the system in steady state and with input change. According to [23, Ch. 14], a large spread in the system eigenvalues gives stiff system dynamics not suitable for explicit state solvers. An implicit solver is sufficient for these systems where the solution may vary fast.

To perform an analysis of this system, MATLAB has an integrated "Linear Analysis Tool" where step and frequency response along with the system transfer function is evaluated. The transfer function is an open-loop configuration from the input to the output. For the models intended to be used here, the input is the compressor speed and the output is the plenum pressure. Since the Greitzer model is also the basis for the centrifugal model, the first one is linearized with this tool. The Input-Output (IO) configuration is shown in Figure 4.5

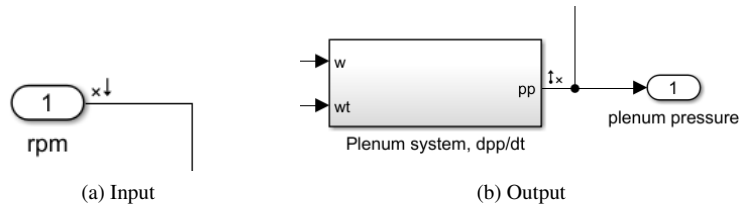


Figure 4.5: I/O of open-loop analysis

The plenum pressure state output from the Greitzer model is linearized around a stable operating point achieved after an elapsed time of 0.2 seconds. The linearized system eigenvalues are found using the built in MATLAB function  $\text{eig}(A)$ , where  $A$  is the system matrix, giving the following result

$$\lambda = \begin{pmatrix} 0.0 + j0.0 \\ -0.49 + j3.26 \\ -0.49 - j3.26 \end{pmatrix} \cdot 10^3 \quad (4.1)$$

The eigenvalues  $\lambda_2$  and  $\lambda_3$  does have negative real part, indicating stability [23], [53]. However,  $\lambda_1$  has a zero real part. The zero real part of  $\lambda_1$  indicates that the linear system is *marginally stable* and that the non-linear system will either be unstable or stable, from the definition in [23, Ch. 1, sec. 2.7], [53, Ch. 9]. The system eigenvalues has a difference with magnitude of  $10^3$  from  $\lambda_1$  to  $\lambda_2$ . This may indicate that a non-linearity with rapid varying numerical solutions might be present.

## 4. Simulation and control

---

On behalf of this analysis, the fixed-step implicit solver *ode14x* is chosen<sup>1</sup>. The time-step is found to be 0.0001 seconds representing proper accuracy of the output from the state variables. The time-step is considerably small due to the fast dynamics of the system, to make it possible to compute the state derivatives.

### 4.4 Initial conditions and process dynamics

The Greitzer model and the centrifugal model are initialised with the same process parameters. This is to be able to view each model behaviour in the light of the same process conditions, similar to the conditions in the WGC laboratory. The models are simulated with the initial parameters seen in Table 4.2. The following assumptions are made to the setup and the models:

1. The gas flow is characterised with the properties of air
2. Constant inlet temperature at 20°C in the laboratory
3. Constant inlet gas density
4. Constant sonic velocity of gas flow
5. The pressure  $p_0$  is atmospheric
6. The choke limit for the compressor is treated approximately. This assumption is drawn from [40]

Assumption 6 originates from the fact that both models do not deal with the dynamics of choke presence in the compressor. As seen from a compressor map, with reference to speed line 135000 rpm in Figure 3.3, the compressor mass flow stagnates and the pressure starts to drop at approximately at (24 lbs min<sup>-1</sup>, 1.4). To shift the operation point away from the choked flow, the compressor speed must be reduced. However, as the speed is reduced the risk of rapidly shifting the operating point into the stall and surge region is present. In this model simulation, the presence of choke flow is not dealt with due to limited time to model the dynamics. The assumptions are approximated from the actual gas, which in this case is air, located in the laboratory.

Table 4.2: Initial simulation model parameters. The asterisk marks that the specifications are taken from the work in [10]

Description	Notation	Value
Inlet gas density*	$\rho_1$	1.205 kg m <sup>-3</sup>
Specific heat capacity, constant pressure*	$c_p$	1004.6 J kg <sup>-1</sup> K <sup>-1</sup>
- , constant volume*	$c_v$	717.4 J kg <sup>-1</sup> K <sup>-1</sup>
Inlet stagnation temperature*	$T_{01}$	293.15 K
Speed of sound of gas (air) at 20°C	$a_0$	343 m s <sup>-1</sup>

---

<sup>1</sup>The model has also been tested with explicit Runge Kutta RK4 (*ode4* in MATLAB) which seems to be sufficient for a numerical solution method. However, if the step-size is altered in this method it is more likely to become unstable [23]

In the simulation model, a varying inlet pressure is applied to account for changes in the turbocharger suction pressure at the laboratory. To account for the variations, the inlet pressure is simulated with an added sinusoidal on the form

$$p_{01}(t) = p_0 + p_{\text{Amp}} \sin(\omega_i t) \quad (4.2)$$

where  $p_0$  is the constant atmospheric pressure in the laboratory,  $p_{\text{Amp}}$  is the pressure amplitude and  $\omega_i$  is the wave frequency in  $\text{rad s}^{-1}$ . The steady state behaviour is now ready to be logged. The two models will in this section be simulated with constant speed as input, with no other control. This is to capture the dynamics of the system both after an elapsed time and when a load change in the system has occurred.

##### 4.4.1 Steady state behaviour of the Greitzer model

From the model introduction in Chapter 2.3, Greitzer assumed that there existed dynamics influencing the compressor characteristic  $\Delta p_c$  [43]. The characteristic dynamics are modelled as a first-order transient response model presented in (2.7)<sup>2</sup>. The time-lag was modelled in this transient response and it is dependent by a constant, describing the number of rotor revolutions before initiating stall behaviour. The physical description of  $t_c$  is given as

$$t_c = \frac{2\pi N_s R_s}{U} \quad (4.3)$$

where  $N_s$  is the number of rotor revolutions until a full rotating stall cell pattern has developed [43],  $R_s$  is the mean rotor radius and  $U$  is the mean rotor velocity. In this simulation,  $N_s$  is investigated by tuning and  $U$  is given by  $U = \omega r$  from the constant speed of the compressor. The throttle mass flow is included in the model as an individual state in (2.5). The pressure drop across the throttle is derived as

$$\Delta p_t = w_t^2 \frac{1}{2\rho k_t^2 A_t^2} \quad (4.4)$$

where  $\rho$  is the gas density and  $k_t$  is the throttle gain included to adjust the throttle valve opening. This parameter is analogous to adjusting the area  $A_t$ , but in this simulation this area is treated as a constant. Including  $k_t$  allows controlling a parameter with span from [0,1] instead of adjusting small values ( $A_t = 0.002$ ). The compressor characteristic state variable  $\Delta p_c$ , the throttle mass flow state  $w_t$  and the steady-state characteristic  $\Delta p_{c,ss}$ , drawn from the empirically determined function will be used in the simulation of the Greitzer model. The system is initialised with the values presented in Table 4.3.

---

<sup>2</sup>In the analysis by [43], the compressor characteristic was denoted  $\Delta p_c$  for the pressure increase. The variable is equal to the centrifugal model pressure ratio  $\Psi_c$  in [40]

Table 4.3: Initial simulation parameters, Greitzer model

$p_p$	$1.2 \cdot 10^5$ Pa
$w$	$0.12$ kg s <sup>-1</sup>
$w_t$	$0.05$ kg s <sup>-1</sup>
$\Delta p_{c,ss}$	1.95
$N$	135000 rpm
$p_{Amp}$	100 Pa
$\omega_i$	$400$ rad s <sup>-1</sup>

The initial conditions are representing an operating point on the 135000 rpm curve, for the GT2252 compressor map. The compressor mass flow, throttle mass flow and plenum pressure response for a throttle valve opening reduction at  $t = 0.1$  s is seen in Figure 4.6. The system dynamics are as mentioned previously, very fast. The system plenum pressure settles at  $t \approx 0.15$  s.

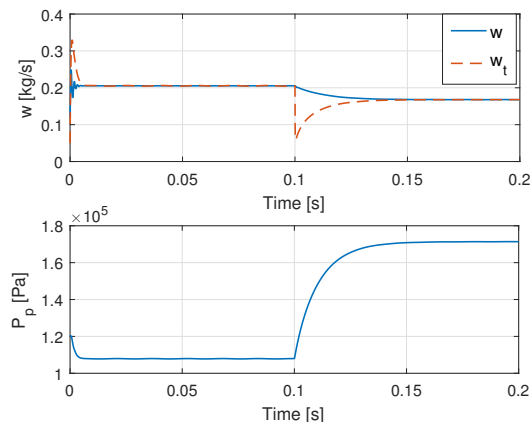


Figure 4.6: The steady-state dynamics of the Greitzer model. Throttle valve reduction is performed at  $t = 0.1$  s

The dynamics of the transient response in (2.7) can be seen from the compressor map in Figure 4.7<sup>3</sup>. The initial starting point at  $t = 0$  is marked with an asterisk and the end point with a "x". In Figure 4.7a, the number of rotor revolutions  $N_s$  is chosen to be 1. It can be seen that after starting the simulation, the operating point shifts towards the choke line and settles around ( $w = 0.22, \Delta p_c = 1.1$ ) after exerting some unstable operation. This instability behaviour does however occur rather quick, since it can be noticed some oscillations shortly after  $t = 0$  in Figure 4.6. However, reducing  $N_s$  results in a reduction in the circular behaviour, which is equal to neglecting the pressure ratio dynamics seen in Figure 4.7b. The variable is kept constant at  $N_s = 1$  in the further work.

<sup>3</sup>In all of the compressor map plots, the starting direction of the curve is towards east, with start marked as an asterisk (\*) and ending with x.

#### 4.4. Initial conditions and process dynamics

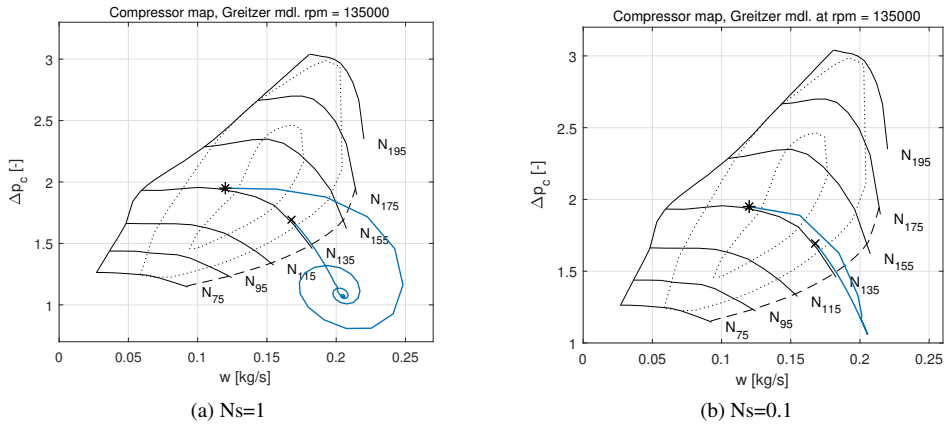


Figure 4.7:  $\Delta p_c$  versus  $w$ , Greitzer model. The plot shows the effect of reducing  $N_s$  to a lower value

The behaviour might not be characterised as surge, since the oscillation amplitude are damped after a short time and a new stable operating point is set. The new point is also seen to be on the 135000 rpm line in the map. This is where the throttle characteristics (given by (4.4)) intersects the compressor characteristics given by the empirical function found in Section 3.3.2.

From the original analysis in [43, p. 194, Fig. 5(b)], the behaviour seems analogous to the dynamics in Figure 4.7a. Greitzer used  $N_s = 2$  throughout his analysis in [43, Part I]. However, in the analysis the steady-state operation ends in steady rotating stall, unlike in this simulated dynamics where the point is on the characteristic curve in the normal operating region of the map.

Forcing a reduction in throttle mass flow increases the pressure on the discharge side of the compressor, which was seen from the response in plenum pressure in Figure 4.6. If the valve gain  $k_t$  is reduced to a certain value within a short time, it is reasonable to predict surge behaviour since the pressure is increased and the mass flow drops significantly within a short time interval [42]. The operating point is then shifted out to the left of the surge line. Introducing a step in the throttle gain from  $k_t = 0.8$  to 0.1 (a reduction of 70%) results in the system response seen in Figure 4.8.

## 4. Simulation and control

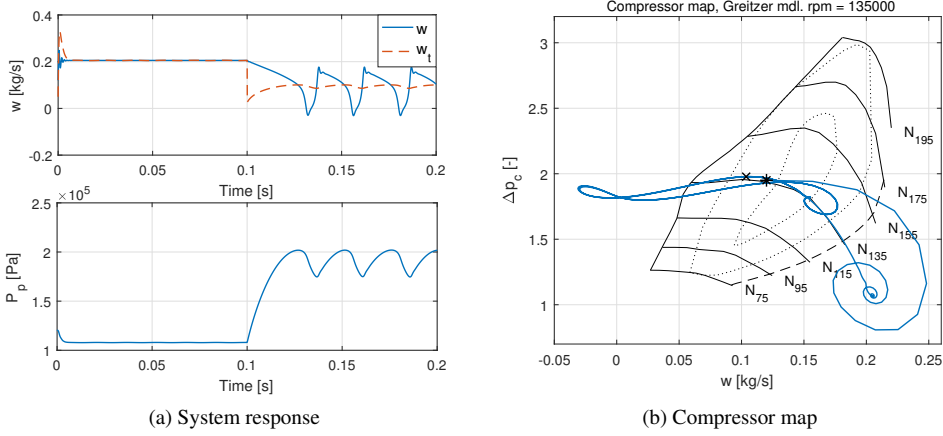


Figure 4.8: Greitzer model with surge behaviour

The oscillations in mass flow seen in Figure 4.8a characterises deep surge with reverse flow [19]. The plenum pressure oscillations have an amplitude of approximately  $0.27 \cdot 10^5$  Pa with a period of  $t_p \approx 0.024$  seconds. Seen in the plot, the system is not returning to a stable equilibrium but continue to oscillate around the surge line. After settling at the operation point ( $w = 2.2, \Delta p_c = 1.1$ ), seen in Figure 4.8b, the throttle gain is reduced and the operation point is shifted further left on the constant speed line leading to the oscillations.

### 4.4.2 Steady state behaviour of the centrifugal model

This section will validate the dynamics of the centrifugal model. The model is simulated with the same initial conditions as the Greitzer model. These are drawn from Table 4.2 and 4.3 with the exception of  $w_t$  and  $\Delta p_{c,ss}$  since these are not state variables in the centrifugal model. In this model,  $\Delta p_c$  changes notation to  $\Psi_c$  for convenience. The spool dynamics where  $\omega$  is a state variable, is not included in the model simulation. The input to the final model when including this state, will then be the turbine torque. In the WGC laboratory scenario, pressurised air with temperature around  $20^\circ\text{C}$  is used to control the speed of the shaft. However, a turbine model is not developed in this work. Therefore, assuming an ideal transfer from the turbine torque, given an valve opening adjusting the inlet turbine air pressure, the rpm is controlled directly in the model simulation.

In this model the throttle mass flow  $w_t$  is not included as a state variable. The throttle flow is restricted to a linear equation given in [40] given as

$$w_t = k_t A_t \sqrt{p_p - p_0} \quad (4.5)$$

where  $k_t$  is the same variable parameter as in Section 4.4.1,  $p_p$  is the plenum pressure and  $p_0$  is the atmospheric pressure at the throttle outlet. In this model, the first principle characteristic is used. The function value given by psiC is mirrored for negative flow rates, resembling the reverse flow characteristic in the unstable compressor map region. Figure 4.9 shows the compressor and throttle mass flow and the plenum pressure for the centrifugal model.

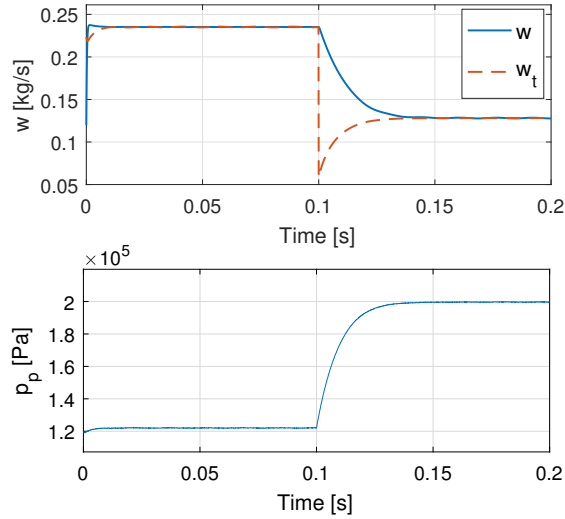


Figure 4.9: The steady-state dynamics of the centrifugal model. Throttle gain reduction is performed at  $t = 0.1$  s

The system finds a new stable operating point after a throttle valve opening reduction at  $t = 0.1$  s. The compressor map is seen in Figure 4.10. The difference between the centrifugal and the Greitzer model is seen from the dynamics in the characteristic of  $\Psi_c$ . In the centrifugal model, the transient response model is not implemented. The equilibrium point at ( $w = 0.23$ ,  $\Psi_c = 1.18$ ) seems to follow the characteristic curve for 135000 rpm, defined in Chapter 3.

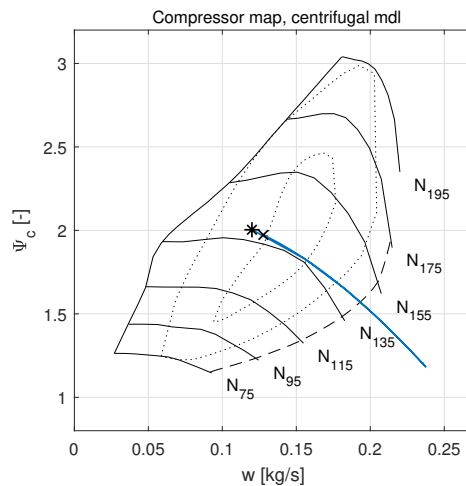


Figure 4.10:  $\Psi_c$  versus  $w$  for the centrifugal model

## 4. Simulation and control

The system seems to identify with the Greitzer model, which is not unexpected since the centrifugal model incorporates the same set of ordinary differential equations for mass flow and plenum pressure. The simulation is further continued to capture the dynamic response to a larger reduction in throttle gain. Figure 4.11 illustrates the response to a reduction of the throttle gain from 80% to 8% (the model responded to surge at an increase of 2% from the Greitzer model response). The reverse flow pattern is visible on the characteristic curve.

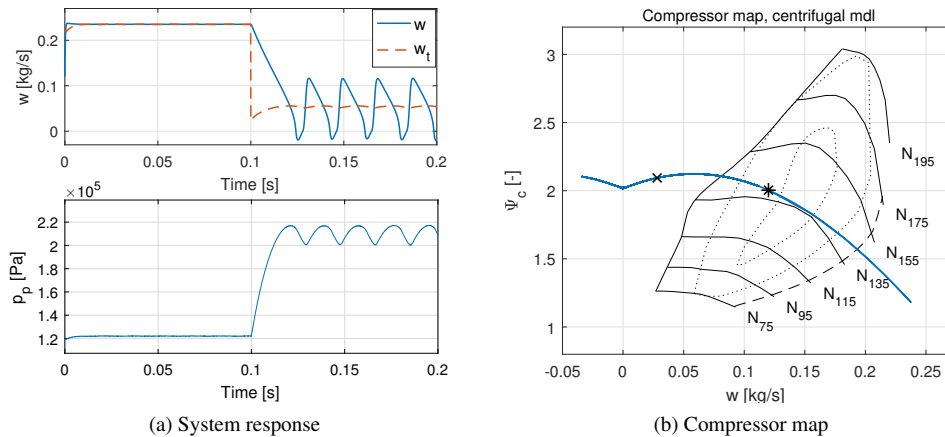


Figure 4.11: Centrifugal model with surge behaviour

The plenum pressure oscillates with an amplitude of approximately  $0.17 \cdot 10^5$  Pa and holds a wave period of  $t_p = 0.018$  s. Comparing the compressor map in Figure 4.8b with the result in Figure 4.11b, the surge cycles for the centrifugal model are restricted to follow the constant speed curve. This is because the model does not incorporate the compressor characteristic dynamics in (2.7).

Furthermore, these models are the basis for predicting the behaviour of the wet gas compressor in the laboratory. The content in this section is a preliminary study to identify typical compressor dynamic behaviour with load disturbances. Moreover, the implementation of a controller to stabilize process changes made by users and by the downstream equipment is needed. The scope of the controller study will then be in the normal operating region of the compressor confined by the surge and choke line.

## 4.5 Controller tuning study

This study will address effective methods of tuning a PID-controller and the method of applying a controller in the turbocharger system.

According to [67], the PID controllers found in the industry are configured by trial and error to find the proper tuning parameters and many are not optimally tuned at all. This leads to an analysis of the process parameters. From the process response, being subject to setpoint or load changes, the open or closed-loop behaviour of the process model can be estimated and the parameters can be gained. These have a direct relation to many of the published tuning-methods (see [98]). Therefore, it is convenient to start with a open-loop characterisation of



the compressor system. The advantage of using simulation-based controller tuning is that the actual process is not exposed to process variations that could eventually damage personnel or equipment. However, simulation-based design will require knowledge of the actual process conditions and assumptions might be applied to establish enough information to simulate the process. This is to ensure that the controller is acting in an environment as close as possible to the actual process [67]. However, there will exist an uncertainty in the initial parameters achieving by tuning when adapting them to actual process controller [57].

The GT2252 turbocharger consists of a compressor and a turbine. The centrifugal model is the one that incorporates the centrifugal properties, such as impeller geometry, and is also made on the purpose of developing compressor control. This model will be used in the further tuning study and when establishing a robust controller to be implemented in the laboratory.

#### 4.5.1 System step response and tuning parameters

To evaluate the compressor system dynamics, process parameters such as *gain*, *time constant* and *dead time* are necessary. The gain is defined as the relationship between changes in process output to process input, given as

$$K = \frac{\Delta y}{\Delta u} \quad (4.6)$$

where  $K$  is the gain factor,  $\Delta y$  is the change in process output and  $\Delta u$  is the change in process input. The process time constant  $\tau_1$  and dead time  $\theta$  defines how fast the dynamics of the system are and the response according to an input change. These parameters are also important when determining controller parameters. The parameters can be found in the model equations or by experimental analysis. Since the compressor model is non-linear, it needs to be linearized to achieve the parameters from the model. The model is already implemented in Simulink and achieving the process parameters can rather be done by experimental analysis (The MATLAB "Linear Analysis Tool" is also useful in determining  $k$ ,  $\tau_1$  and  $\theta$ ) [57], [67].

Figure 4.12 presents the open-loop response of the compressor with a input step of  $\Delta u = 10000$  rpm.

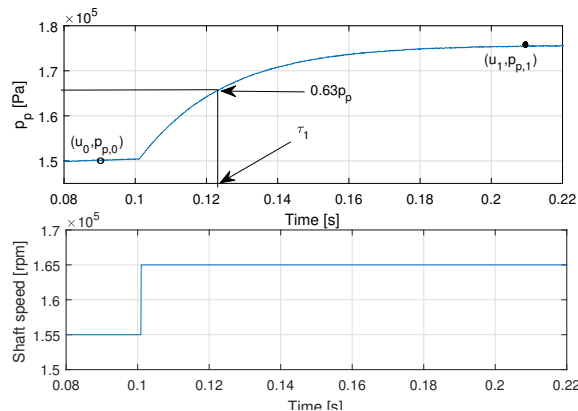


Figure 4.12: Input step response for the centrifugal model with an open-loop configuration

## 4. Simulation and control

---

In the compressor model, the spool speed is defined as input and the plenum pressure is defined as the process output. The input step is initiated at  $t = 0.1$  s and the response is from steady-state point  $(u_0, p_{p,0})$  to a new point at  $(u_1, p_{p,1})$ . Once again, the fast dynamics of the system can be seen as there is almost no time-delay from the input step to where the process variable reacts. Furthermore, the system seems to be critically damped, being close as possible to a potential overshoot of the process variable before it settles [67]. The process gain is found as

$$K = \frac{(1.75 - 1.50) \cdot 10^5 \text{ Pa}}{10000 \text{ rpm}} = 2.5 \frac{\text{Pa}}{\text{rpm}} \quad (4.7)$$

According to [57], the process time constant  $\tau_1$  is found at 63% of the Process Value (PV) when going from  $p_p(t = 0)$  to the new steady-state value in  $p_p(t = 0.63p_p)$ . In Figure 4.12, this is at the plenum pressure value  $p_p = 1.66 \cdot 10^5$  Pa and the corresponding time constant is then

$$\tau_1 = 0.024 \text{ s} = 24 \text{ ms} \quad (4.8)$$

The dead time  $\theta$ , being the delay from the step to the rise start of the process variable is small. The simulation time for the result is 0 to 0.25 s and it is difficult to see if there exist a value for the dead time due to the fast dynamics of the system. Therefore, to analyze the differences with and without a system dead time, this analysis will include two approaches:

1. Tuning the controller parameters with dead time  $\theta = 0.5$  ms, five times the simulation time-step. In the time-domain of the simulation model, the dead time of 0.5 ms is 0.05 % of total step time to reach a new stable operating point<sup>4</sup>
2. Tuning the controller with no dead time,  $\theta \approx 0$

With the collected process parameters available, open-loop tuning methods can be used. Ziegler-Nichols PID tuning rules are well known and the rules are applied both for closed-loop and open-loop tuning. However, the method require that the process is brought to an unstable operating point with a steady-oscillating process variable. This is done by increasing the controller proportional gain. If a compressor with an installed controller is tuned with this approach, it leads to an oscillating discharge pressure. This can be damaging for both the compressor and the downstream system, as it can be analogous to initiating surge behaviour (seen in Figure 4.8 for example). Therefore, open-loop tuning with methods that rely on the step-response parameters is considered more convenient.

Both the Skogestad Internal Model Control (SIMC) tuning rules proposed in [98] and the PI-tuning rules in [52] utilize the process parameters in their methods. The latter is a revision on the tuning-rules by Ziegler-Nichols, resulting in better performance. These two are chosen on behalf of a literature search, with focus on the comparison performed in [58] for PI controller tuning. Since the dynamics of the system is fast and there may occur rapid changes in the PV, the derivative action is often discarded. This is due to the large derivative gain, created by a rapid change in PV error, which may create instability.

---

<sup>4</sup>This is taken into consideration to reflect that the dead time is a representable fraction of the time-domain of the system even though it is small.

According to [52], the step-response in Figure 4.12 characterise of first-order model response<sup>5</sup> defined in as

$$g(s) = \frac{K e^{-\theta s}}{(\tau_1 s + 1)} \quad (4.9)$$

where  $K$ ,  $\theta$  and  $\tau_1$  are the process parameters. In [98], a PI control law is suggested to handle such processes. The first-order process approximation is named a "KLT" process in [52], where  $L = \theta$  and  $T = \tau_1$ . For the SIMC method, the controller proportional gain is given as

$$K_c = \frac{1}{K} \frac{\tau_1}{\tau_c + \theta} \quad (4.10)$$

where Skogestad introduces the closed-loop response time as  $\tau_c$  acting as a tuning parameter. The integral time is given as

$$\tau_i = \min[\tau_1, 4(\tau_c + \theta)] \quad (4.11)$$

and the derivative time is  $\tau_D = 0$  in these settings. The Hagglund & Åström's revisited KLT PI settings for the proportional gain is (using the same notation as above)

$$K_c = \frac{0.14}{K} + \frac{0.28 \tau_1}{\theta} \quad (4.12)$$

and the integral time is derived as

$$\tau_i = 0.33 \theta + \frac{6.8 \theta \tau_1}{10\theta + \tau_1} \quad (4.13)$$

As seen in (4.12), a small dead time gives a large proportional gain. This can lead to an aggressive controller, adjusting too fast towards the new setpoint value. There is also a problem for  $\theta = 0$  since the parameters are not defined for this condition. However, a second approach to the Hagglund & Åström's revisited settings is used to calculate a less aggressive proportional gain. The derived settings are for a process where  $\theta/\tau_1 \rightarrow 0$ , which is said to be "lag-dominant" [52]. Here,  $K_c$  and  $\tau_i$  is given as

$$K_c = \frac{0.35 \tau_1}{K\theta} \quad (4.14)$$

$$\tau_i = 7\theta \quad (4.15)$$

### 4.5.2 Tuning results

The calculated parameters from the SIMC rules and the Hagglund & Åströms PI rules for both KLT (HAA-1) and "lag dominant" processes (HAA-2) are summarised in Table 4.4. The initial closed-loop response time  $\tau_c$  is set to  $\tau_c = \theta = 0.0005$ , using SIMC tuning rule of thumb for fast response and good robustness against load disturbances [98]. A different approach is also used since  $\theta$  is small enough to be neglected. This is to set  $\tau_c = \tau_1$  giving pure process time-constant dynamics with a lower proportional gain [57, Ch. 10].

<sup>5</sup>It is also considered a "rule of thumb" according to [5] to discard the derivative action if the response is similar to a first-order model

#### 4. Simulation and control

Table 4.4: Tuning parameters for the compressor PI-controller. SIMC - Skogestad IMC tuning, HAA - Hagglund & Åström PI-tuning rule

	$\theta$	$K_c$	$\tau_i$
SIMC-1	0	0.4	$\tau_c = \tau_1 = 0.024$
SIMC-2	0.0005	9.6	0.004
HAA-1	0.0005	13.49	0.003
HAA-2	0.0005	6.72	0.0035

Integrating the PI controller in Simulink for the centrifugal compressor model is presented in Figure 4.13. To avoid "unreal" actuator signals, a saturation block has been included in the model to limit the control signal to the speed limits of the GT2252 turbocharger. Integrator wind-up is compensated for by using back-calculation of the integrator output if the output saturates [5].

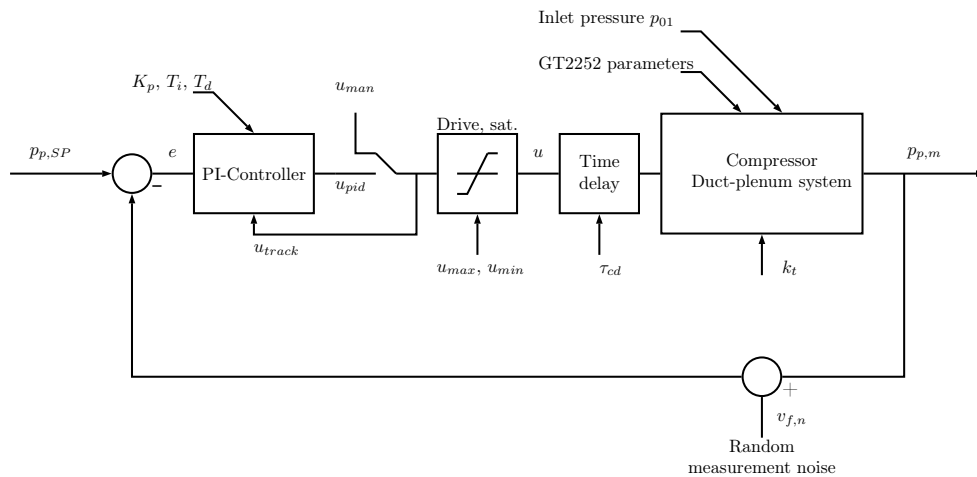


Figure 4.13: Block diagram representation of the Simulink model with PI control

To model measurement noise, a random signal in the range of  $\pm 0.1\%$  of the setpoint value is added to the PV. Also, the same varying inlet suction pressure from Table 4.3 is kept throughout the simulation. The control signal ( $u_{pid}$  in the figure) is processed through a delay, to simulate some delay from initiating the compressor control. The four tuning-settings are gathered in the output presented in Figure 4.14. The process setpoint value is changed from  $1.5 \cdot 10^5$  Pa to  $2.0 \cdot 10^5$  Pa at  $t = 0.5$  s to test the stability in setpoint changes and load change is performed at  $t = 1$  s.

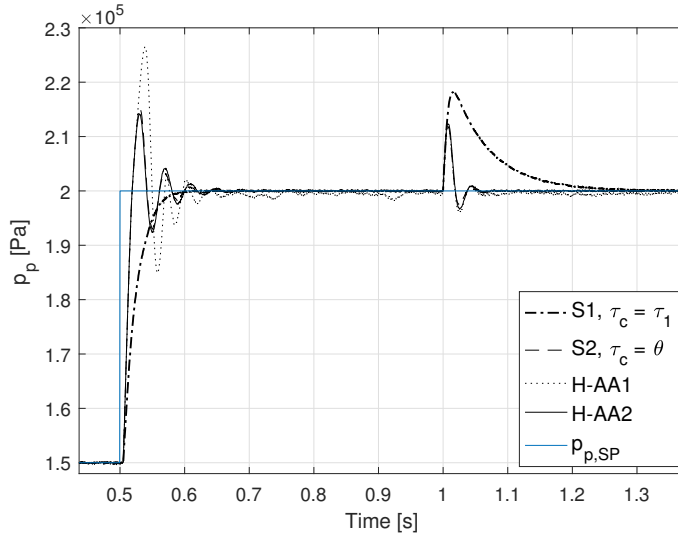


Figure 4.14: Result of tuning the compressor PI control with four settings. S1 and S2 = Skogestad IMC-PI tuning, HAA = Hagglund & Åstrøm

The throttle simulates the load by changing the throttle gain from 80% to 30%. The setpoint step result favours the "SIMC-1" settings (S1 in the figure) with  $\tau_c = \tau_1$ , with no dead time between input to PV response. The gain seems to be too large for the other settings, but the "HAA-2" settings shows better load disturbance compensation than "SIMC-1". This is again due to larger proportional gain. The different controller setting performances are compared with the  $IAE_{SP}$  for setpoint changes and  $IAE_D$  for load changes. The IAE values are given by the integral

$$IAE = \int_{t_i}^{t_f} |e(\tau)| d\tau \quad (4.16)$$

where  $t_i$  and  $t_f$  are the time values before and after the setpoint or load change and  $e$  is the control error. The lower the IAE values are, the better the performance (keeping the error low throughout the process change) [57]. The performance data is collected in Table 4.5.

Table 4.5: Tuning parameters for the compressor PI-controller. SP - setpoint change, D - load disturbance

	$IAE_{SP}$	$IAE_D$
SIMC-1	$1.28 \cdot 10^3$ Pa	$1.36 \cdot 10^3$ Pa
SIMC-2	982.65 Pa	207.45 Pa
HAA-1	$1.62 \cdot 10^3$ Pa	398.52 Pa
HAA-2	$1.01 \cdot 10^3$ Pa	230.32 Pa

The results show that the disturbance compensation is worse for the SIMC-1 parameters. However, these parameters does not show to develop too large overshoot for changes in the setpoint. The SIMC-1 parameters are used in the further controller development. A possible

## 4. Simulation and control

---

option is to reduce the closed-loop response time  $\tau_c$  to achieve a more rapid load disturbance compensation.

The linear PI controller, with adequate tuning seems to handle the dynamics of the system in the normal operating region of the compressor map. However, the tuning found in this section and results are highly dependent on the operation point. The non-linear model might also not reveal the same first-order response at other operating points as seen here. To compensate for changing process dynamics and following process gain changes, an adaptive control method is preferred.

### 4.6 Gain scheduling controller

The tuned performance of the PID controller is influenced by the non-linearity of the compressor model. In Section 4.5.1, one operating point were chosen to establish  $K_c$  and  $\tau_i$  for the controller ( $\tau_D$  was excluded). However, if the process is marginally stable and the system shifts to other operational points due to process changes, the same controller parameters might not be adequate due to different process gain values [53]. Since the process gain depends on the system operation point due to a non-linear system, the compressor control will be extended with GS control.

GS control algorithms have been developed for compressor control of rotating stall and surge, more specifically on the Moore-Greitzer compressor model (see for example [35] and [107]). These are developed with similar procedures described in Section 2.5.1. The controller developed in [107] utilise the compressor mass flow as scheduling variable. The GS procedure in this section is inspired by [92], where a controller for automatic cruise control in a vehicle was developed. The throttle was used to define the operating points and was selected as the GS variable.

Seen in the steady-state behaviour of the dynamics for the compressor models, the compressor mass flow is highly dependent on the mass flow through the throttle. Reducing the throttle mass flow  $w_t$ , increases the pressure  $p_p$  to a point where the non-linear system is no longer stable. The compressor mass flow is reduced, bringing the operating point towards the surge line. The changes in throttle mass flow, can be related to changes in the process dynamics downstream of the compressor. However, in the simulation model the throttle valve is representing the downstream pressure changes. The process dynamics are then manipulated with the throttle gain parameter  $k_t$  in the model. The valve downstream of the compressor is not intended to be adjusted during WGC laboratory operation. Furthermore, the scenario is used in the simulation and control to be able to demonstrate the downstream process dynamics.

In the laboratory, the pipeline pressure at suction and discharge side are monitored for the turbocharger. A suggestion is to use one of these two variables for the GS controller. However, in the simulation model the suction pressure is set to a constant oscillating sinusoidal. Therefore, this is not a proper GS variable in this scenario. The throttle mass flow is a variable that is varying in the model simulation and it is easily manipulated to verify the GS controller response. This mass flow will then be the proposed GS variable for simulation purposes. Two assumptions are then made to the model mass flow:

1. The throttle mass flow cannot be larger than the actual compressor mass flow in the system at steady-state<sup>6</sup>. This implies that a upper limit is set to the GS variable corresponding to the throttle flow limit.
2. The compressor and throttle mass flow are measurable. The scheduling variable must be available for measurement to use GS control in the WGC laboratory.

A total of six operating points with six different settings for the throttle mass flow are chosen. According to the compressor map, see Figure 4.10, the highest efficiency is achieved in the area around  $w = 0.095$  to  $0.175 \text{ kg s}^{-1}$ . The six scheduling variables are spread evenly from  $0.09$  to  $0.2 \text{ kg s}^{-1}$ .

The steady-state behaviour for each of the GS variables are found from step-response plots similar to Figure 4.12, revealing the process gain and time-constant. The transfer function  $H(s)$  is obtained by linearization with the MATLAB function `linearize(sys, io, ts)`, where `sys` is the Simulink model, `io` is the defined IO of the open-loop system and `ts` is the operation point in simulation time to be linearized. The steady state behaviour of the PV is achieved after  $ts \approx 0.1 \text{ s}$ . For each of the GS variables, the process gain, time constant and linearized transfer function  $H(s) = Y(s)/U(s)$  from input to output is presented in Table 4.6.

Table 4.6: GS variable, process gain and time constant and linear process transfer function

$w_t$	$K$	$\tau_1$	$H(s)$
0.09	2.13	0.0076	$\frac{5.105 \cdot 10^5}{s^2 + 768.3s + 2.215 \cdot 10^5}$
0.112	2.14	0.0091	$\frac{3.816 \cdot 10^5}{s^2 + 1760s + 2.215 \cdot 10^5}$
0.134	2.18	0.012	$\frac{4.668 \cdot 10^5}{s^2 + 2244s + 2.215 \cdot 10^5}$
0.156	2.17	0.014	$\frac{1.53 \cdot 10^7}{s^2 + 1.46 \cdot 10^5 s + 2.215 \cdot 10^5}$
0.178	2.19	0.017	$\frac{3.936 \cdot 10^5}{s^2 + 3450s + 2.215 \cdot 10^5}$
0.2	2.22	0.0196	$\frac{3.526 \cdot 10^5}{s^2 + 3857s + 2.215 \cdot 10^5}$

The operation point  $H(s)$  for GS(4) has a large value in the nominator with  $10^2$  difference from the other operation points. However, the undamped resonance frequency of this  $H(s)$  seems to be constant and equal to the other operating point frequencies. The source of these differences are not known at this stage, but the focus will here instead be held on the trends in process gain and time constant over the operational area. The process gain seems to be a little lower for lower mass flows in the compressor and have a lower time constant compared to when the throttle flow is increased. The change in  $K$  is minor, but the time constant is more than doubled from GS(1) to GS(6).

Using a PI controller, the tuning can be directly done from the gain and time constant in Table 4.6 with the SIMC method from Section 4.5.2. The initial PI tuning parameters, with  $\tau_c = \tau_1$ , for the proportional gain and the integral time is given in Table 4.7.

<sup>6</sup>For system transients, the mass flow at the throttle might be larger than the compressor mass flow

#### 4. Simulation and control

Table 4.7: Initial PI settings for each scheduling point with  $\tau_c = \tau_1$  and  $\theta = 0$

GS-PI	$K_c$	$\tau_i$
1	0.4695	0.0076
2	0.4673	0.0091
3	0.4587	0.0122
4	0.4608	0.0144
5	0.4566	0.0170
6	0.4505	0.0196

To avoid sudden changes to the controller gain, a *bumpless transfer* between the scheduled PI parameters must be used. The term bumpless originates from avoiding upsets when switching between controllers for the process, especially between manual and automatic control [38]. To compensate for steep changes in between the controller parameters for  $K_c$  (seen for GS(2) to GS(4)) the scheduling is performed with a 3rd-degree function. The 3rd-degree fit is plotted in Figure 4.15 for the proportional gain  $K_c$  (Figure 4.15a) and the integral time gain  $\tau_i$  (Figure 4.15b).

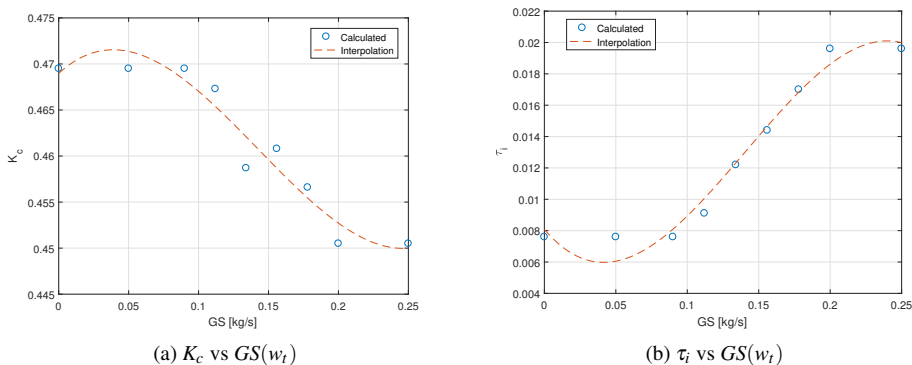


Figure 4.15:  $K_c$  and  $\tau_i$  versus GS variable  $w_t$  with 3rd-degree fit

The calculation is performed continuously during simulation run-time for the time-varying GS variable. In between each of the scheduling points, the developed MATLAB function `gainSchedule` calculates new values for  $K_c$  and  $\tau_i$ . This approach is similar to the discrete version in [57].

The polynomials used for determining new controller settings are calculated "offline", meaning that the two functions for  $K_c$  and  $\tau_i$  are not changing during run-time. For scheduling values outside of the defined span, the controller gain and integral time are set equal to the smallest or largest value.

The system response is seen in Figure 4.16 for the first stage GS controller. At  $t = 0.1$  s the system switches from manual to automatic GS control. A setpoint step is performed at  $t = 0.25$  s and a throttle gain reduction from  $k_t = 0.8$  to  $0.3$  is done at  $t = 0.35$  s. The first implementation of the GS controller is seen to adapt the same performance in terms of the single PI with SIMC-1 parameters.



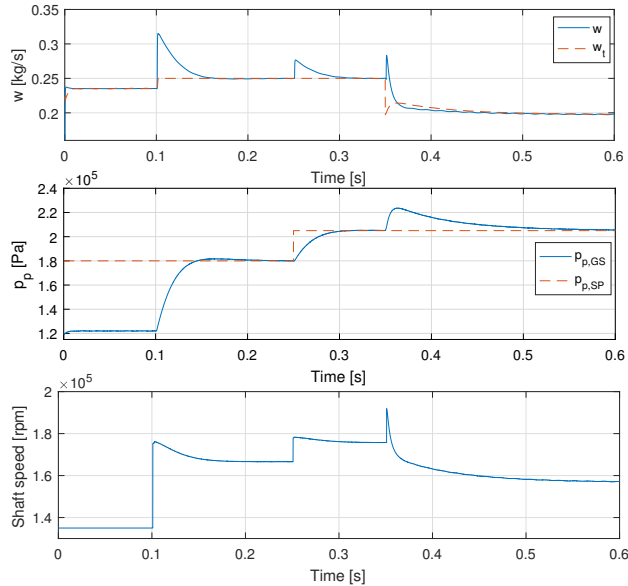


Figure 4.16: System output with first stage GS control

The PV for load disturbance is returning to the setpoint, but rather slowly. The closed loop response time  $\tau_c$  is the tuning parameter in the SIMC tuning method. To compensate for the load disturbance, a smaller value for  $\tau_c$  where reported in [98] to achieve better robustness. To improve the GS controller, the PI settings are recomputed with  $\tau_c = 0.002$  and  $\theta = 0.0005$  in (4.10) and (4.11). This approach gives a larger  $K_c$  and a integral time which can be assumed to be constant. The new controller parameters are presented in Table 4.8.

Table 4.8: Tuned PI settings for each scheduling point with  $\tau_c = 0.002$  and  $\theta = 0.0005$ 

GS-PI	$K_c$	$\tau_i$
1	1.43	0.0076
2	1.70	0.0091
3	2.23	0.0100
4	2.66	0.0100
5	3.10	0.0100
6	3.55	0.0100

The result for the tuned GS controller is presented in Figure 4.17. A step in setpoint is done at  $t = 0.1$  s and a throttle gain reduction at  $t = 0.15$  s from 80 to 30%. The PV reaches the setpoint faster, (a settling time reduction of approximately 0.025 s) and the load disturbance is almost mitigated. An observation is that the shaft speed increases when using a larger proportional gain for the controller and the drive saturates at 195000 rpm for the setpoint step.

#### 4. Simulation and control

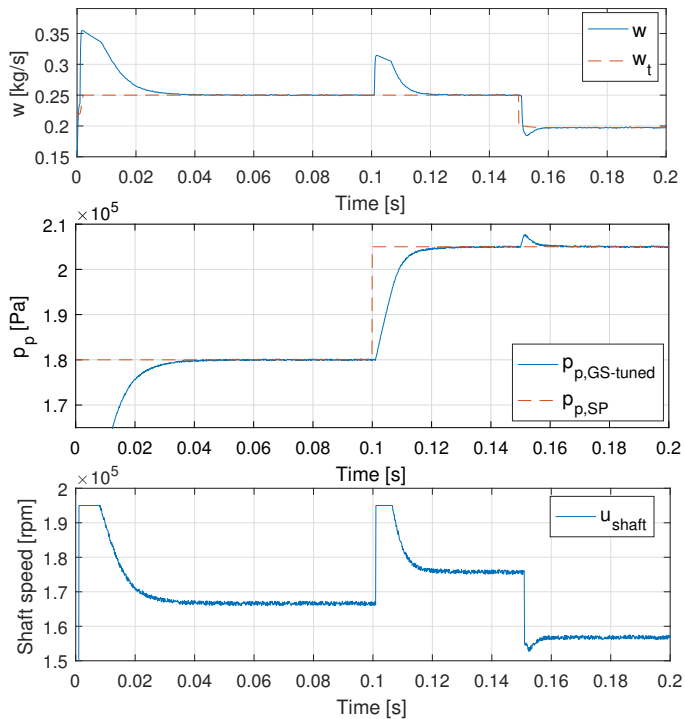
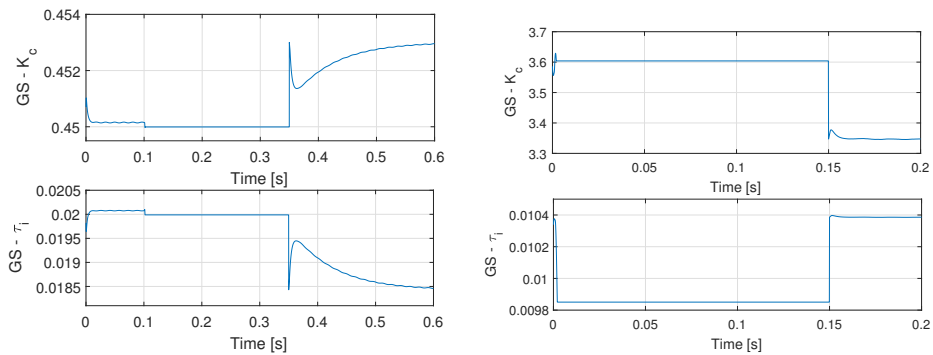


Figure 4.17: Tuned GS controller system response to setpoint and load change

The scheduling of both the initial and tuned controller PI settings are seen in Figure 4.18. Both with 3rd-degree polynomials to calculate the new parameters. Since the change in scheduling variable is abrupt, the gain change for the controller is responding likewise.



(a) Initial GS-settings, for system in Figure 4.16

(b) Tuned GS settings, for system in Figure 4.17

Figure 4.18:  $K_c$  and  $\tau_i$  for initial and tuned GS PI settings using 3rd-degree interpolation

The drastic change in throttle flow might introduce large variations in the output signal for the controller, resulting in unstable performance. For measurement signals, filtering techniques are used to smooth the input signal which may reflect variations with small frequency and different amplitude. For controllers in general, a noisy measurement signal is a problem as it can amplify the output to the actuating element (valve, motor drive etc.) [57]. To extend the GS controller, a low pass filter on the scheduling variable is proposed to improve the PI scheduling and the resulting control signal. The filter equation is given as

$$T_f \dot{y}_f = y - y_f \quad (4.17)$$

where  $T_f$  is the filter time-constant,  $y$  is the input signal and  $y_f$  is the filtered output signal. However, there is a downside for poorly chosen filter time values. Increasing  $T_f$  may cause the gain change to be performed too slow, increasing the control error. If  $T_f$  is too small, there will be little to no smoothing of the large step in  $w_t$ . The delay in process variable response for increasing the value of  $T_f$  is seen in Figure 4.19. The initial parameters from Table 4.7 are used to illustrate the filtering effect. The GS controller is initiated at  $t = 0.2$  s.

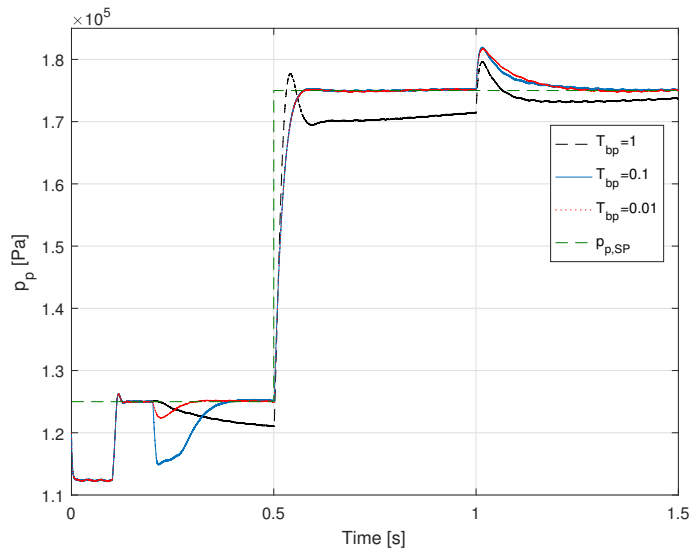


Figure 4.19: Process output  $p_p$  for three different filter time constants  $T_f$

In the continued simulation, the filter time-constant is set to  $T_f = 0.01$  s which showed the best result in Figure 4.19. The filter will produce a smoother switching between  $K_c$  and  $\tau_i$  for the controller. The result of utilising the filter in (4.17) for the GS controller is seen in Figure 4.20.

## 4. Simulation and control

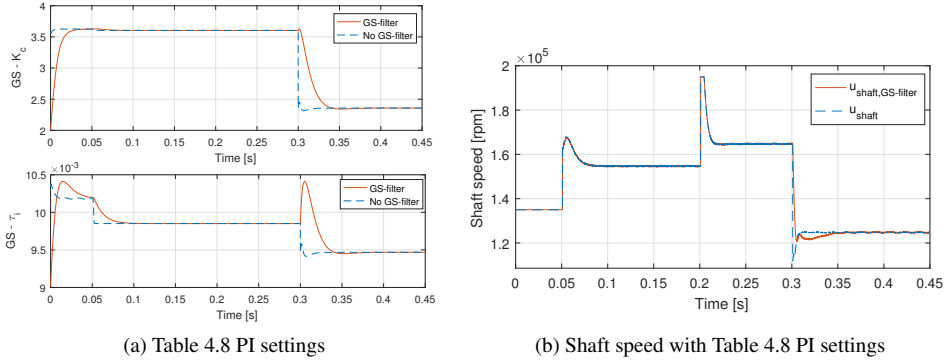


Figure 4.20:  $K_c$  and  $\tau_i$  with and without filter on GS variable

The improvement is minor for the shaft speed in terms of less abrupt changes. The filter, presented Figure 4.20b, is seen to influence the input  $u$  at load changes ( $t = 0.3$  s). By smoothing the input signal of the scheduling variable, the controller is shown to be less aggressive. However, this implies that the robustness performance will be poorer. The final performance evaluation, in terms of IAE values, is done for four scenarios. These are presented in Table 4.9.

Table 4.9: Comparing three GS controller options to single PI controller. The single PI parameters are  $K_c = 2.45$  and  $\tau_i = 0.0095$

	GS-PI initial w/filter	GS-PI tuned	GS-PI tuned w/filter	Single PI w/filter
IAE <sub>SP</sub>	428.4 Pa	164.61 Pa	164.61 Pa	166.21 Pa
IAE <sub>D</sub>	$1.40 \cdot 10^3$ Pa	23.33 Pa	68.80 Pa	102.98 Pa

The result is close to what was predicted previously, that the filter increases the IAE for load disturbance. The optimal GS controller is seen in scenario 2, the tuned GS PI settings with no filter. Therefore, this controller will be used in the continuation of this chapter. The difference from a single PI controller is not large and indicates that tuning a single PI controller at a "difficult" operating point results in good stability and robustness.

### 4.6.1 Controller performance with empirical characteristic

The robustness in terms of model uncertainties has not yet been performed on the compressor GS controller. This section describes the performance outcome of changing the characteristic function from the first principle to the empirical. The controller was tuned for the first principle adapted characteristic from Section 3.2.5. With a change of characteristics, the compressor behaviour will act according to the defined characteristic in Figure 3.10b rather than Figure 3.9. The result of using the GS controller with the empirical characteristic and the first principle for comparison is seen in Figure 4.21.

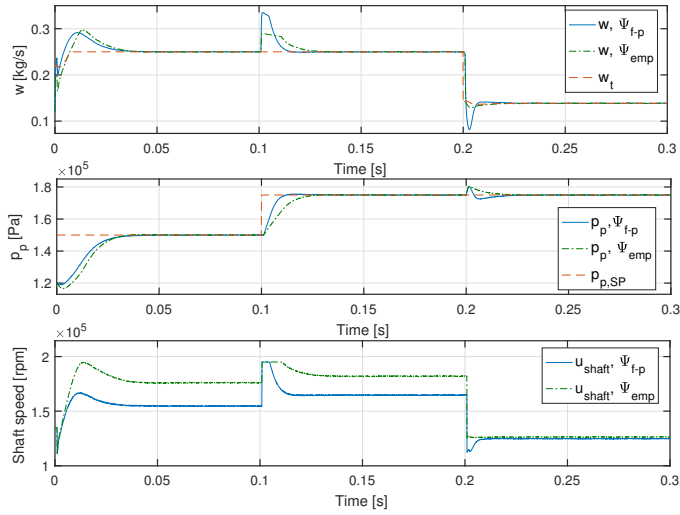


Figure 4.21: Setpoint and load step response for GS controller with empirical characteristic

A setpoint increase is performed at  $t = 0.1$  s with  $\Delta p_p = 0.25 \cdot 10^5$  Pa. The throttle gain reduction  $k_t = 0.8$  to  $0.25$  is done at  $t = 0.2$  s. The controller compensates for the new required plenum pressure, but must increase the process input to reach the control objective. The increased requirement in control output implies that the compressor requires more power from the drive to adapt to the changes. This is better seen in the proportional and integral term plot in Figure 4.22 for the two settings. The integral term holds a larger value, due to the increased error when using the empirical characteristic.

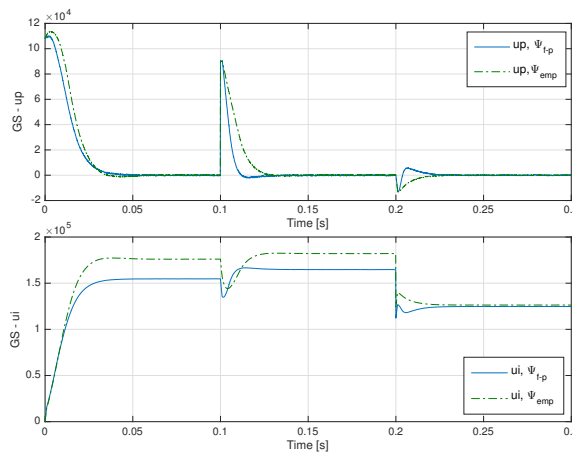


Figure 4.22: Control input contributions ( $u_p$ ) and ( $u_i$ ) for GS controller with empirical characteristic

The response for the controller, handling the process with the empirical characteristic is poorer than for the first principle one. Again, the tuning is made for the step-response with the first principle which is characterised with unique time-constants for different operating points. The controller performance with allowable overshoot and constraints of the control output must be defined to verify if the performance seen in Figure 4.21 is acceptable. However, there is no unstable control output and the overshoot is small verifying that the GS controller can deal with this type of model uncertainty.

### 4.7 Wet gas impact on the centrifugal compressor model

The GS controller is according to Table 4.9 a better controller than a single PI controller with fixed  $K_c$  and  $\tau_i$ . However, to design a controller that will be appropriate to implement in the WGC laboratory it must be proven to be robust towards changes in model parameters related to wet gas. The centrifugal model is not ideal and equal to actual compressor conditions. Simulating the GS controller with wet gas parameter modifications is an approximate prediction and the same behaviour one might encounter in the laboratory is most likely not to fit the reality.

The motivation to perform the parameter variations is to be able to declare the compressor controller as proficient for the WGC laboratory. The compressor model in Section 3.2 is intended for dry, ideal gases. For wet gas implementation, experiments are typically made on the centrifugal dry gas compressors [79]. The parameter variations for the centrifugal compressor model must be related to the results found in documented wet gas experiments. This section is then based on the typical parameters that changes performance outcome presented in Section 2.1.3 for a dry gas centrifugal compressor with wet gas flow. In this section, the wet gas parameters are  $\rho_1$  the inlet gas density,  $c_p$  the specific heat capacity at constant pressure and  $k_f$  the impeller gas flow friction factor.

#### 4.7.1 Preliminary wet gas parameter study

According to the observations presented in Section 2.1.3, the internal losses in the compressor increase with increasing liquid fraction in the flow. The compressor model developed by [40], considers the frictional loss as part of the limiting factor for an increased pressure ratio over the compressor. The friction loss was derived in Section 3.2.1 and is given as

$$\Delta h_f = \frac{C_h l w^2}{2D \rho_1^2 A_1^2 \sin(\beta_{1b})} \quad (4.18)$$

where  $C_h$  is the surface friction loss coefficient,  $l$  is the mean channel length of the impeller,  $w$  is the mass flow rate ( $w = \rho AC$ ),  $D$  is the mean hydraulic diameter,  $\rho_1$  is the inlet fluid density,  $A_1$  is the inlet area and  $\beta_{1b}$  is the fixed inducer blade angle. The factor  $C_h$  is given by the friction factor for single-phase fluids, which can be drawn from a Moody diagram (see for example [15]) for laminar and turbulent flow. For oil & gas pipeline flow, [49] states that the NORSOK standards recommends a maximum gas flow velocity of  $60 \text{ m s}^{-1}$  and  $6 \text{ m s}^{-1}$  for liquid flow in carbon steel pipelines. The gas flow velocity is considerably larger than for liquid and has a lower density. Higher velocities increases the friction loss, with turbulent flow. Seen in a Moody diagram, the friction factor decreases for turbulent flow and

the velocity dominates the friction factor  $k_f$ . For liquid flow, the velocity is lower and the moody friction factor increases (towards laminar flow). However, the scale of the friction factor in a moody diagram is small (0.008 to 0.1) [15]. This indicates that the fluid velocity will be the dominating factor in (4.18).

According to [111], the pressure drop due to friction for a gas-liquid mixture in horizontal pipe flow is given by:

- The friction between each fluid phase and the pipe wall
- The phase interaction between gas and liquid
- The effect of entrainment (liquid droplets in the core gas flow)

In [36], the liquid phase in the gas flow is said to increase the frictional losses between the fluids and the rotor for a dry gas compressor. However, the ideal gas friction factor determined for the centrifugal model impeller implies challenges in terms of the defined wet gas parameters. According to [12], gas holds less heat capacity than a liquid, and if a mixture of both phases occurs the result holds a larger heat capacity. This implies that the ratio of specific heats  $\kappa$  changes for wet gas and the pressure ratio in (3.25) may increase for decreasing GVF for the flow. An increase in pressure ratio contradicts the findings in [46], stating that the total pressure ratio is reduced. The loss associated with wet gas is found to occur in the diffuser and volute section in this article and the pressure increase occurs at the impeller. Therefore, it might not be valid approach to assume that the correct pressure ratio for wet gas flow in the compressor is calculated with (3.25). However, as the internal losses is a phenomena found by experiments and not modelled, it is difficult to have any opinion on the thermodynamic issues for wet gas and to relate them to a model governed by ideal gas laws. The solution in this modelling approach is to use an strict empirical relation to increase the friction loss, since the accurate modelling of wet gas friction flow in an impeller is not the task in this work.

### 4.7.2 Centrifugal model wet gas characteristic

The assumptions taken in this work are based on the previous analysis on what parameters can reflect a "wet gas" behaviour of the model. It is important to express that the approach is strictly an empirical relation. This is to connect the increasing friction factor, gas density and heat capacity to emulate a wet gas compressor characteristic to use in the simulation model. In the simulation to illustrate an approximate wet gas behaviour for the centrifugal model, the following assumptions are applied:

1. The inlet temperature is kept constant at 293.15 K. For wet gas, the liquid fraction reduces the temperature due to higher mass of liquid in the flow [79]
2. The specific heat for constant pressure for the gas is in the denominator of (3.25). If this factor is modelled equal to (2.3), yielding  $c_p = c_h$ , the factor will increase with decreasing GVF and reduce the pressure ratio. This assumption implies strict empirical relations for the specific heat and may not be considered a reality. This is because  $\kappa$  must be kept constant to avoid an increasing  $\Psi_c$ . In the compressor model derived by [40],  $\kappa$  is considered a constant
3. The friction factor is proportional to the decreasing GVF, giving an increase in friction loss  $k_f w^2$ . The use of GMF is giving a larger increase in friction loss and the relation in (2.2) is used to derive the new friction loss

#### 4. Simulation and control

Table 4.10 presents the GVF and GMF values used to calculate the wet gas parameters.

Table 4.10: GVF and GMF values used in the simulation of wet gas

	GVF	GMF
	1.0	1.0
	0.9997	0.8009
	0.9995	0.7070
	0.9993	0.6328
	0.9990	0.5467

The result of decreasing GVF and GMF for the compressor ratio is seen in Figure 4.23 for a constant speed of 120000 rpm.

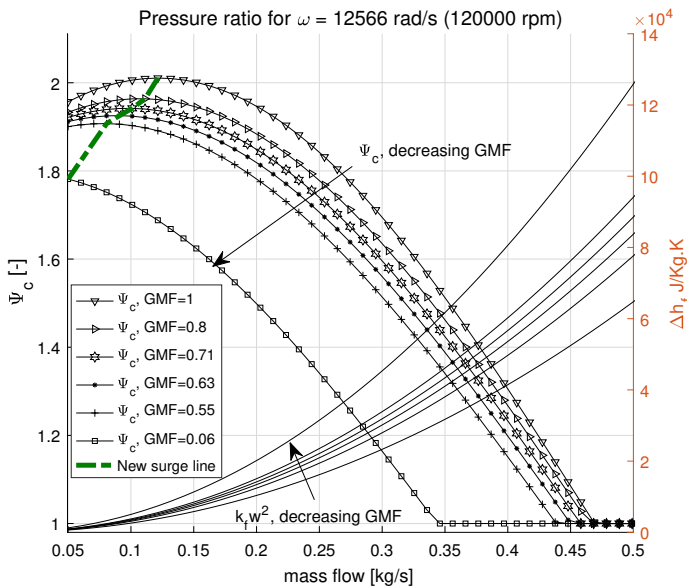


Figure 4.23: Empirically modelled wet gas characteristic. The green dashed line indicates the maximum  $\Psi_c$  value for each curve.

The empirical relation for the friction factor is calculated such that  $GMF = 0$  when the friction loss is unchanged (dry gas). It is defined as

$$k_f = k_{f,0} (1 + (1 - GMF)) \quad (4.19)$$

where  $k_{f,0}$  is the dry gas friction factor. The local maximum for each of the characteristics is connected with a dashed green line. Mentioned previously, was that the surge line was connected where the slope of the characteristic was zero. The zero-slope points is included to illustrate that the surge line is shifted, when injecting wet gas in the compressor model. Seen in Figure 4.23, decreasing the GVF for the flow will constrain the capacity of the compressor, reducing the achievable mass flow and pressure ratio.



The area which the controller is intended to be working is to the right of the new surge line, in the negative slope area of the characteristics. The behaviour of the compressor pressure ratio can be seen to be similar to what the experiments on centrifugal dry gas compressors has shown (see for reference Figure 4 in [46] and Figure 6 [45]).

### 4.7.3 Controller robustness

To simulate a delay from the reference rotational speed to the achieved rotational speed of the compressor, a first order time delay model is included (low pass filter). It can be drawn towards the unmodelled dynamics of the turbine, supplying the drive torque to the shaft for the turbocharger. Since the turbine air supply is adjusted by a control valve in the WGC laboratory, it is reasonable to assume that there exist a delay before the actual speed of the shaft is reached. This model is included as an additional measure in this analysis to indicate the robustness performance of the controller. The time constant for the turbine dynamics is set equal to the GS filter time constant. The initial conditions for the wet gas flow tests on the model are included in Table 4.11.

Table 4.11: Initial conditions for wet gas performance test

	Description	Value
$p_p$	Plenum pressure	$1.2 \cdot 10^5$ Pa
$w$	Compressor mass flow	$0.12$ kg s <sup>-1</sup>
$N$ ( $u_{\text{man}}$ )	Rotational speed	135000 rpm
$p_{01}$	Inlet pressure	$0.001 \cdot 10^5 \sin(400t + 1)$ atm)
$v_f$	Amplitude of white noise on $p_p$	$0.002 \cdot 10^5$ Pa
$k_t$	Throttle coefficient	0.8
$T_{\text{td}}$	Shaft dynamics time constant	0.01 sec
$\rho_g$	Gas density (air at 20° C)	$1.205$ kg m <sup>-3</sup>
$\rho_w$	Liquid density (water at 20° C)	$998.21$ kg m <sup>-3</sup>
$c_{p,g}$	Specific heat constant pressure, gas	$1004.6$ J kg <sup>-1</sup> K <sup>-1</sup>
$c_{p,w}$	Specific heat constant pressure, water	$4182$ J kg <sup>-1</sup> K <sup>-1</sup>

The geometric parameters for the compressor is fixed and equal to the ones presented in Table 3.1. The wet gas flow variables (density, heat capacity and friction factor) are connected to the compressor characteristic block `psiC`. This MATLAB function script is extended to incorporate the changes made to the GVF and GMF for the wet gas flow in the code.

The calculation of  $\rho_1$ ,  $c_p$  and  $k_f$  is done in the simulation model and Algorithm 4 presents the pseudocode. These parameters are routed to the `psiC` function in the compressor block for the simulation model `centrifugal_md1.slx`.

## 4. Simulation and control

---

---

**Algorithm 4** Pseudocode for wet gas parameter calculations in centrifugal compressor model

---

```
1: procedure CALCULATEWGCPARAMETERS(GVF, GMF)
2:   while simulation stop  $\neq$  true do ▷ Code run during simulation
3:     if wgc simulation = true then
4:        $\rho_l = \rho_g \text{GVF} + (1 - \text{GVF})\rho_l$  ▷ Calculate constant values
5:        $c_p = c_{p,g} \text{GVF} + (1 - \text{GVF})c_{p,l}$ 
6:        $k_f = k_{f,dry}(1 + (1 - \text{GMF}))$ 
7:     else
8:        $\rho_l = \rho_g$  ▷ If false, keep the original parameters
9:        $c_p = c_{p,g}$ 
10:       $k_f = k_{f,dry}$ 
11:     end if
12:     simTime = simTime + Ts ▷ Iterate to next time step in simulation
13:   end while
14: end procedure
```

---

Two scenarios are tested with the GS controller:

1. Constant gas flow GVF from 1 to 0.999, equivalent to reducing the GMF to approximately 50%
2. Ramping down the GVF during simulation

For scenario number one, the result of exposing the controller for five constant GVF values in Table 4.10 from 1 to 0.999, is seen in Figure 4.24. The reduced GVF is seen to make the process slower and prolong the controller settling time of zero offset error for compressor plenum pressure and mass flow. The controller compensates for the change in gas density by applying more input to the drive shaft seen in the lower subplot of Figure 4.24. The enthalpy friction loss is plotted for the five different GVF settings in Figure 4.25. The limitation is that the maximum compressor mass flow is reduced with reduced GVF, seen in the upper plot of Figure 4.24.

The reduced GMF with larger liquid density is more demanding on the drive unit for the compressor, which has its limitations. The upper limit for the simulation model is 195000 rpm, defined by the compressor map for GT2252. This is seen in the lower plot, where the limit is reached when  $\text{GVF} < 99.93$  equal to a  $\text{GMF} < 0.6328$ . Moreover, the controller is able to meet the setpoint demand for the plenum pressure for  $\text{GVF} \geq 99.95$  but at this point it is not able to handle further demand for increased pressure.

## 4.7. Wet gas impact on the centrifugal compressor model

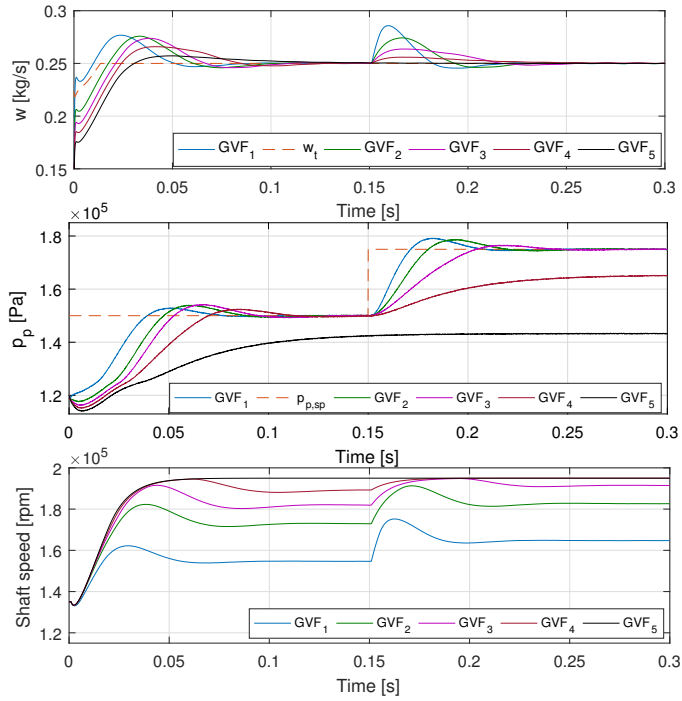


Figure 4.24: System step response for constant GVF from 1 to 0.999

For scenario number two, a ramped signal output is used to simulate an increasing water content in the gas flow. The lower limit of the GVF is 99.95% after the observations made in scenario 1. The plenum pressure setpoint is set to  $1.6 \cdot 10^5$  Pa. Since the pressure in the system drops with an increasing liquid fraction of the gas flow and increasing the control input is the measure to maintain stable pressure, the process gain might be changing.

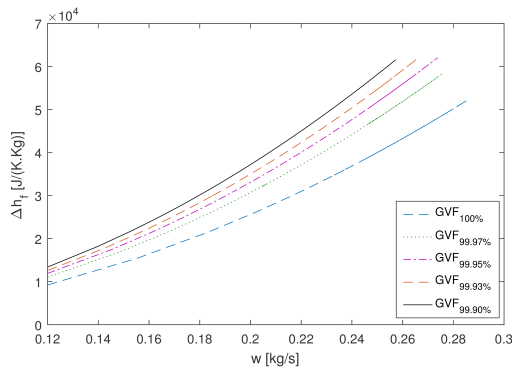


Figure 4.25: Compressor enthalpy friction loss for constant GVF values

## 4. Simulation and control

A step-response is performed with GVF of 0.999, giving a process gain of 0.16 compared to the one found in Section 4.5.1 of 2.5. Since the proportional gain  $K_c$  is inverse proportional to the process gain, it needs to be increased to compensate for a lower gain. The gain ratio  $\Delta K = 2.5/0.16 = 15.63$  is the theoretical factor to scale  $K_c$ . The PV output for three different values of the gain ratio factor is plotted in Figure 4.26, where the output before  $t = 0.1$  s is with GVF=1.

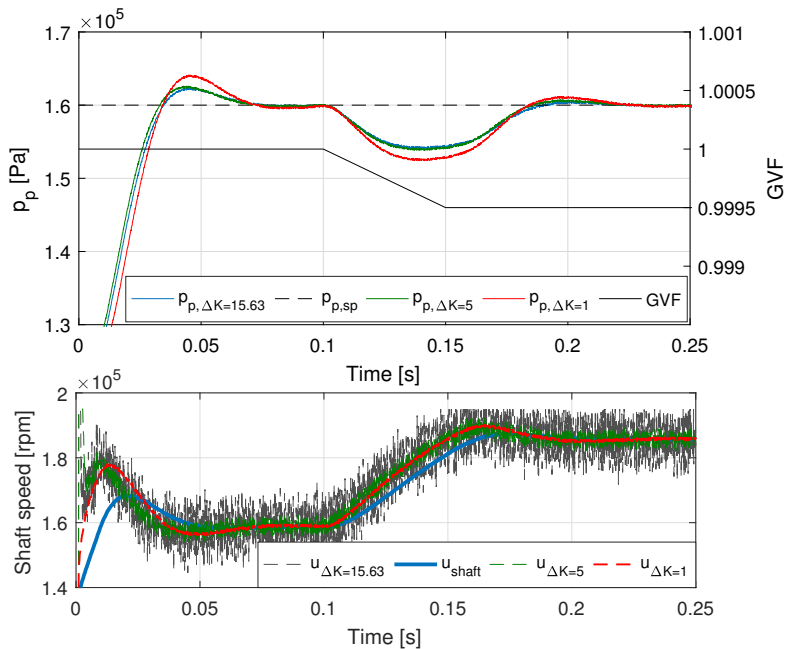


Figure 4.26: System response for ramped GVF from 100 to 99.95%

Using the increased gain ratio factor is observed to give a little reduction in the settling time when simulating with increased density, heat capacity and friction. However, the downside is that the controller input is heavily influenced by the increased gain factor. The controller signal is determining the actuator opening of the inlet air supply valve to the turbine side. With a large oscillatory signal, the valve seat might be worn out quickly due to large variations over short time. The effect of increasing the proportional gain due to lower process gain is not seen to improve the controller and will only be used to illustrate the effect of using the theoretical gain factor.

In terms of the simulation model, the effect of using the proposed turbine dynamics is equal to include a low-pass filter on the control signal. This eliminates the higher frequency output from the controller. A summary of the IAE performance values for scenario 2 in this section is presented in Table 4.12. The IAE value is calculated from  $t \approx 0.1$  s towards the simulation end time. This is due to the increase in gain is valid for the application of wet gas and is not representative for the case where  $\text{GVF}=1$ .

Table 4.12: IAE for plenum control with wet gas

GVF	IAE <sub>wgc</sub> for $\Delta K \cdot K_{c,0}$		
	$K_{c,0}$	$5K_{c,0}$	$15.63K_{c,0}$
Ramped, $1 \rightarrow 0.999$	426.62 Pa	345.06 Pa	100.92 Pa

The GS controller is able to comply with the model changes in terms of wet gas parameter increase for the inlet density  $\rho_1 = \rho_h$ , heat capacity  $c_p = c_h$  and friction factor  $k_f$ . The limitation is on how much liquid content being present in the pipeline, corresponding to an increased drive input to the system. The saturation limits for the drive were reached in the simulation model.

## 4.8 Summary of chapter

The simulation scenario used in this chapter was based on an open-loop setup of the WGC laboratory turbocharger. Using a fixed-step implicit solver, the simulation of the models showed to capture the dynamics of both steady state behaviour and the dynamics of surge. Surge behaviour were initiated through a reduction in the throttle valve opening downstream of the turbocharger. A controller study resulted in four settings were the SIMC-1 parameter showed to have the lowest overshoot on a setpoint change and the settling time after a load disturbance was not excessive. However, it had the largest IAE values. The suggestion to improve the tuning was to decrease the closed loop response time  $\tau_c$  and increase the proportional gain  $K_c$  to improve the robustness.

A GS controller with throttle mass flow as the scheduling variable was developed as a first stage WGC controller for the turbocharger. Two 3rd-degree polynomials, used for the interpolation technique to determine the offline GS functions, were used for the PI settings to calculate new parameters during simulation run-time. The controller settings was further tuned with  $\tau_c = 0.002$  and a dead time of  $\theta = 0.0005$ . The GS controller showed to reduce the IAE value for both setpoint and load disturbances compared to the single PI SIMC-1, but with small margin. A filter were proposed on the GS variable, to lower the abrupt changes in actuator response, but it was shown to not improve the controller significantly. The controller showed to compensate for a model uncertainty when changing from the first principle to the empirical characteristic.

The results from forcing a wet gas parameter change for the simulation model, resembled the performance of a compressor under wet gas. Empirical quantities were used to emulate wet gas parameters  $\rho_1$ ,  $c_p$  and  $k_f$  in the centrifugal model. The characteristic were developed for increased density and heat capacity, together with a linear increase in impeller friction factor for decreasing GMF of the fluid flow. The main goal was to further test the robustness of the GS controller towards model uncertainties with parameter changes. The GS controller were simulated with constant GVF and GMF values at setpoint of  $1.5 \cdot 10^5$  Pa and was able to handle a step of  $\Delta p_p = 0.25 \cdot 10^5$  Pa for GVF decrease from 100% to 99.95% (GMF of approximately 70%). However, the control output exceeded the saturation limit for the drive of 195000 and was not able to comply with the new control objective.

#### 4. Simulation and control

---

The process gain in the model decreased when the wet gas parameter increased. The gain factor of 15.63 was calculated when using a constant GVF of 99.9%. The dynamics was slower and a proportional gain increase of 15.63 was tested to improve the performance. The results showed a small improvement, but the control output to the actuator were changing rapidly. This may lead to deterioration of the actuating item (in the WGC laboratory the actuator is the inlet air supply control valve for the turbine side of GT2252).

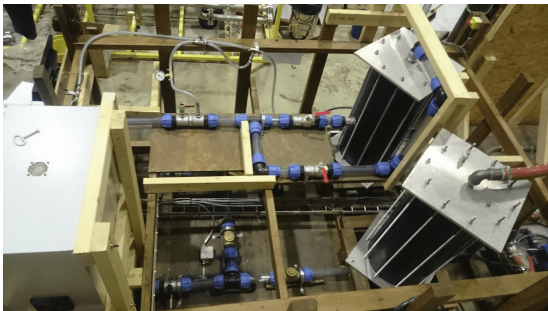
## Chapter 5

# Results from laboratory build and commissioning

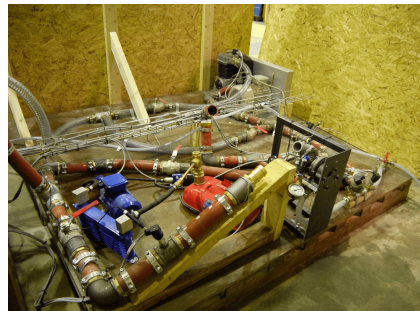
This chapter includes an overview of the laboratory setup, operation and documentation. The latest documentation is included along with pictures of the status of the laboratory in the end of the thesis period. The chapter is intended to introduce the reader to the facility located at MTP. The specific work the author has contributed with is included and the material can be found in the electronic appendix file. The full documentation of the laboratory is a separate thesis delivered this spring produced by Daniel Nedregård at the department of MTP.

### 5.1 System overview

The laboratory is designed with the specific purpose of performing experiments related to a small scale SGCS. Direct wet gas to compressor inlet and separation of gas and liquid before compression are the two main scenarios intended to be experimented on. The laboratory consists of two separate sections shown in Figure 5.1.



(a) LPLT zone



(b) HPHT zone

Figure 5.1: WGC laboratory sections

## 5. Laboratory results

According to [10], the design is based on the actual SGCS at the Ormen Lange test pilot facility and the Gullfaks Sør gas compression. This is similar to the PFD presented in Figure 2.2. In the WGC laboratory, water and air are used to simulate wet gas flow. This section provides an overview of the laboratory installation with the instrumentation, equipment and the developed control system.

The section in Figure 5.1a surrounded by wood structure is the separation and cooling section. It is referred to as the low-pressure-low temperature (LPLT) side. The rotary machinery used for gas compression is installed on the lower platform in Figure 5.1a, surrounded by protective walls. This section is called the high-pressure-high-temperature (HPHT) side and holds the piston compressor and turbocharger.

The laboratory is described by a single P&ID which is included in Appendix B. The standards used to draw this diagram are ISO 10628-1 for chemical and petrochemical process applications and ISO 14617-1 for general symbol notations and graphical notation of mechanical components. During the spring, the drawing has been subject to several revisions improving the design and taking into account the process loop alterations.

### 5.1.1 Test scenarios

A reduced PFD for the laboratory is presented in Figure 5.2 with representative valves and process equipment. The manual valve setup enables bypass of the separator, piston compressor or turbocharger to configure the preferred test scenarios. For full gas compression, the wet gas flow is directed through the separator unit for separation of gas and liquid. The gas flow is directed to the piston compressor for increased differential pressure and discharged to the turbocharger determining the final gas pressure. After the gas flow is discharged from the turbocharger, it is cooled in a counter flow heat exchanger and joined with the liquid flow from the water pump unit. The anti-surge line recycles the gas flow, keeping the minimum flow limit for the turbocharger.

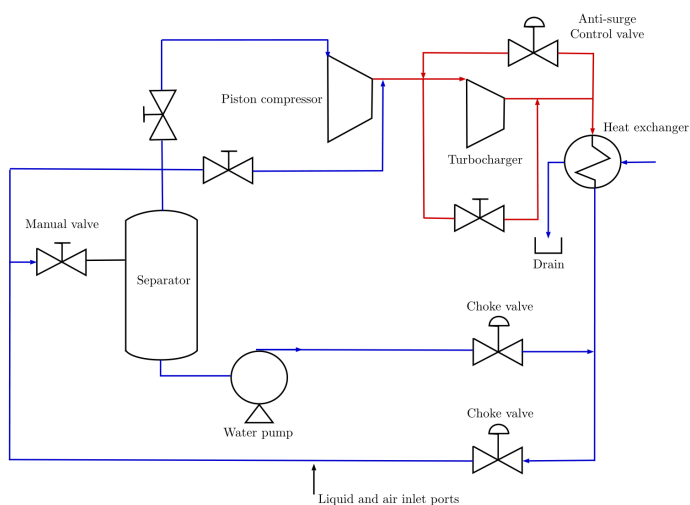


Figure 5.2: Reduced overview PFD for the WGC laboratory. Blue marks the LPLT zone and red marks the HPHT zone



Additionally, not seen in Figure 5.2, is the turbocharger external oil lubrication loop for the bearings inside the housing and the pneumatic air supply to the turbine inlet. These topics are covered by the full documentation presented in the P&ID. The laboratory is intended to be used in the following to three scenarios:

1. Separation and gas compression
2. Wet gas compression, bypassing the separator and piston compressor
3. Dry gas compression

The limitation for scenario 1 is that the piston compressor is not compatible with gas flow having a water fraction or other fluid substances in the compression process according to the manufacturer specifications. Therefore, it will not be used even if the separator unit is utilized in the process loop. This is because there is no humidity sensing element in the process loop downstream of the separator gas outlet.

The system piping together with the separator and cooler volume determine the total GVF content for the laboratory. The GVF values have been calculated from the measurements of the total pipeline and equipment. The result presented shown in Table 5.1.

Table 5.1: Volume and GVF specifications for the laboratory. \* - no separation

Item	Volume (m <sup>3</sup> )	GVF	LVF	V <sub>w</sub> L	V <sub>w</sub> L *	V <sub>g</sub> m <sup>3</sup>	V <sub>g</sub> m <sup>3</sup> *
System piping	0.038	99	1	1.36	0.39	0.135	0.000392
Separator / Heat-exchanger	0.098	98	2	2.72	0.78	0.133	0.000784
Total volume	0.1360	97	3	4.08	1.18	0.132	0.00117

The practical result of the content in this table is the litres of water necessary to pour into the pipeline prior system startup, seen in column 3 and 4.

### 5.1.2 Laboratory instrumentation

To be able to analyse the process variables in the laboratory during operation and to enable control of the process, sufficient instrumentation is needed. The measurement areas, process variables and the control method are presented in Table 5.2.

Table 5.2: Wet gas laboratory process measurements and control. P - Pressure, T - Temperature

Area	Variable	Measurement	Available control input
Pipeline	Gas flow	P/T	Choke valves/Cooler fluid input
Piston compressor	Pressure	P/T measurement	Electrical motor drive
Turbocharger	Pressure/Flow rate	Shaft speed	Turbine inlet pressure
Separator	Liquid	Level	Water pump

Siemens Sitrans P200 pressure transmitters have been installed to monitor the pipeline pressure [97]. The transmitters have an analog output signal of 4 to 20 mA or from 0 to 10 V and require 12 VDC supply voltage. The input signal to the data acquisition unit (DAQ), communicating with the Labview software need to be converted to 0 to 10 V. The measurement range is from 1 to 60 barg, and it is capable of measuring gas, liquids or vapors in absolute or gauge pressure.

## 5. Laboratory results

---

The temperature measurement are divided into two sections: Low temperature section and high temperature section. The low temperature section is where the separation and heat exchangers are located. In this section two temperature sensors of the type Jumo PT100 are installed. These have a temperature range of  $-50$  to  $80^{\circ}\text{C}$ . The temperature is measured with a PT100 resistance element [66]. In the high temperature section, the temperature measurement are covered by two Lutron PT100 probes [71]. The P200 pressure transmitter and the Lutron PT100 sensor probes are seen in Figure 5.3 measuring the pipeline pressure and temperature upstream of the turbocharger.

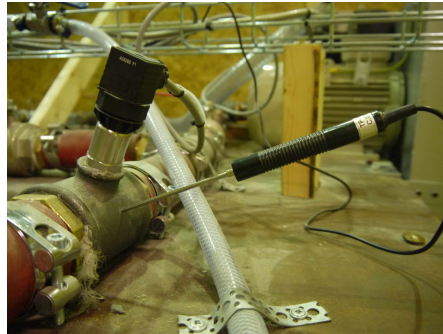


Figure 5.3: Siemens P200 and Lutron PT100 transmitter in the high temperature side

The range of the Lutron PT100 sensors are from  $-50$  to  $400^{\circ}\text{C}$  corresponding to a specific value in Ohms given by the PT100 element. Both temperature sensors are push-in mounted probes in the pipeline. The output resolution transferred to the DAQ is in volts and it is dependent on the mA signal induced on the circuit.

The turbocharger shaft speed is measured by a speed transmitter, giving an output signal in pulse form when the impeller blade passes. The pre-drilled sensor port is marked with an arrow in Figure 5.4.

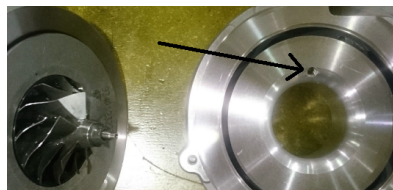


Figure 5.4: Impeller blades and rpm sensor port

For increased shaft speed, the number of pulses per time unit increase i.e. the frequency increases. The relationship from output frequency and rpm is given as [31]

$$\text{RPM} = 60 \cdot 8 \frac{f_{\text{out}}}{n_{\text{blades}}} \quad (5.1)$$

where  $f_{\text{out}}$  is the sensor output signal and  $n_{\text{blades}}$  is the number of blades on the impeller. The number 60 is a conversion from seconds to minute and 8 is a correction factor due to the output frequency is  $1/8$  of the actual measured frequency.

The laboratory also incorporates level measurements for the liquid in the separator. The sensor is a flotation unit, switched normally open. If the separator water level reaches the height of the installed sensor, it closes<sup>1</sup> a voltage supply to a solid state relay on the circuit board. This relay routes 24 VDC supply voltage to the auxiliary contact pair on the water pump 230 VAC supply contactor, starting the water pump<sup>2</sup>. The flotation level sensor is seen in CAD drawing presented in Figure 5.6.

### Control valves

To switch between the laboratory scenarios, manual ball valves are installed in the pipeline. The valves enabled for remote control by the user are called control valves. In the laboratory, four control valves are installed. Two of these are choke valves for the process flow. The two types are presented in Figure 5.5.

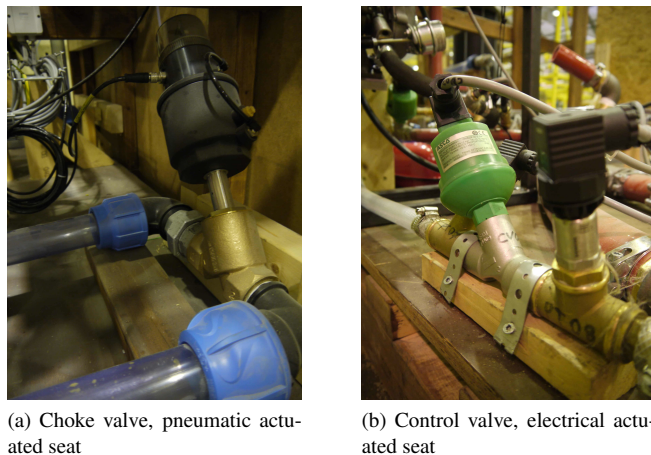


Figure 5.5: WGC laboratory control valves

The gas pressure and flow are equalized or reduced downstream of the installed choke valves of the type Asco 290 series angle seat Proportional Positioner [24]. These are pneumatically actuated with a positioner keeping the seat in a locked position specified by the control system. The positioning is controlled by a 4 to 20 mA signal sent from the control system via the DAQ unit, equal to a linear opening from 100 to 0%. The choke valves are fail safe, returning to normally closed position for loss in power supply to the actuator.

The second control valve type is a motorized Asco 290<sup>3</sup> series angle seat valve. The motorized version is used both for controlling the gas flow through the recycle anti-surge line and turbine inlet air supply for the turbocharger. Common for both of these systems is that the valve response time is required to be small, due to rapid adjustment necessary if surge occurs.

<sup>1</sup>Normally closed

<sup>2</sup>Originally, this was intended to be performed by a Arduino circuit in the previous student project [10].

<sup>3</sup>The Asco 290 series proportional positioner is available for larger pipe sizes than the motorized version.

## 5. Laboratory results

---

The motorized Asco 290 was selected for the anti-surge valve due to the faster response time<sup>4</sup> [10]. The anti-surge valve is a full-open or full-close valve actuated by a 24 VDC signal. The turbine inlet air supply valve is proportional control, enabling full control of the seat position.

### 5.1.3 Processing equipment

#### Separation

The separator unit was hand-made by the students due to cost reduction compared to buying from a manufacturer [10]. The vertical separator design is presented in Figure 5.6. The separation principle relies on gravitational force acting on the fluid molecules. This forces the heavier fluid (in terms of density) fall to the bottom and the lighter fluid (gas) rise to the top outlet. The level sensor is seen in the bottom right of the figure.

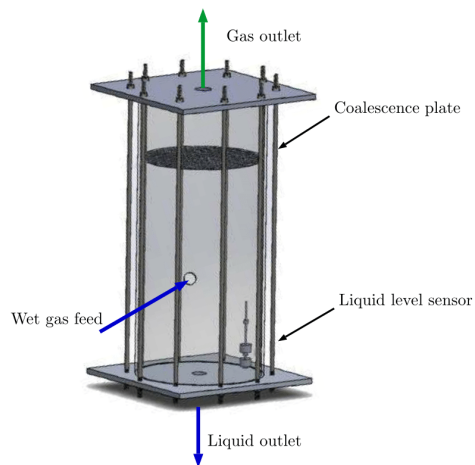


Figure 5.6: Laboratory vertical separator [10]

A coalescence plate has been installed with the purpose of merging droplets being carried by the gas flow towards the top outlet. The fusion of droplets creates a heavier resulting mass for the merged droplets, forcing it towards the bottom of the column.

#### Compression

The gas compression in the laboratory is performed by the series or single configuration of the piston compressor and turbocharger. The turbocharger, being the main subject for this thesis has been covered in Section 2.2.1.

The piston compressor is a reciprocating type, drawing gas from the suction side into a fixed volume chamber and utilising a piston to reduce the chamber volume resulting in compressed gas with higher pressure. This type of compressor is said to be a "constant flow rate" machinery as the characteristic is almost vertical on a pressure ratio versus flow rate

---

<sup>4</sup>The motorized version has a 1.3 second response time compared to the choke valves 2 seconds for full open.

map [48]. Furthermore, the piston compressor is driven by a 4 kW three phase motor and the speed of the motor is intended to be controller with a variable frequency drive from Siemens Sinamics G120C for 4 kW loads [96].

## Cooling

The discharged gas from the turbocharger enters a heat exchanger for cooling. The heat exchanger is also made by [10], as a counter flow cooler. The principal of operation comprises an inlet gas flow at the top of the column, flowing through spiral copper threads down to the outlet of the column. The liquid cooling port is installed at the bottom, and fills the column with coolant from bottom to the top.

## Boosting & pumping

To enable boosting of the liquid fraction of the flow drawn from the bottom outlet of the separator column, a single phase 230 VAC water pump is used. The water pressure is equalised by the downstream choke valve.

### 5.1.4 Control system

The control system for the laboratory is designed in National Instruments Labview graphical programming software by Daniel Nedregård. The separation and compression section of the P&ID front panel view in the control system are seen in Figure 5.7. All the sensor data are processed by the control system, consisting of the logical decisions for operation of the control valves for gas flow mixing after separation and cooling, turbine inlet pressure and turbocharger anti-surge valve.

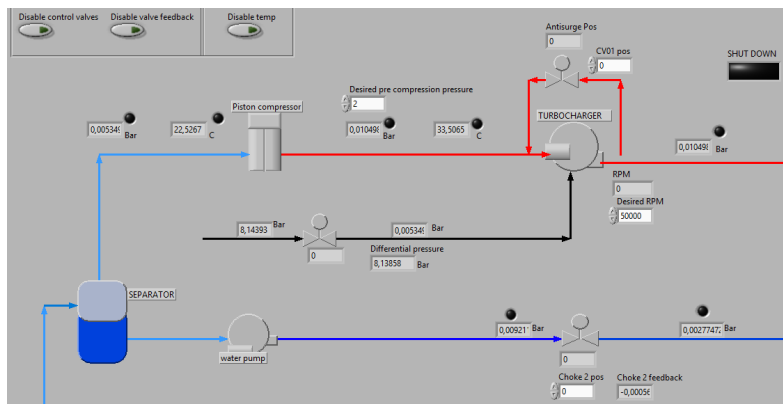


Figure 5.7: A section of the WGC control system front panel (courtesy of Daniel Nedregård)

The control system incorporates safety measures to avoid hazards occurring in the laboratory, damaging personnel and equipment. This is done by indication alarms on the front panel for pressure and temperature readings exceeding limits set by the user. The alarm log list can be found in the tab environment in the program, which the user can use to navigate through the system. The tab selection is presented in Figure 5.8.

## 5. Laboratory results

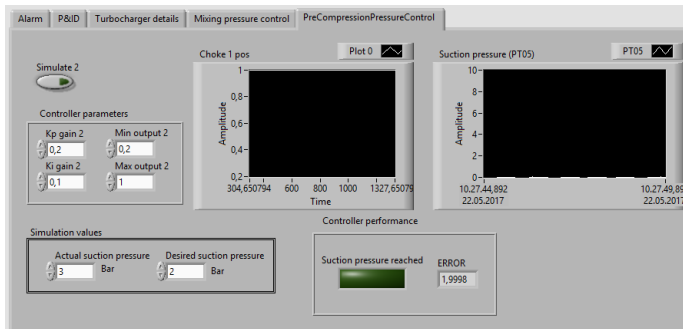


Figure 5.8: Tab view of the control system (courtesy of Daniel Nedregård)

The system process control is divided into three sections, with three PI control algorithms:

1. In the turbocharger speed control tab, the user can get an overview of turbocharger differential pressure, rotational speed and PI settings.
2. In the mixing pressure control tab, the choke valves are controlled to ensure correct pressure for the flow from the heat exchanger and the liquid flow from the separator.
3. In the turbocharger suction pressure control tab, the pressure transmitter at the suction side of the compressor is used for the control of correct suction pressure. The choke valve 2 upstream for the suction inlet is used to control the pressure.

The control system builds on the same design as for the laboratory P&ID.

### 5.2 Electrical circuit design

The laboratory is powered by the electrical infrastructure where it is located and requires a 400 VAC line supply to the rig. The supply powers the main circuit board, consisting of automatic circuit protection fuses, contactors, a frequency converter and two switching power supplies. Both the control cabinet and the inside circuit board are shown in Figure 5.9. In the autumn of 2016, the control cabinet was mounted to the LPLT rig side, instead of being an individual unit. The user operated control station is located to the left of the cabinet in Figure 5.9a which is not shown in this figure.

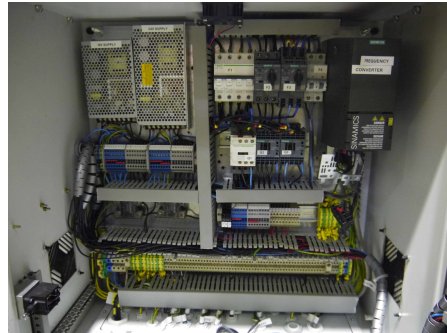
The schematic overview of the circuit board is presented in Appendix D. The documentation for the electrical circuits consists of two drawings and a terminal block diagram. These drawings are:

- Main circuit for 400/230 VAC equipment
- Control circuit for 24 VDC equipment
- Terminal block diagram for DAQ

The last drawing in the list covers the outward going connections to the Labview control system. The electrical circuit schematics are found in Appendix C for both 400/230 VAC main circuit and the 24 VDC control circuit.



(a) Control cabinet



(b) Circuit board (Turn switch wiring on the right door panel is not shown)

Figure 5.9: WGC laboratory control cabinet and circuit board

The author is a certified electrician<sup>5</sup> and is therefore instructed on wiring electrical installations. Moreover, this is the reason why the extended electrical design and installation have been performed by the author, with a control check by the NTNU electrical maintenance personnel.

### 5.2.1 Electrical design revisions

During the spring, a set of design revisions have been done in the laboratory after the initial design in [10]. This is due to new measurement equipment being installed in the loop and extensions in the control cabinet. Below follows two lists of revisions and the outcome of updating the existing structure for both 400/230 VAC circuit and 24/12 VDC circuit. Reference is given to the drawings made by [10] in Chapter 3, Section 3.7 and the revised circuit design for the main circuit and the control circuit presented in Appendix C.

#### 400/230 VAC circuit

1. Installed 4 pole main circuit breaker and contactor for overload and short circuit protection
  - The previous 400 VAC circuit breaker were a 3 pole, shutting off the current on L1 to L3 phases. However, the grid system supplying the lab is "TN-S", where the "S" is short for separated protective earth (PE) and neutral. The neutral leader supplied is not carrying any current in the wire, but is used to reduce the voltage to 230 V for equipment requiring it. Moreover, it can by fault carry current causing short circuit situations. According to [83, §23, §24, appendix 1], both the phase wire and the neutral wire must be disconnected. A new circuit breaker, along with a coherent 4 pole contactor was ordered and installed to comply with the regulations.

<sup>5</sup>The Norwegian certification is called "gruppe L - Lavspenning" for installations with voltage ratings up to 1000 VAC and 1500 VDC.

## 5. Laboratory results

### 2. F4 circuit breaker for switching power supply units

- The overload and short circuit protection for switching power supply for 12 and 24 VDC are routed through the automatic fuse F4 rated 13 A. Instead of using F1, rated 25 A, the switching power supply units are now more selectively protected (cannot hold larger overload than what F4 is rated for).

### 3. F4 circuit breaker for extra equipment

- F4 is made available for extra equipment in further extensions. This is due to the low power consumption by RS-100-12/24.

### 4. Protective earth terminal is changed to accommodate more wiring inputs

- The original PE-rack was placed at the circuit board lower end, and did not hold more than 16 input terminals. It was changed out with the industry standard PE-terminal blocks to have a uniform layout to the circuit board.

A section of the new AutoCAD drawing for the 400/230 VAC circuit is shown in Figure 5.10. The equipment (frequency converter and contactors) are evenly distributed on the L1 to L3 phases together with the neutral wire N. The terminal block connections are shown. These aid the user in terms of troubleshooting and future extensions of the electrical wiring.

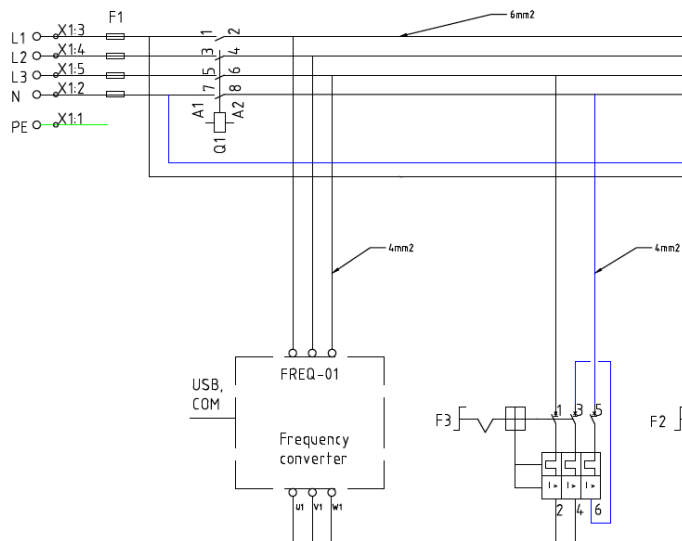


Figure 5.10: A section of the 400/230 VAC circuit drawing

## 24/12 VDC circuit

### 1. Organised terminal block layout

- The existing terminal block layout on the circuit board has been extended and uniformed with two types of blocks. There are five groups of terminal blocks as seen in Appendix D, separating the 12 and 24 V circuits and the 400/230 VAC circuit.



### 2. Removed the Arduino circuit

- The Arduino was originally intended to control the on/off power supply to the water pump depending on the signal input from LS01 - Separator level sensor. However, due to inefficient use of space and that the unit was only intended to control a single switch, it was replaced by a solid state industrial relay controlled by a DAQ unit with Labview.

### 3. Updated the 24 VDC individual circuit fuse protection layout

- Each 24 VDC circuit (main control branch, control valves etc.) were protected with an individual element fuse in the original drawing. Using F4 as protection<sup>6</sup> for both 12 and 24 VDC circuit gives more available space for other equipment. For the operation at MTP, the whole laboratory can be shut down during fault detection.

## 5.3 Commissioning

Commissioning of the WGC laboratory includes verification of schematics, the installed equipment and that testing is completed according to the laboratory responsible requirements. This includes performing a Factory Acceptance Test (FAT) of the installed equipment and connections. For the WGC laboratory, the FAT test concerns:

1. The electrical schematics (main and control circuit) are cross-checked towards the wiring done in the control cabinet
2. The P&ID is checked and verified towards the actual process loop in the laboratory
3. Field equipment (pressure transmitters and control valves) installation are cross checked towards factory specifics and connection schematics
4. The control system designed in Labview is tested with simulated signals, verifying the controller response

After completing the FAT, a Site Acceptance Test (SAT) must be performed with the laboratory responsible. This test ensures that the process loop is installed correctly, both by visual check and by performing a startup, operation and shutdown of the facility. All the safety measures (emergency stop switches and interlocks) must be tested to ensure the correct functionality [86]. The FAT for the WGC laboratory were conducted from 10 to 13 of March 2017. An excerpt of the full documentation for the 24 VDC control circuit is shown in Figure 5.11 to illustrate how the check were performed. After all the corrections were sorted out, the drawing and revision number were updated.

---

<sup>6</sup>Each switching power supply (RS-100-12/24) includes overload and short circuit protection, where the relay closes after the fault is removed [76]

## 5. Laboratory results

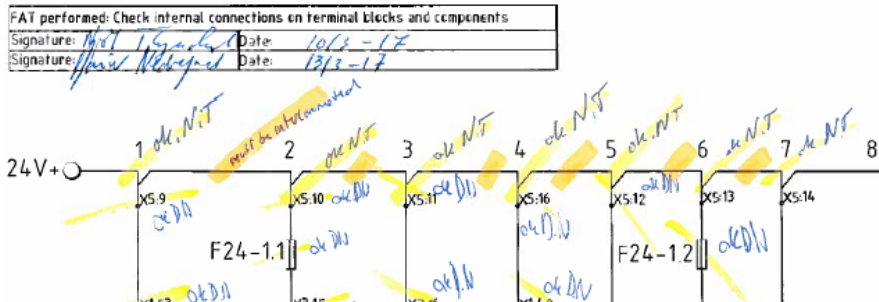


Figure 5.11: FAT test markings on the 24 VDC schematic

The FAT revealed the following results:

### 1. 24 VDC control circuit

- Minor notation errors in the schematic circuit layout
- Missing interconnection of the wire branches on 2 locations
- One faulty N/T connection of a wire on branch 5

### 2. 400/230 VAC main circuit

- Minor notation errors in the schematic circuit layout
- One poor wire termination on the bottom connection of F4 fuse towards the low voltage switching power supply

### 3. P&ID cross check with visual inspection

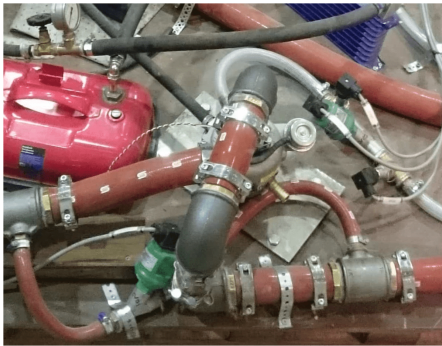
- The turbocharger bypass loop were missing in the documented revision used in the FAT
- Valve V1-013 was missing in the drawing, indicating the liquid injection port

## 5.3.1 Individual functionality testing

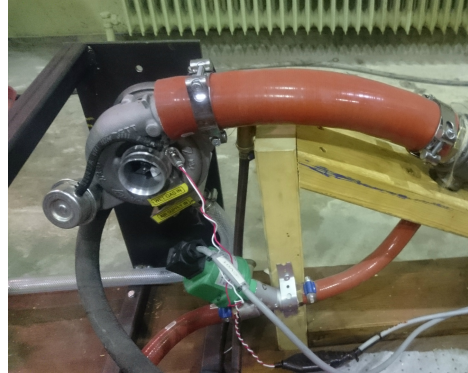
This section presents the work performed by the author in connection with the startup testing and troubleshooting of the laboratory.

### Turbocharger installation

The installation of the turbocharger were performed in the summer 2016, before the start of the specialisation project and master thesis. The first layout is seen in Figure 5.12a where the turbocharger is oriented with the compressor inlet upwards.



(a) Vertically installed



(b) Horizontally installed

Figure 5.12: WGC laboratory turbocharger installation

In the guidelines for installing a Garrett type turbocharger, the tilt of the oil drain side of the turbocharger must not be larger than  $35^\circ$  such that the oil can drain freely by gravity [32]. The first attempt of running the oil loop resulted in a leakage of oil through the shaft seals into the turbine and compressor housing. This was due to the larger downstream pressure of the turbocharger, since the oil cooler was placed before the reservoir.

After cleaning the compressor and turbine side, the turbocharger were installed with the common shaft oriented horizontally, seen in Figure 5.12b, enabling the oil to drain freely from top to the reservoir. The alteration of the setup implied that the anti-surge line and turbine inlet air supply hose needed to be re-installed.

Due to the limited experience with this equipment in the startup phase of the year and since the turbocharger already was installed by the institute in the summer of 2016 it was assumed that the correct installation method where used.

### Electrical troubleshooting

The electrical system were started after completing the FAT for the control cabinet and equipment out in the field of the laboratory. The troubleshooting is divided into three categories: motor operation, cabinet and control valves. The description of the problems and solutions are listed below.

#### 1. Motor operation, oil and water pump

- The fan on the motor drive for the oil pump indicated incorrect rotation direction (anti-clock wise). This was solved immediately by re-directing the phase wires L1 to L3 and L3 to L1, enabling a switched phase direction to the motor induction coil.

## 5. Laboratory results

---

- The level sensor did not trigger the relay QR01 in the control cabinet and the Q3-contactor for the water pump was activated when the switching power supply were on. The direction of wiring on the solid state relay is determined by the internal diodes and circuitry. The problem was solved by switching the output terminal connections on the relay to Q3, which was before only directing the voltage to the contactor without any relay operation.

### 2. Control cabinet, control valves front panel pilot light (PL4)

- The pilot light for the control valves, indicating that the power supply of 24 VDC was on, were not working. This was due to the pilot light series alignment in supply branch for the control valves, ending in ground potential and not on the negative 24 VDC branch. This was solved by connecting the light in parallel with the valves seen in Appendix C, Figure C.1.

### 3. Control valves, Choke valve re-wiring

- A larger part of the troubleshooting was spent aiding the work of getting the control valves operational. The choke valves Asco 290-series Proportional Positioner was installed and wired with a molded cable. The connections were tested according to the datasheet of the 5 pin DIN plug. However, the connections were incorrectly wired on the terminal side on the choke valve. After re-wiring each of the two valves, the 24 VDC supply were seen to initiate the valve (LED glowing) and by visual inspection it was able to operate the seat with the pneumatic air supply.
- A common problem for both choke valves and the turbine inlet air control valve were that the chosen DAQ unit outputs are limited to approximately half of the 20 mA control signal. The circuit were wired on a breadboard, converting the 0 to 5V output of the DAQ to a corresponding 4 to 20 mA signal. However, the impedance of the output port is too large to generate the portion of the signal beyond approximately 10 mA. This limited the stroke operation of the valve, not being able to reach full-open. Since the anti-surge valve is either full-open or full-closed and controlled by a solid-state relay, this is not a problem for this valve. The solution was to order an auxiliary powered DAQ signal unit, to supply the valves with sufficient input signal.

An excerpt of the 24 VDC circuit is presented in Figure 5.13. Referring to 2 in Section 5.3.1, the parallel wiring is seen in branch number 2 with for PL4. In this drawing, the voltage supply for the control valves are presented and not the switching logic associated with the DAQ. This is to separate the 24 VDC from the 10 and 5 VDC wiring the DAQ units are configured with. The drawing is limited to the 24 VDC switching logic and equipment supply for the laboratory.

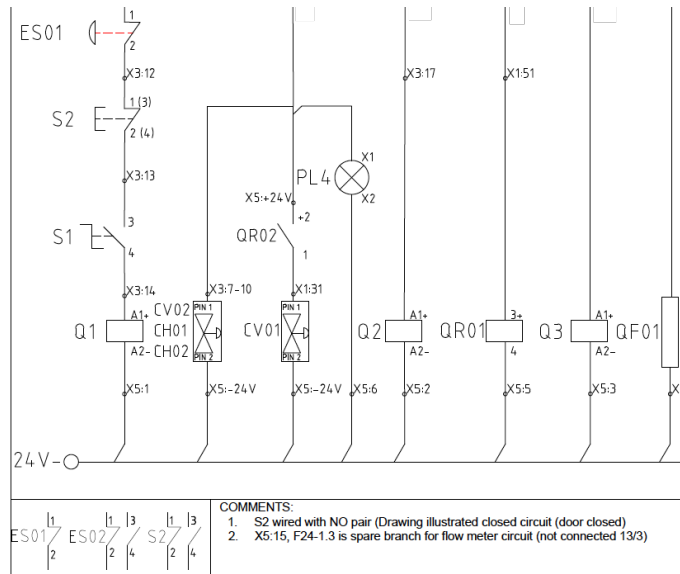


Figure 5.13: A section of the 24 VDC control circuit drawing

### 5.3.2 Protocol operation

A part of this thesis has been to contribute with the documentation of the WGC laboratory. An operational protocol, describing the startup, operation and shutdown of the laboratory is developed by the author. This document, being available at the laboratory location, is intended to direct the personnel to perform the correct operation of manual valves and software corresponding to each individual test scenario.

The protocol includes information of HSE according to NTNU specifications and contact information for the HSE, operators and personnel being responsible for the laboratory. The full document is included in Appendix E.



# Chapter 6

## Discussion, conclusions and recommendations for further work

This chapter includes the discussion on important topics from the work, the final conclusions and further recommendations for continued work on the topic.

### 6.1 Discussion

#### Corrections to the empirical compressor characteristic

The empirical characteristic relies on the supplied compressor map from the GT2252 turbocharger. The zero mass flow pressure ratio point on the map was estimated with (3.31), for isentropic gas flow and gave the assumed minima for each characteristic curve. This result was used since it was considered the best estimate in the low mass flow region of the map. However, the negative flow region of the compressor map is not shown for GT2252 and estimating this region is not covered by the first principle model. In this work, the approach similar to the work in [42] was taken to extend the empirical characteristic in this region by evenly distribute negative pressure ratio points with an estimated interval. Then, a characteristic curve reflected the pressure ratio in the negative flow region by comparing it to literature findings. However, the result and the approach for the negative flow region are a rough simplification and will most likely not predict the actual behaviour of GT2252 operating in this region.

#### A discussion on model selection

The two models, Greitzer and the centrifugal compressor model are describing the dynamic behavior of a compressor. In the specialisation project, the Greitzer model and the performance calculations developed by Shultz were argued to be a proper foundation for predicting accurate compressor behaviour. However, the two dynamic models are different from the Shultz procedure being a static iterative procedure calculating the pressure ratio and state variables for the compressor. The static modelling does not consider the performance during run-time of the process, only calculating the final product at a defined step in the procedure. In the dynamic model, the time plays an essential role were process conditions are displayed

## 6. Discussion and conclusions

---

during each time step. Due to the model differences, the Greitzer model incorporating an empirical compressor characteristic from known datasheet was used as a comparison foundation to the centrifugal models physical phenomena characteristic.

### Choke flow in the models and controller design

The result of simulating the compressor models with constant speed drove the compressor operating point into the choke flow region when the mass flow and plenum pressure reached an equilibrium state. This is a problem if the dynamics are adapted to the equivalent realistic turbocharger in the laboratory since choke flow stalls the mass flow and leads to a sudden pressure drop. The models are based on predicting surge and general compressor performance. In this work, this has not been included in the simulations and control due to the complex phenomena and difficulty in modelling. However, it is important to state that the uncertainties for the work on developing a controller is increasing with the unmodelled phenomena of choke flow in the compressor.

The speed of sound of the gas flow is significantly reduced for reduced GVF in the typical definition spectre of wet gas (down to 95% GVF) [62]. This dependency was not included in the simulations with wet gas parameters for the centrifugal compressor model. The speed of sound were modelled into the plenum mass balance equation and decreasing this yields a larger rate of change for the plenum pressure. Reduced speed of sound also increases the chances for choke flow, as the impeller gas flow relative velocity might reach the sonic velocity of the local gas flow faster in the impeller. However, the wet gas parameter study were limited, due to the complexity of including all of the interactions a gas flow with liquid presents in a compressor.

### GT2252 impeller design towards wet gas tests

One aspect of the impeller design is the shroud, encapsulating the impeller blades. For dry gas impeller tests with wet gas, see for example [45] (open-loop setup, performed at NTNU), [13, 63] (both closed-loop setup), the shrouded impeller design has been used. It is pointed out in [45], that the unshrouded design of the impeller is not applicable for wet gas test. The shrouded design is coherent for low design flow coefficient, indicating higher flow resistance and larger pressure drop due to increased friction in the impeller passages [25]. For GMF down to 48% the test in [45] showed a small increase in pressure ratio. The wet gas compression tests which will be conducted in the WGC laboratory is on a unshrouded impeller design. On the note pointed out here, the test might not be valid.

It is also a challenge in the dry gas centrifugal model, to develop a characteristic with wet gas properties showing pressure ratio increase for low gas flows. Therefore, the experiments in the simulations were restricted to the developed controller with a model imitating a quasi-wet gas behaviour.

### Validity of gain scheduling controller

The GS controller have been developed for process control in the normal operating region of the compressor (seen between the surge and choke line in Figure 2.11). In relation to the initial phase of the WGC laboratory, the anti-surge control method is surge avoidance.



A recycle valve is installed to ensure minimum flow to the compressor inlet. If the GS controller is implemented for the GT2252 turbocharger in the WGC laboratory, this control algorithm is separated from the anti-surge part. Pointed out by [77], is that the anti-surge control algorithm is an extensive study, where stand alone PI control might not be sufficient. Therefore, the argument of towards not developing a controller for surge mitigation is related to the practical setup of the process loop installed by [10]. A consequence of this argument was that the controller were not tested towards surge in the simulations.

The tuned GS controller integral time  $\tau_i$  did not reflect a large change for the maximum and minimum GS variable, compared to the proportional gain  $K_c$  being increased by a factor close to 2. The values was presented in Table 4.8. The controller was not tested with a constant  $\tau_i$ . However, keeping  $\tau_i$  fixed with GS-control would probably show the same performance as with a GS with varying  $\tau_i$ . The opposite scenario was shown to occur for the initial GS settings in Table 4.7, where  $K_c$  could be considered constant.

The result of increasing the proportional gain of the GS controller for decreasing GVF of the gas flow showed a high frequency control signal. A low pass filter were used to represent some unmodelled dynamics of a turbine, to emulate a delay in the rotational speed build up for the compressor. The high frequency control signal simulated to adjust the turbine inlet pressure control valve, were smoothed by the low pass filter. By just taking into account the gain factor  $\Delta K$ , the high frequency signal was shown to be worst for the theoretically calculated factor from the process gain. Using this in the real system, implies that the controller valve is working rapidly. Since it is built with mechanical components, the assumption of early breakdown may be reasonable due to overload on the shaft with the valve seat. The assumptions of only changing the proportional gain may not be adequate, since the time constant dynamics will most likely change with the dynamics of wet gas.

The GS controller is considered a first step for the WGC laboratory turbocharger, with or without wet gas flow. The parameters used in the simulation are based on the laboratory fluid properties, temperatures and dimensions. The first principle characteristic, being the main compressor property attained from the GT2252 map has been validated with the simulation model. The accuracy is not declared properly, since correction factors are commonly applied for the compressor map generation. This was not done when illustrating the steady state behaviour of the models. However, the outcome of simulation with both characteristics is suggested to be used in the laboratory as an initial step. The GS controller will most likely be re-tuned and validated when implemented in the laboratory.

### Laboratory test run 26th of May 2017

A short test run of the facility was performed in the end of May, to test the functionality of all the valves, separator, cooler and turbocharger. Manual control were used for the choke and control valves through the Labview control system. The test was performed with dry gas (air) at atmospheric temperature and pressure. The pipeline were pressurised up to 2 barg, being the standard procedure. After starting the turbocharger, the inlet turbine supply valve (CV02) was kept at 65%, with a differential pressure of 4.9 barg. The valve opening gave a rotational speed of approximately 51000 rpm resulting in a compressor pressure ratio of 1.2, with a flow discharge temperature of approximately 65°C. The counter flow cooler sufficiently cooled the gas flow down to 21°C. Operation of the choke valves showed little to

## 6. Discussion and conclusions

---

none pressure change at the suction port of the compressor and was kept constant at 100% open.

The results of further increasing the opening of CV02 gave little increase in the turbocharger speed. The inlet pressure dropped in the pneumatic supply line, resulting in an insufficient pressure and gas flow on the turbine side. This occurred rather quickly and the build up time with CV02 closed was approximately 5 minutes from 3 barg to 8 barg being the maximum capacity of the workshop air supply. Alone, the turbocharger may not be sufficient to produce the required flow rate, with the inlet pneumatic air supply from the facility. The rapid decrease in pneumatic air supply when operating the turbocharger also limits the achievable rotational speed and pressure ratio.

With a decreasing pneumatic air supply as a result of turbocharger operation, the rest of the system is also likely to be influenced. The opening of the choke valves are actuated with the pneumatic air supply, and therefore they may be non-functional for insufficient air supply. The solution to this situation will be to install a separate rig pneumatic air supply, ensuring sufficient air pressure and flow for turbocharger operation.

### 6.2 Conclusions

The GT2252 turbocharger has been the subject for simulation modelling and control in this work. The compressor components on the turbocharger has been analyzed. The impeller is a backwards curved, unshrouded design with 12 blades where 6 are splitter blades. The impeller inducer and exducer blade angle has been measured for use in the simulation of compressor models. The GT2252 compressor map has been sampled in MATLAB. The map presents the performance in terms of pressure ratio, corrected mass flow and limitations towards operational speed. This was done to establish two compressor characteristics for the compressor.

Two compressor models have been presented. The centrifugal model derived in [40] and the Greitzer model in [43] were selected in the specialisation project review, on behalf of the potential for wet gas compressor modelling (Gravdahl) and the comparison towards a semi-empirical compressor model (Greitzer) for accuracy of dry gas modelling. The first principle characteristic developed by [40] has been presented and evaluated with LSQ curve fit tool in MATLAB. The parameters for this characteristic has been optimised towards the best fit for each constant speed line. The zero mass flow points for the characteristic were calculated with the derivation showed in [42]. An empirical characteristic drawn directly from the sampled compressor map speed lines has been developed. The approach was equal to the work in [42]. The zero mass flow points were equal to the first principle characteristic and the negative region of the map were estimated to produce a complete characteristic for comparison. The result is in favour for the empirical characteristic, where the 155000 rpm curve had a mean absolute error of 0.051 for a 3rd degree polynomial fit compared to the first principle fit of 0.1324.

The simulation validity of both the centrifugal and the Greitzer model has been performed. The first principle characteristic were implemented in the centrifugal model and the empirical one in the Greitzer model. Both steady-state were simulated and surge behaviour were initiated for the two models by simulating a throttle gain reduction. The centrifugal model has been subject to a controller tuning study, for direct single PI control on the com-

pressor speed. SIMC tuning rules in [98] and Ziegler-Nichols revisited PI rules in [52] were used. The tuning result achieved with SIMC tuning with closed loop response time  $\tau_c = \tau_1$  showed the best overall performance given the criteria of no overshoot for the model plenum pressure. However, the settings had the largest IAE values for both setpoint change and load disturbance perturbations.

The SIMC tuning rules were further used in the development of a compressor GS controller. The control area were constrained to the normal operating region of the GT2252 compressor map. The throttle mass flow was selected as the scheduling variable and 6 operating points were used to define the non-linear behaviour for the centrifugal compressor model. The scheduling algorithm was developed with predetermined 3rd-degree polynomial characteristics, calculating new controller settings continuously during run-time for a time-dependent scheduling variable. The GS controller was tuned with  $\tau_c = 0.002$  and  $\theta = 0.0005$  s (Simulation time step  $t_s = 0.0001$  s) increasing the performance towards set point and load disturbances (throttle gain reduction) compared to a single PI controller tuned with the same procedure. The tuned GS controller were proficient towards model changes. This was tested by interchanging the compressor characteristics for the centrifugal model.

A wet gas compressor characteristic has been developed empirically with the compressor parameters inlet gas density, gas heat capacity at constant pressure and impeller gas flow friction loss. The characteristic showed to resemble the properties of what has been found in experiments conducted on centrifugal dry gas compressors (see [45, 63]). The GS controller has been subject to testing with this wet gas characteristic and the performance has been evaluated with 5 constant GVF values and a ramped GVF from 100 % to 99.95 %. The simulated wet gas increased the necessary control input in terms of drive shaft speed. The saturation limit of 195000 rpm was reached for GVF levels lower than 99.95 % corresponding to a GMF of 70.7 %. This result corresponds with an increase in power requirement on the drive, for centrifugal dry gas compressors being tested with wet gas.

The GS-controller developed in this work is proficient as an initial controller for the WGC laboratory turbocharger, based on the simulation model parameters. The parameters used to define the controller and simulation environment can act as a first stage for the control system.

The author has contributed in the extended planning and construction of a small scale wet gas compression test rig at the Department of Mechanical and Industrial Engineering. The main responsibility has been the laboratory electrical wiring, with high voltage side in the control cabinet. Control circuit and main power supply circuit drawings have been revised and approved with a factory acceptance tests. An operational procedure document for startup, operation and shutdown have been produced by the author as a necessary supplement to the rig. The rig has been tested with initial pipeline pressure of 2 barg, working separator, cooler and turbocharger. However, the limitation was proven to be on the turbine inlet supply side where insufficient air flow and pressure constrained the allowable shaft speed on the compressor.

### 6.3 Recommendations for further work

The author has given critics and discussed potential improvement to the work in this thesis. The topics are on corrections to the empirical characteristic, modelling the choke flow condition and impeller design validity towards wet gas testing. Taking this into consideration, and the conclusion topics from the previous section, a set of recommendations for further work on the thesis subject are given.

1. The WGC laboratory must be completed and operational before testing the controller developed in this work. The final stage on the laboratory is to ensure sufficient air supply to the turbine inlet, throughout the experiments.
2. Extend the control system environment with gain scheduling control on the turbocharger.
3. After 2 is performed: Implement and evaluate the gain scheduling controller towards both dry gas (air) and wet gas (air-water mixture) in the WGC laboratory.
4. Confirm the emulated wet gas characteristic found in this work towards wet gas in the laboratory, by establishing an empirical wet gas characteristic for the GT2252 turbocharger.

Recommendation 4 is only valid if the impeller geometry is shrouded, being a subject pointed out in [45]. Due to the scale of the laboratory, and the work of installing a new compressor with a shrouded impeller, preliminary test should be performed on the GT2252 turbocharger.

## References

- [1] S. Abdallah and R. Schwind. A look at compressor impeller technologies for turbochargers focusing on surge mitigation. *Glob J Tech Opt*, 06(03), 2015.
- [2] L. C. P. Aguilera. Subsea wet gas compressor dynamics. Master's thesis, Norges Teknisk-Naturvitenskapelige Universitet, Fakultet For Ingeniørvitenskap og Teknologi, 2013.
- [3] A. Anderson. Simple first-order models for surging in pump and compressor systems. *Proceedings of the Institution of Mechanical Engineers, Part C: Journal of Mechanical Engineering Science*, 209:149–154, 1995. ISSN 09544062.
- [4] ASME. ASME PTC 10: Performance test code on compressors and exhausters, 1997.
- [5] K. J. Astrom and T. Hagglund. *Advanced PID Control*. ISA, 2005.
- [6] Y. Bai and Q. Bai. *Subsea Engineering Handbook*. Elsevier Science, 2010. ISBN 9781856176897.
- [7] J. D. Bendtsen, J. Stoustrup, and K. Trangbaek. Bumpless transfer between observer-based gain scheduled controllers. *International Journal of Control*, 78(7):491–504, 2005.
- [8] T. Bjørge and L. Brenne. Subsea gas compression; available technology and future needs. In *Statoil Hydro Presentation, The Research Council of Norway*. The Research Council of Norway, 2010.
- [9] H. P. Bloch and C. Soares. *Process Plant Machinery*. Elsevier Science, Burlington, 1998.
- [10] M. B. Bordal, E. Flatlandsmo, and J.-H. K. Medby. Subsea gas boosting laboratory: Design and construction. Master's thesis, Department of Production and Quality Engineering, Norwegian University of Science and Technology, 2016.
- [11] M. P. Boyce. Principles of operation and performance estimation of centrifugal compressors. In *Proceedings of Turbomachinery Symposium*, volume 22, pages 161–177, 1993.
- [12] O. Bratland. Pipe flow 2. In *Multiphase Flow Assurance*. (n.p.), 2013. ISBN 978-616-335-926-1.

## References

---

- [13] L. Brenne, T. Bjørge, J. L. Gilarranz, J. Koch, and H. Miller. Performance evaluation of a centrifugal compressor operating under wet-gas conditions. In *Proceedings of the 34th Turbomachinery Symposium*, pages 111–120, 2005.
- [14] L. Brenne, T. Bjørge, L. E. Bakken, and Ø. Hundseid. Prospects for sub sea wet gas compression. *ASME Turbo Expo 2008: Power for Land, Sea, and Air*, 7:671–672, 2008. doi: doi:10.1115/GT2008-51158.
- [15] G. O. Brown. The history of the darcy-weisbach equation for pipe flow resistance. In *Environmental and Water Resources History*, pages 34–43. ASCE National, Washington D.C, 2003.
- [16] Cameron. Subsea multiphase compressor, 2016. URL <http://cameron.slb.com/onesubsea/technology-and-innovation/processing-systems/multiphase-compressor>. Accessed 20.11.2016.
- [17] F. Chu, F. Wang, X. Wang, and S. Zhang. A model for parameter estimation of multistage centrifugal compressor and compressor performance analysis using genetic algorithm. *Sci. China Technol. Sci.*, 55(11):3163–3175, 2012. ISSN 1674-7321.
- [18] A. Cortinovis, D. Pareschi, M. Mercangoez, and T. Besselmann. Model predictive anti-surge control of centrifugal compressors with variable-speed drives. *IFAC Proceedings Volumes*, 45(8):251–256, 2012. ISSN 1474-6670.
- [19] B. de Jager. Rotating stall and surge control : a survey. *Proceedings of the 34th Conference on Decision and Control*, 34:1857–1862, 1995. ISSN 0-7803-2685-7.
- [20] R. Dehner, A. Selamet, P. Keller, and M. Becker. Simulation of deep surge in a turbocharger compression system. *Journal of Turbomachinery*, 138, 2016. doi: 10.1115/1.4033260. URL [http://turbomachinery.asmedigitalcollection.asme.org/data/Journals/JOTUEI/935297/turbo\\_138\\_11\\_111002.pdf](http://turbomachinery.asmedigitalcollection.asme.org/data/Journals/JOTUEI/935297/turbo_138_11_111002.pdf).
- [21] S. L. Dixon and C. A. Hall. *Fluid Mechanics and Thermodynamics of Turbomachinery (Sixth Edition)*. Butterworth-Heinemann, Boston, 2010. ISBN 978-1-85617-793-1. doi: <http://dx.doi.org/10.1016/B978-1-85617-793-1.00001-8>. URL <http://www.sciencedirect.com/science/article/pii/B9781856177931000018>.
- [22] J. Doke. Grabit, extracts data points from an image file, 2016. URL <https://se.mathworks.com/matlabcentral/fileexchange/7173-grabit>. Accessed: 23.01.2016.
- [23] O. Egeland and J. T. Gravdahl. *Modelling and Simulation for Automatic Control*. Marine Cybernetics, Trondheim, Norway, 2002. ISBN 82-92356-01-0.
- [24] Emerson. Asco series 290, 2017. URL <http://www.asco.com/en-us/Pages/solenoid-valve-series-290.aspx>. Accessed: 17.05.2017.
- [25] A. Engeda. Design considerations for a very low flow coefficient impeller. *Proceedings of the 1999 3rd ASME/JSME Joint Fluids Engineering Conference, FEDSM'99, San Francisco, California, USA, 18-23 July 1999 (CD-ROM)*, page 1, 1999.

- [26] K. Eriksson and K. Antonakopoulos. Subsea processing systems: Optimising the maintenance, maximizing the production. *Offshore Technology Conference, OTC 24688*, 2014. doi: DOI:10.2118/24688-MS. Aker Solutions.
- [27] L. Eriksson and L. Nielsen. *Modeling and Control of Engines and Drivelines*. Chichester, UK: John Wiley & Sons, Ltd, Chichester, UK, 2014. ISBN 9781118479995. doi: 10.1002/9781118536186.
- [28] V. Ferrara. *Wet gas compressors - stability and range*. PhD thesis, Department of Energy and Process Engineering, Norwegian University of Science and Technology, Trondheim, 2016.
- [29] D. A. Fink, N. A. Cumpsty, and E. M. Greitzer. Surge dynamics in a free-spool centrifugal compressor system. *Journal of Turbomachinery*, 114:321–332, 1992. ISSN 0889504X.
- [30] W. E. Forsthoffer. 3 - compressor best practices. In *Forsthoffer's Best Practice Handbook for Rotating Machinery*, pages 93–228. Butterworth-Heinemann, Boston, 2011. ISBN 978-0-08-096676-2. doi: <http://dx.doi.org/10.1016/B978-0-08-096676-2.10003-7>.
- [31] Garrett by Honeywell. Gt2252, 2016. URL <https://turbobygarrett.com/turbobygarrett/turbochargers/gt2252>. Accessed: 17.01.2016.
- [32] Garrett by Honeywell. Turbo tech advanced, 2016. URL [https://turbobygarrett.com/turbobygarrett/turbo\\_tech\\_advanced](https://turbobygarrett.com/turbobygarrett/turbo_tech_advanced). Accessed: 09.02.2016.
- [33] G. O. . Gas. Statoil's snøhvit project, 2017. URL <https://www.geoilandgas.com/case-study/statoils-snohvit-project>. Accessed: 31.03.2017.
- [34] A. Ghanbariannaeni and G. Ghazanfarihashemi. Protecting a centrifugal compressor from surge. *Pipeline & Gas Journal*, 239(3), 03 2012. URL <https://pgjonline.com/2012/04/02/protecting-a-centrifugal-compressor-from-surge/>.
- [35] L. Giarré, D. Bauso, P. Falugi, and B. Bamieh. Lpv model identification for gain scheduling control: An application to rotating stall and surge control problem. *Control Engineering Practice*, 14(4):351–361, 2006.
- [36] J. L. Gilarranz, H. A. Kidd, G. Chochua, and W. C. Maier. An approach to compact wet gas compression. *Proceedings of ASME Turbo Expo 2010:GT2010-23447*, 2010.
- [37] R. S. R. Gorla and A. A. Khan. *Turbomachinery: Design and Theory*. Mechanical Engineering. Baton Rouge : CRC Press, Baton Rouge, 2003. ISBN 0-8247-5636-3.
- [38] S. F. Graebe and A. L. Ahlen. Dynamic transfer among alternative controllers and its relation to antiwindup controller design. *IEEE Transactions on Control Systems Technology*, 4(1):92–99, 1996.
- [39] J. T. Gravdahl. *Modeling and control of surge and rotating stall in compressors*. PhD thesis, Department of Engineering Cybernetics, Norwegian University of Science and Technology, 1998.

## References

---

- [40] J. T. Gravdahl and O. Egeland. *Speed and surge control for a low order centrifugal compressor model*. Proceedings of the 1997 International Conference on Control Applications. Hartford, CT,, 1997. ISBN 0-7803-3876-6. doi: 10.1109/CCA.1997.627573.
- [41] J. T. Gravdahl and O. Egeland. Compressor surge control using a close-coupled valve and backstepping. In *American Control Conference, 1997. Proceedings of the 1997*, volume 2, pages 982–986. IEEE, 1997.
- [42] J. T. Gravdahl, O. Egeland, and S. O. Vatland. Active surge control of centrifugal compressors using drive torque. *Proceedings of the IEEE Conference on Decision and Control*, 2:1286–1291, 2001. ISSN 01912216.
- [43] E. M. Greitzer. Surge and rotating stall in axial flow compressors—part i: Theoretical compression system model. *Journal of Engineering for Power*, 98:190, 1976. ISSN 00220825. doi: 10.1115/1.3446138. URL [http://gasturbinespower.asmedigitalcollection.asme.org/data/Journals/JETPEZ/26724/199\\_1.pdf](http://gasturbinespower.asmedigitalcollection.asme.org/data/Journals/JETPEZ/26724/199_1.pdf).
- [44] E. M. Greitzer. Surge and rotating stall in axial flow compressors—part ii: Experimental results and comparison with theory. *Journal of Engineering for Power*, 98:199, 1976. ISSN 00220825. doi: 10.1115/1.3446139. URL [http://gasturbinespower.asmedigitalcollection.asme.org/data/Journals/JETPEZ/26724/199\\_1.pdf](http://gasturbinespower.asmedigitalcollection.asme.org/data/Journals/JETPEZ/26724/199_1.pdf).
- [45] T. G. Grüner and L. E. Bakken. Wet gas impeller test facility. In *ASME Turbo Expo 2010: Power for Land, Sea, and Air*, pages 705–712. American Society of Mechanical Engineers, 2010.
- [46] T. G. Grüner and L. E. Bakken. Instability characteristic of a single-stage centrifugal compressor exposed to dry and wet gas. In *ASME Turbo Expo 2012: Turbine Technical Conference and Exposition*, pages 881–890. American Society of Mechanical Engineers, 2012.
- [47] T. G. Grüner, L. E. Bakken, L. Brenne, and T. Bjørge. An experimental investigation of airfoil performance in wet gas flow. In *Proceedings of ASME Turbo Expo 2008: Power for Land, Sea and Air*, 2008.
- [48] J. S. Gudmundsson. Kompresjon og kompressorer. In *TPG4135*, pages 1–29. Univeristy Lecture at NTNU, 2010.
- [49] J. S. Gudmundsson. Trykktap i rørledninger. In *TPG4135*, pages 1–33. Univeristy Lecture at NTNU, 2010.
- [50] J. S. Gudmundsson. Tofase. In *TPG4135*, pages 1–13. Univeristy Lecture at NTNU, 2010.
- [51] J. S. Gudmundsson. Feltutbygging. In *TPG4135*, pages 1–27. Univeristy Lecture at NTNU, 2010.
- [52] T. Hägglund and K. J. Åström. Revisiting the ziegler-nichols tuning rules for pi control. *Asian Journal of Control*, 4(4):364–380, 2002.



- [53] M. A. Haidekker. *Linear Feedback Controls : The Essentials*. Elsevier insights Linear feedback controls. Elsevier Science, Burlington, 2013.
- [54] A. Hall, D. Griffin, and R. Steven. A discussion on wet gas flow parameter definitions. In *25th North Sea Flow Measurement Workshop*, 10 2007.
- [55] P. C. Hanlon. *Compressor handbook*. McGraw-Hill handbooks. McGraw-Hill, New York, 2001. ISBN 0070260052.
- [56] K. E. Hansen, P. Jorgensen, and P. S. Larsen. Experimental and theoretical study of surge in a small centrifugal compressor. *Journal of Fluids Engineering, Transactions of the ASME*, 103:391–395, 1981. ISSN 00982202.
- [57] F. Haugen. *Reguleringsteknikk*. Akademika forlag, Trondheim, 2012.
- [58] F. Haugen, R. Bakke, B. Lie, and F. Haugen. Temperature control of a pilot anaerobic digestion reactor. *Modeling, Identification and Control*, 34(3):99–117, 2013.
- [59] W. R. Hawthorne and J. H. Horlock. Actuator disc theory of the incompressible flow in axial compressors. *ARCHIVE: Proceedings of the Institution of Mechanical Engineers 1847-1982 (vols 1-196)*, 176(1962):789–814, 1962. ISSN 0020-3483.
- [60] J. V. Helvoirt. *Centrifugal Compressor Surge, Modeling and Identification for Control*. PhD thesis, Technische Universiteit Eindhoven, 2007.
- [61] M. Hjelmeland, A. B. Olsen, and R. Marjohan. Iptc 14231, advances in subsea wet gas compression technologies. *International Petroleum Technology Conference*, 2011.
- [62] Ø. Hundseid and L. E. Bakken. Wet gas performance analysis. *Proceedings from GT2006-91035*, 5:625–632, 2006. ISSN 0791842401.
- [63] Ø. Hundseid, L. E. Bakken, T. G. Grüner, L. Brenne, and T. Bjørge. Wet gas performance of a single stage centrifugal compressor. In *ASME Turbo Expo 2008: Power for Land, Sea, and Air*, pages 661–670. American Society of Mechanical Engineers, 2008.
- [64] G. Ingram. *Basic Concepts in Turbomachinery*. Grant Ingram & Ventus Publishing ApS, 2009. ISBN 978-87-7681-435-9.
- [65] ISA. ISA-5.1-2009, 2009.
- [66] J. G. . C. KG. Push-in rtd temperature probe with connecting cable, 2017. URL <http://www.jumo.de/products/temperature/rtd-temperature-probes/overview/902150/push-in-rtd-temperature-probe-with-connecting-cable-902150.html>.
- [67] M. King. *Process Control A Practical Approach*. United States: John Wiley & Sons Inc, 2010.
- [68] B. Kumar, D. DeRemer, and D. Marshall. Stator blade. In *An Illustrated Dictionary of Aviation*. McGraw-Hill Companies, Inc., 2005. URL <http://encyclopedia2.thefreedictionary.com/stator+blade>.

## References

---

- [69] J. Kurzke. Correlations hidden in compressor maps. *Proceedings of ASME Turbo Expo 2011*, 1:161–170, 2011. ISSN 9780791854617.
- [70] B. Lakshminarayana. *Fluid dynamics and heat transfer of turbomachinery*. Wiley, 1996.
- [71] Lutron. Pt100 ohm temperature probe, 2017. URL [http://lutron.com.tw/ugC\\_ShowroomItem\\_Detail.asp?hidKindID=1&hidTypeID=67&hidCatID=&hidShowID=556&hidPrdType=&txtSrhData=](http://lutron.com.tw/ugC_ShowroomItem_Detail.asp?hidKindID=1&hidTypeID=67&hidCatID=&hidShowID=556&hidPrdType=&txtSrhData=). Accessed: 12.05.2017.
- [72] MathWorks. Least-squares fitting, 2017. URL <https://se.mathworks.com/help/curvefit/least-squares-fitting.html>. Accessed: 15.02.2017.
- [73] MathWorks. Simulink: Simulation and model-based design, 2017. URL <https://se.mathworks.com/products/simulink.html>. Accessed: 26.04.2017.
- [74] MathWorks. Simulink solvers: Choose a solver, 2017. URL <https://se.mathworks.com/help/simulink/ug/types-of-solvers.html#f11-44943>. Accessed: 26.04.2017.
- [75] G. K. McMillan. *Centrifugal and Axial Compressor Control*. The Instrument Society of America, North Carolina, USA, 1983. ISBN 0-87664-744-1.
- [76] Mean Well. Single output switching power supply rs-100-series, 2017. URL <http://www.mouser.com/ds/2/260/RS-100-SPEC-806359.pdf>. Accessed: 02.03.2017.
- [77] S. Mirsky, J. Whirter, W. Jacobson, M. Zaghoul, and D. Tiscornia. Development and design of antisurge and performance control systems for centrifugal compressors. In *Proceedings of the Forty-Second Turbomachinery Symposium*, pages 1–3, 2012.
- [78] G. Mogseth and C. Holden. Subsea production. In *TPK4126*. Univeristy Lecture at NTNU, 2015. Accessed: 10.10.2016.
- [79] G. O. Musgrove, M. A. Poerner, M. Cirri, and M. Bertoneri. Overview of important considerations in wet gas compression testing and analysis. *3rd Turbomachinery & 30th Pump Users Symposia (Pump & Turbo 2014)*, 2014.
- [80] S. W. News. Norway gives green light for ormen lange plant expansion, 2017. URL <http://subseaworldnews.com/2017/02/10/norway-gives-green-light-for-ormen-lange-plant-expansion/>. Accessed: 21.03.2017.
- [81] Offshore Energy Today.com. The development of a true wet gas compressor, 2015. URL <http://www.offshoreenergytoday.com/the-development-of-a-true-wet-gas-compressor>. Accessed: 02.06.2017.
- [82] OG21. Strategy revision 2016, 2016. URL <http://www.og21.no/prognett-og21/2016/1254020156965>. Accessed 20.11.2016.
- [83] F. om elektriske lavspenningsanlegg (FEL). Vedlegg i. nasjonale tilpasninger, 1999. URL [https://lovdata.no/dokument/SF/forskrift/1998-11-06-1060#KAPITTEL\\_6](https://lovdata.no/dokument/SF/forskrift/1998-11-06-1060#KAPITTEL_6).

- [84] J. M. Øverli. *Strømningsmaskiner : 1 : Grunnlag*, volume 1. Tapir, Trondheim, 3 edition, 1992. ISBN 8251911001.
- [85] J. Pinsley, G. Guenette, A. Epstein, and E. Greitzer. Active stabilization of centrifugal compressor surge. In *ASME 1990 International Gas Turbine and Aeroengine Congress and Exposition*. American Society of Mechanical Engineers, 1990.
- [86] D. Prasad. The difference between a fat and a sat, 03 2012. URL <http://www.kneat.com/2012/03/29/the-difference-between-a-fat-and-a-sat/>. Accessed: 29.04.2017.
- [87] R. M. Ramberg and S. Davies. Statoil operating gullfaks, aasgard subsea compression systems. *Oil & Gas Journal*, 02 2016. URL <http://www.ogj.com/articles/print/volume-114/issue-5/special-report-offshore-petroleum-operations/statoil-operating-gullfaks-aasgard-subsea-compression-systems.html>. Accessed: 11.05.2017.
- [88] Z. A. Rofiqi. Review of wet gas compressor performance. Master's thesis, Norges Teknisk-Naturvitenskapelige Universitet, Fakultet For Ingeniørvitenskap Og Teknologi, 2014.
- [89] W. J. Rugh and J. S. Shamma. Research on gain scheduling. *Automatica*, 36(10): 1401–1425, Oct. 2000. ISSN 0005-1098. URL <http://www.sciencedirect.com/science/article/pii/S0005109800000583>.
- [90] SAFE. Fakta om kårstø, 2017. URL <http://statoil.safe.no/hjem/safe-land/lokal-info-land/karsto/>. Accessed: 11.05.2017.
- [91] B. Sandal. Undervannskompressor løftet på plass på kårstø. Aibel, 2013. URL <http://aibel.com/no/news-and-media/news/subsea-compressor-lifted-into-place-at-karsto>. Accessed: 11.05.2017.
- [92] P. Shakouri, A. Ordys, D. S. Laila, and M. Askari. Adaptive cruise control system: Comparing gain-scheduling pi and lq controllers. *18th IFAC World Congress*, 44 (1):12964–12969, Jan. 2011. ISSN 1474-6670. URL <http://www.sciencedirect.com/science/article/pii/S1474667016457034>.
- [93] A. N. Shell. Ormen lange, 2016. URL <http://www.shell.no/products-services/ep/ormenlange/no.html>. Accessed 20.11.2016.
- [94] Siemens. Siemens turbocompressor - single shaft horizontal split, axial design, 2017. URL <http://www.energy.siemens.com/mx/en/compression-expansion/product-lines/single-shaft-horizontal-split/stc-sx.htm#content=Design%20Concept>. Accessed: 30.03.2017.
- [95] Siemens. Siemens turbocompressor - single shaft, vertically split casing, 2017. URL <http://www.energy.siemens.com/co/en/compression-expansion/product-lines/single-shaft-vertical-split/stc-sv.htm#content=Design%20Concept>. Accessed: 30.03.2017.

## References

---

- [96] Siemens. Sinamics g120c built-in units, 2017. URL <http://w3.siemens.com/mcems/mc-drives/en/low-voltage-inverter/sinamics-g120c/Pages/sinamics-g120c-portlet.aspx>. Accessed: 18.05.2017.
- [97] Siemens. Sitrans p200/p210/p220, 2017. URL <http://w3.siemens.com/mcems/sensor-systems/en/process-instrumentation/pressure-measurement/pages/sitrans-p200-p210-p220.aspx>. Accessed: 12.05.2017.
- [98] S. Skogestad. Simple analytic rules for model reduction and pid controller tuning. *Journal of Process Control* 13 (2003) 291-309, 13(4):291–309, June 2003. ISSN 0959-1524. URL <http://www.sciencedirect.com/science/article/pii/S0959152402000628>.
- [99] J. Smeulers, W. Bournan, and H. Van Essen. Model predictive control of compressor installations. In *IMECHE Conference Transactions*, volume 6, pages 555–566. Mechanical Engineering Publications, 1999.
- [100] B. R. Sørensen. Forelesningsnotater, smn 6194 varmelære. In *Termodynamikk*, page 80. Høgskolen i Narvik, 2009.
- [101] Statoil. Subsea processing. In B. N. Tvetter, editor, *Statoil Presentation*. Univeristy Lecture at UiO, 2014. URL <http://www.uio.no/studier/emner/matnat/math/MEK4450/h14/undervisningsmateriale/module-1/uio-9sep2014-subsea-processing-birgitte--lecture-notes.pdf>. Accessed: 20.04.2017.
- [102] A. H. Stenning. Rotating stall and surge. *Journal of Fluids Engineering*, 102:14, 1980. ISSN 00982202. doi: 10.1115/1.3240618. URL [http://fluidsengineering.asmedigitalcollection.asme.org/data/Journals/JFEGA4/26955/14\\_1.pdf](http://fluidsengineering.asmedigitalcollection.asme.org/data/Journals/JFEGA4/26955/14_1.pdf).
- [103] N. Subpro. Laboratories and test facilities at subpro, 2017. URL <https://www.ntnu.edu/web/subpro/facilities>. Accessed: 11.05.2017.
- [104] N. Subpro. System control, 2017. URL <https://www.ntnu.edu/subpro/systemcontrol>. Accessed: 11.05.2017.
- [105] H. Tamaki. Effect of piping systems on surge in centrifugal compressors. *Journal of Mechanical Science and Technology*, 22:1857–1863, 2008. ISSN 1738-494X.
- [106] N. Tengesdal. *Wet Gas Compressors: State of the Art*. Specialization project report autumn 2016, 2016.
- [107] K.-H. Tu and J. S. Shamma. Nonlinear gain-scheduled control design using set-valued methods. In *American Control Conference, 1998. Proceedings of the 1998*, volume 2, pages 1195–1199. IEEE, 1998.
- [108] R. Vepa. *Dynamic Modeling, Simulation and Control of Energy Generation*, volume 20 of *Lecture Notes in Energy*. Springer London, London, London, 2013.
- [109] N. Watson and M. S. Janota. *Turbocharging the internal combustion engine*. Macmillan, London, 1982.

- [110] F. Willems and B. de Jager. Modeling and control of compressor flow instabilities. *Control Systems, IEEE*, 19:8–18, 1999. ISSN 1066-033X.
- [111] P. Yu, Y. Li, J. Wei, Y. Xu, and T. Zhang. Modeling the pressure drop of wet gas in horizontal pipe. *Chinese Journal of Chemical Engineering*, pages –, 2016. ISSN 1004-9541. doi: <https://doi.org/10.1016/j.cjche.2016.10.024>. URL <http://www.sciencedirect.com/science/article/pii/S1004954116306541>.



# Appendices





# Appendix A

## Measurements and calculations

This appendix includes the estimated angles on the impeller and data set for the zero mass flow points sampled in MATLAB.

### A.1 GT2252 impeller angle measurements

The impeller angles are determined manually by inspection and measured five times each. This gives an average for each of the two angles that are better approximated than performing the measurement once. This is due to the difficulty and uncertainty factor when measuring.

The inducer blade angle  $\beta_{1b}$  is assumed to follow the upper (at inlet) section of the blade, towards the hub. This is illustrated in Figure A.1. In the figure,  $U_1$  is the tangential velocity vector given by  $\omega r_1$ .

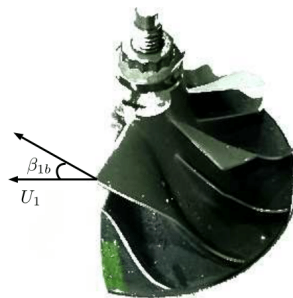


Figure A.1: Measuring the inducer blade angle  $\beta_{1b}$  on the impeller

The full data set for each measured angle is included in Table A.1.

### A.2 GT2252 zero mass flow values

The following expression is used to calculate the zero-mass flow points for each constant speed in rpm

## A. Measurements and calculations

Table A.1: Measured angles on impeller inducer and exit blade for GT2252

Measurement no.	$\beta_{1b}$	$\beta_{2b}$
1	11°	50°
2	44°	58°
3	15°	60°
4	19°	52.5°
5	18°	50°
Average ( $\tilde{\beta}_{1b}, \tilde{\beta}_{2b}$ )		21.4° 54.1°

$$\Psi_c(0, N) = \left( 1 + \frac{N^2 \pi^2 (D_2^2 - D_1^2)}{60^2 c_p T_{01}} \right)^{\frac{\kappa}{\kappa - 1}} \quad (\text{A.1})$$

where  $\Psi_c$  is the compressor pressure ratio,  $N$  is the speed in revolutions per minute,  $D_1$  is the inducer diameter,  $D_2$  is the impeller outer diameter,  $c_p$  is the specific heat at constant pressure in  $\text{J kg}^{-1} \text{K}^{-1}$  and  $T_{01}$  is the stagnation temperature. The process values in (A.1) are drawn from the WGC laboratory design phase by [10] and are summarised in Table A.2

Table A.2: WGC laboratory process values

$c_p$	1004.6	$\text{J kg}^{-1} \text{K}^{-1}$
$\kappa$	1.4	-
$T_{01}$	293.15	K

The temperature at inlet is assumed to 20°C at standard conditions. The calculated valley points  $\Psi_c(0, N)$  for each speed line on the map is presented in Table A.3.

Table A.3: Zero-mass flow values for each speed line, GT2252

$\Psi_c(0, N)$	N (rpm)
1.2140	75000
1.3582	95000
1.5526	115000
1.8092	135000
2.1431	155000
2.5742	175000
3.1276	195000

## Appendix B

# WGC Laboratory - Piping and Instrumentation Diagram

This appendix includes the full P&ID for the WGC laboratory. The standards used to draw the P&ID as part of this project, are ISO 10628-1 for chemical and petrochemical process applications together with the general symbols for graphical notation of mechanical components in ISO 14617-1. The drawing has been improved, using proper tags and symbols and including the new installed equipment. A section of the P&ID is shown in Figure B.1, including the turbocharger (V-002).

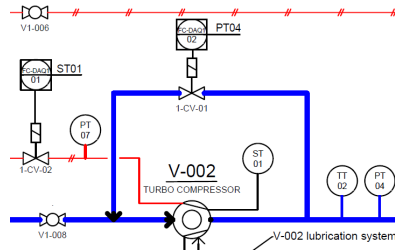


Figure B.1: P&ID for WGC laboratory, turbocharger section. Process line is marked with blue (thick line), pneumatic air line in red (straight line with two diagonal lines)

The numbering system for the instruments are made in ascending order (PT01, PT02, ...), matching it to the work done by the electrician at the laboratory in the autumn of 2016. The equipment tags for valves, vessels, pumps etc. in the schematic are made according to the International Society of Automation standard ISA 5.1 [65] shown in an example below:

V1-001

V - Valve, 1 - Valve category, 001 - Valve number (ascending order)

1-CV-01

1 - Area code, CV - Control Valve, 01 - Valve number (ascending order)

The instrument and equipment tag notation are included in the drawing nomenclature.

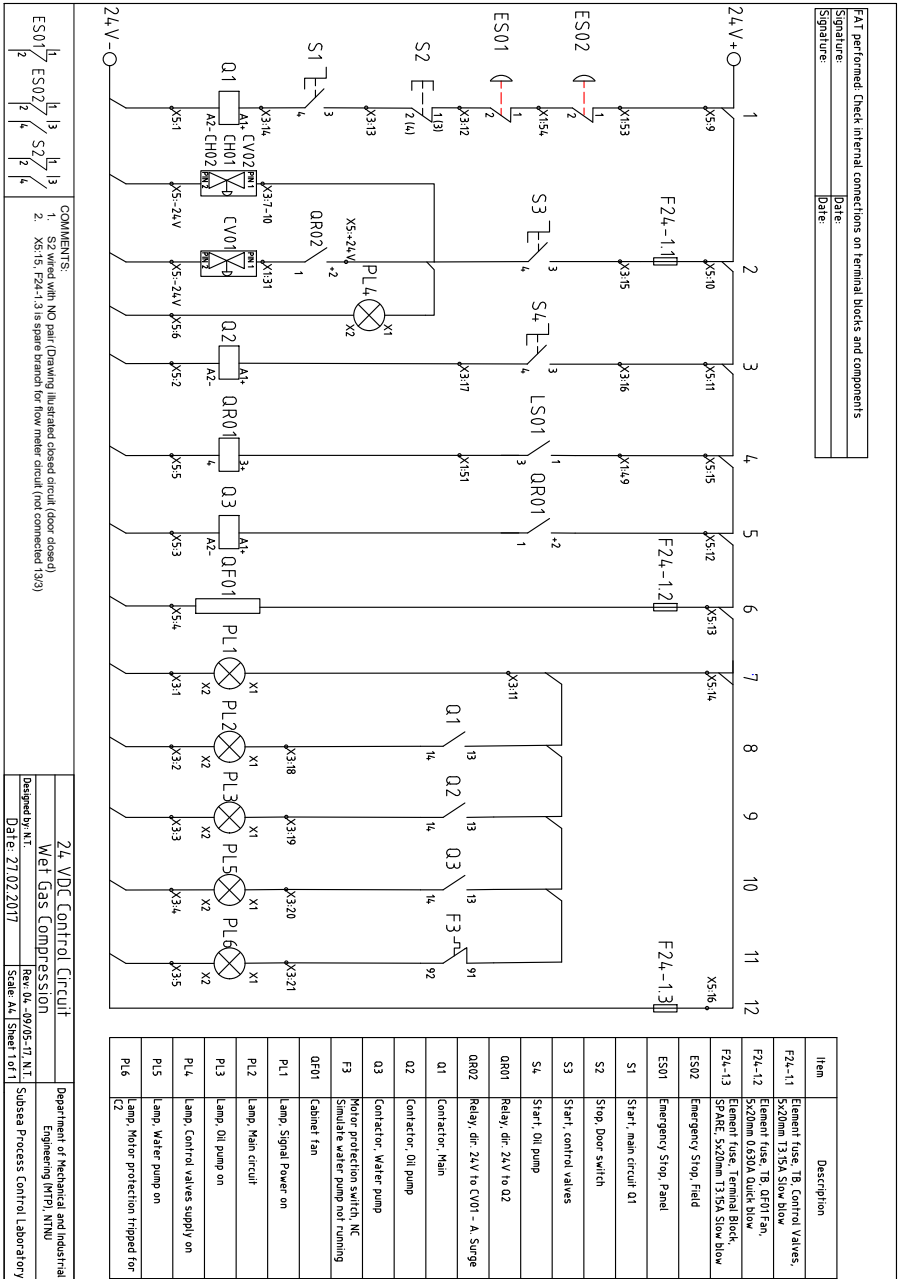


## Appendix C

### WGC Laboratory - Electrical circuits

This appendix includes the 24 VDC control circuit and 400/230 VAC main circuit schematics for the WGC laboratory. Both are originally in A4 format, but is rendered to fit in this thesis.

# C. WGC Laboratory - Electrical circuits



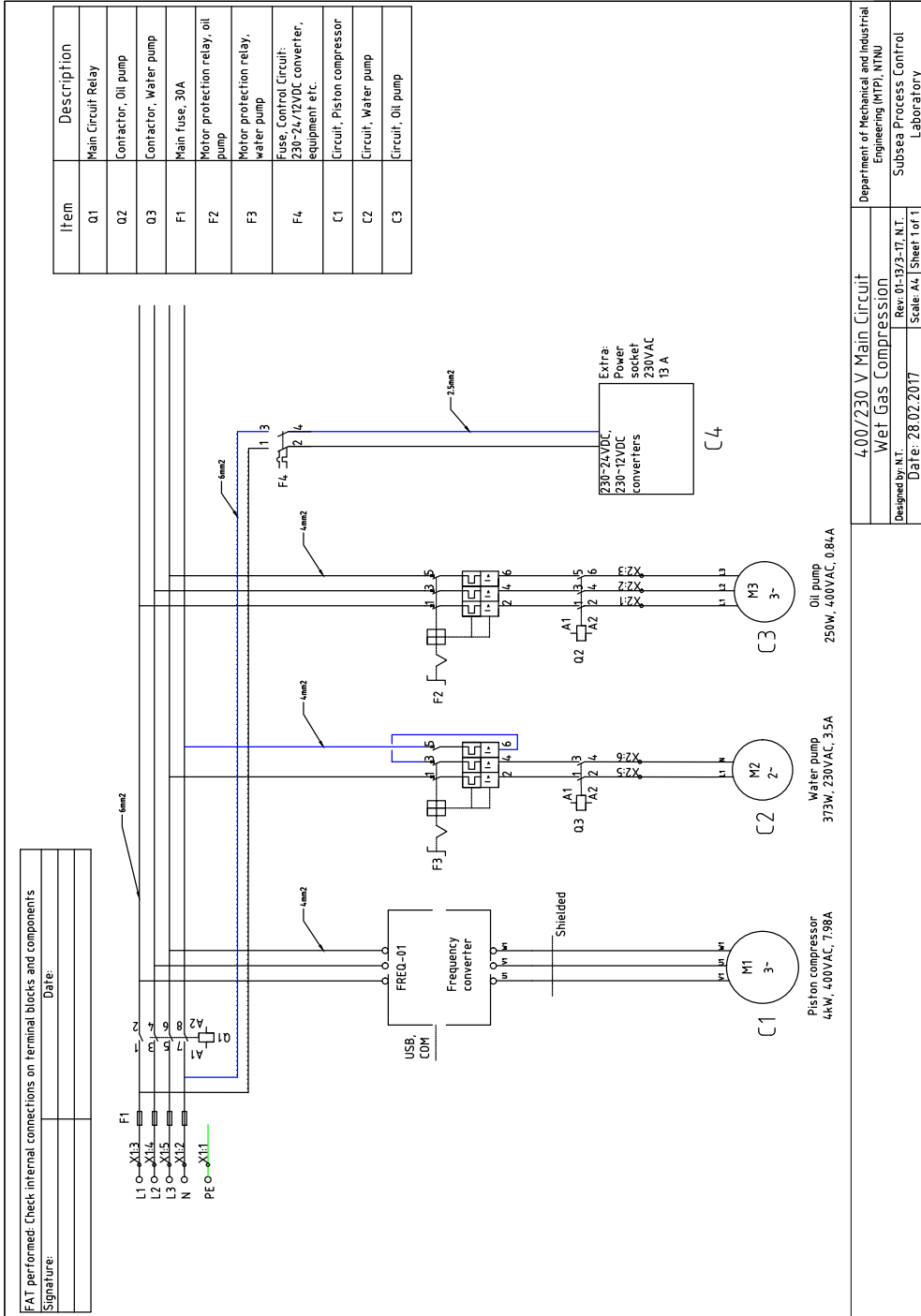


Figure C.2: 400/230 VAC main circuit CAD layout





## Appendix D

### WGC Laboratory - Circuit board arrangement

This appendix shows the circuit board arrangement in the control distribution box located at the WGC laboratory.

## D. WGC Laboratory - Circuit board arrangement

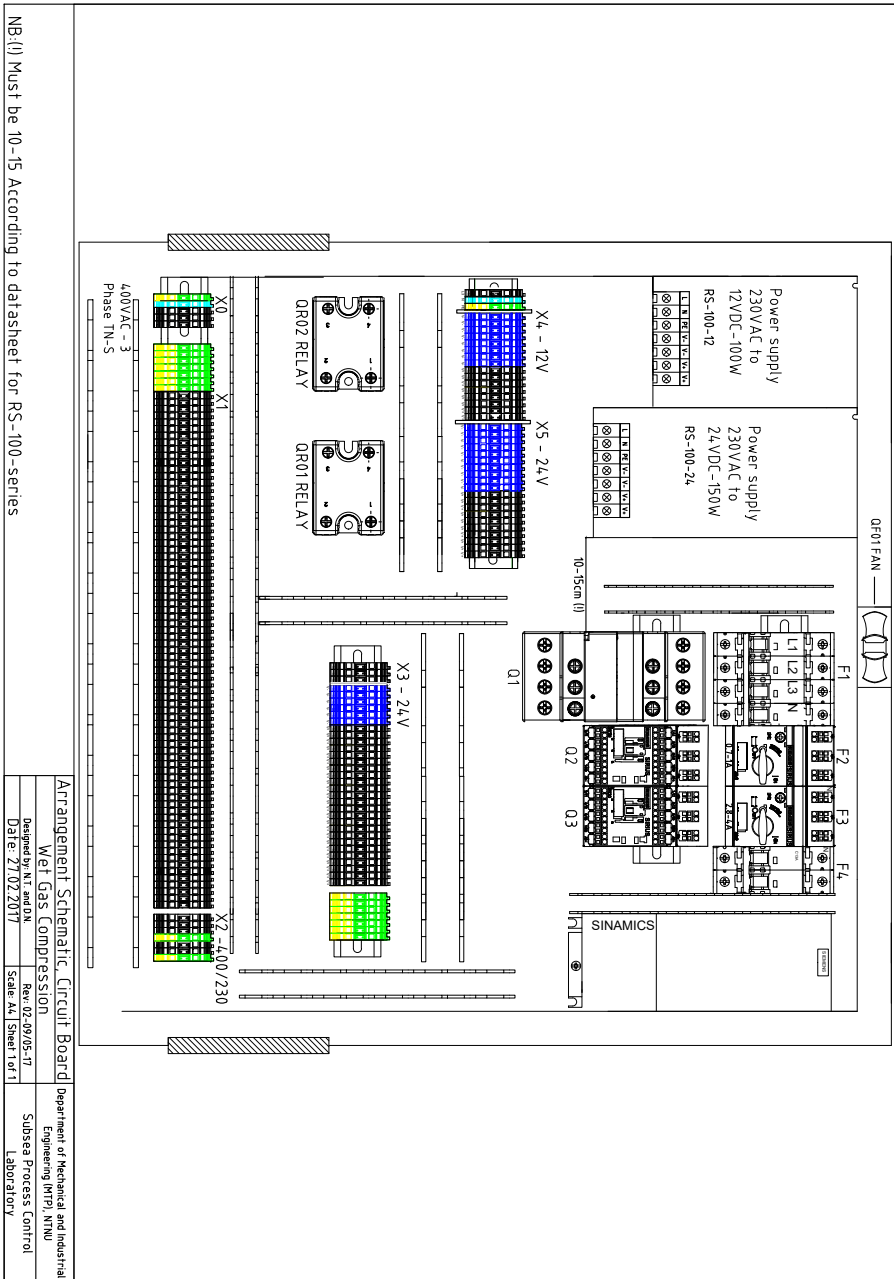


Figure D.1: Circuit board arrangement schematic

## Appendix E

### WGC Laboratory - Operation protocol

The WGC laboratory startup, operation and shutdown is described in this appendix. The operation protocol includes relevant information of test scenarios, HMS, manual and software adjustments to run the facility.

# Startup, operation and shutdown procedure

Wet Gas Compression Laboratory

May 2017

Subsea Process Control Laboratory

---

Title:  <h2 style="text-align: center;">Wet Gas Compression</h2>		
Dok. no.: 01	Rev. no.: 05	Date: 24.05.2017

Author(s): Njål Tengesdal	
Validity of this document: Wet Gas Compression laboratory, control cabinet, Labview software	
Faculty: Faculty of Engineering (IV)	Contact: Christian Holden, phone: 735 93 782
Department: Department of Mechanical and Industrial Engineering	

Approval signature:	Date:
1.	
2.	
3.	

## Table of Contents

1	Introduction .....	4
1.1	Operating scenarios .....	4
1.2	Nomenclature .....	4
1.3	Table nomenclature .....	5
2	HMS .....	6
2.1	Contact information .....	6
3	Commissioning .....	7
3.1	Laboratory startup .....	8
3.1.1	Dry gas startup .....	10
3.1.2	Wet gas startup .....	10
4	Laboratory operation (Case A – F) .....	12
4.1	Wet gas compression cases .....	12
4.2	Dry gas compression cases .....	15
5	Shut down procedure .....	18
6	Troubleshooting .....	19
7	References .....	20

---

## 1 Introduction

This document is made with the sole intention to ensure safe and efficient operation of the wet gas compression laboratory at MTP Valgrinda. The procedure of startup, operation and shutdown of the facility is based on the theoretical design made by [1] and [2].

The laboratory (lab) is a *Subsea Process Control Facility*, with the purpose of simulating the environment of a subsea installation. This includes piping, gas-liquid separation, gas compression (piston and centrifugal type) cooling with heat exchangers and control valves. The lab is instrumented with pressure, temperature, level and speed transmitters to complete the control system signal requirements for optimal control.

### 1.1 Operating scenarios

Modes of operations:

- Case A. Subsea separation and gas compression. Separator, piston and centrifugal compressor are active \*
- Case B. Subsea separation and gas compression. Piston compressor is bypassed
- Case C. Direct wet gas compression. Direct inlet wet gas to the centrifugal compressor, bypassing both the separator and the piston compressor
- Case D. Dry Gas Compression, bypassing the separator (No liquid injected) \*\*
- Case E. Dry Gas Compression II, only piston compressor is active (No liquid injected)
- Case F. Dry Gas Compression III, only centrifugal compressor is active (No liquid injected).

\* The piston compressor is not recommended to operate in the wet gas scenario. Please consult the laboratory responsible, or move on to Case B or C.

\*\* Case D - F follows the same start up protocols as A-C.

Note: The piston compressor is intended to be controlled by a variable frequency drive (VFD) located in the control cabinet, adjusting the speed of the crankshaft.

The procedures A-F explained in this document will have the system [Piping and Instrumentation Diagram \(P&ID\)](#) as reference available, included in Appendix A.

### 1.2 Nomenclature

- |        |                          |
|--------|--------------------------|
| - VFD  | Variable frequency drive |
| - GVF  | Gas Volume Fraction      |
| - LVF  | Liquid Volume Fraction   |
| - Barg | Bar gauge                |

### 1.3 Table nomenclature

This section explains the columns in the startup, operational and shutdown table procedures.

1. MANUAL VALVE ADJUSTMENT PROCEDURE BEFORE STARTUP				
2. Step	3. Action/Activity	4. Description/check	5. Confirm/check	

1. Headline, explaining the objective for the list of tasks
2. Operation steps, indicating the number of the current and following steps to be executed
3. Action or activity to be performed at the current step
4. Descriptive text of what the action or activity yields and/or an indication of what to check for in the environment
5. Confirm or check the result of the action or activity performed in 3.



---

## 2 HMS

The wet gas compression facility must be operated with **at least two** persons present to avoid harm or damage to personnel and equipment.

1. **Never** operate the facility without the permission from laboratory responsible (see Section 3).
2. **Follow** the workshop rules where the facility is stationed
3. **Use** hard boots and eye wear protection when operating the facility
4. **Never** open the control cabinet with electrical wiring without consulting trained personnel

For guidelines and regulations on performing work and experiments at NTNU laboratory and workshops, please consult the *Laboratory and Workshop Handbook* found at:

<https://innsida.ntnu.no/wiki/-/wiki/English/Laboratory+and+workshop+handbook>

Regulations for health, safety and environment according to NTNU in *HSE-Handbook for NTNU*:

[http://www.ntnu.no/c/document\\_library/get\\_file?uuid=bb98f1f9-a03d-4380-95d8-94e248ae7069&groupId=10137](http://www.ntnu.no/c/document_library/get_file?uuid=bb98f1f9-a03d-4380-95d8-94e248ae7069&groupId=10137)

### 2.1 Contact information

#### Laboratory Responsible:

Christian Holden                      Phone: 735 93 782                      Email: [christian.holden@ntnu.no](mailto:christian.holden@ntnu.no)

#### Main Safety Responsible at Valgrinda:

Kari Elise Dahle                      Phone: 735 97 123                      Email: [kari.e.dahle@ntnu.no](mailto:kari.e.dahle@ntnu.no)

#### Technical coordinator, Safety training

Øyvind Andersen                      Phone: 735 93 779                      Email: [ovvind.andersen@ntnu.no](mailto:ovvind.andersen@ntnu.no)

#### Electrical guidance and campus service

Lab inspector: Jørn Ove Blokkum      Phone: 918 97 417                      Email: [jorn.blokkum@ntnu.no](mailto:jorn.blokkum@ntnu.no)

Lead Discipline: Frode Dahl              Phone: 918 97 376                      Email: [frode.dahl@ntnu.no](mailto:frode.dahl@ntnu.no)

### 3 Commissioning

This section contains the startup procedure for dry gas and wet gas in the laboratory. Technical data on the laboratory is included in Table 3.1

Table 3.1 Volume specifications for the laboratory

Item	Description	Volume [ $m^3$ ]
Piping	Plastic, rubber and silicon piping	0.0380
F-001	Vertical gas-liquid separator	0.0967
W-002	Heat exchanger, cooling	0.0012
Total volume	Piping, F-001, W-002	0.1359

Gas volume fraction (GVF) and liquid volume fraction (LVF) measurements are included in Table 3.2. These are based on calculated values, and there may exist deviation from the real process conditions.

Table 3.2 GVF and LVF for the laboratory

GVF [%]	LVF [%]	$V_{water}$ [l]	$V_{water}$ [l]**	$V_{gas}$ [ $m^3$ ]	$V_{gas}$ [ $m^3$ ]**
95	5	6.795	1.96	0.1291	0.00196
96	4	5.436	1.568	0.1305	0.00157
97	3	4.077	1.176	0.1318	0.00118
98	2	2.718	0.784	0.1332	0.000784
99	1	1.359	0.392	0.1345	0.000392
99.5	0.5	0.6795	0.196	0.1352	0.000196
100	0	0	0	0.1359	0

\*\* - no separation

### 3.1 Laboratory startup

This section contains the preliminary procedure for startup and initiation of the facility with dry or wet gas. The following operations indicated in the section tables **must be followed from Table 1 to 3**.

1. MANUAL VALVE ADJUSTMENTS PRIOR LABORATORY STARTUP			
Step	Action/Activity	Description/check	Confirm/check
1	Close pneumatic supply valve	Close the supply valve located in the work shop	-
2	Connect pneumatic supply line to rig	Connect the rig pneumatic supply line from V1-006 to the connection point X01	-
3	Close V1-007	Manual air supply valve to turbine inlet	Leakages around quick-release connection
4	Close V1-006	Air supply valve to pneumatic line	-
5	Close V1-012	Air supply valve to pipeline	-
6	Open pneumatic supply valve	Open the work shop pneumatic supply valve to pressurize the supply line	Leakages around quick-release connection
7	Connect VU-001 to W-002 inlet	Connecting the hose to area water supply for the counter flow cooler	Leakages at the bottom connection
8	Connect water hose to W-002 outlet	Connect outlet of W-002 to water hose and place it in the area drainage	-
9	Open VU-001	Open the water supply valve approximately 10-20%	Leakages, steady flow from the cooler to the drainage
10	Proceed to Table 2.	-	-

2. LABORATORY POWER SUPPLY CONNECTION			
Step	Action/Activity	Description/check	Confirm/check
1	Close the control cabinet door	Closing the door allows powering the main circuit.	For foreign objects inside the cabinet
2	Connect the main power cord	Locate and connect the main power cord (400V-red) to the main socket (red below cabinet)	Connection is proper
3	ES01-02 to NC	Check if the emergency stop switches are set to NC (pull out)	The system will not be power if ES01-02 = NO
4	Turn S1 to ON	System on/off switch S1	PL2 = green

5	Turn S3 to ON	24 VDC power supply to control valves	PL4 = green
6	Verify water pump circuit	Check if the water pump circuit has a fault	PL6 = No light If RED, go to Section 6
7	Verify cabinet fan running	Check if the cabinet fan (QF01) is operational and working	If not, go to Section 6
8	Proceed to Table 3.	-	-

3. LABORATORY SOFTWARE STARTUP			
Step	Action/Activity	Description/check	Confirm/check
1	Start Labview Software	Locate the software in the start menu	-
2	Run global.vi	.vi located in folder "Labview/global/global.vi"	-
3	Connect DAQ to USB	Connect the DAQ to the USB port on the computer	-
4	Set to RUN mode	Set the Labview program to run (upper left corner arrow)	-
5	Verify transmitter readings	Pressure and temperature readings	Readings reflect real values
6	Verify safe working conditions	Locate the alarm list in the HMI and acknowledge	Alarm list, post-fault logs
7	Check control valve positions	Locate the control valve positioning feedback in the HMI <u>and check with Table 3.3</u>	0% - closed 100% - open
8	Proceed to Section 3.1.1 or 3.1.2		

Table 3.3 – Control valve positions

Control valve positioning protocol			
Item	Description	Value	Check
CH01	Choke valve downstream of check valve V3-002	Full open, 1 (100%)	-
CH02	Choke valve downstream of water pump P-001	Full open, 1 (100%)	-
CV01	Anti-surge compressor control valve	Fully closed, 0 (0%)	-
CV02	Turbine air supply valve	Fully closed, 0 (0%)	-

### 3.1.1 Dry gas startup

After performing the tasks in Section 3.1, the dry gas startup can be executed.

DRY GAS STARTUP			
Step	Action/Activity	Description/check	Confirm/check
1	Close V1-013	Liquid injection port valve	Connection leakages
2	Close V1-012	Rig air supply valve to pipeline	-
3	Open V1-007	Manual air supply valve to turbine inlet	-
4	Open V1-006	Rig air supply valve	-
5	Open V1-012	Rig air supply valve to pipeline	MAN02 = 2 barg
6	Close V1-012	Air supply to piping valve after step 4 is done	Leakages (large decline in pressure at MAN02)
7	Proceed to CASE D-F	-	-

### 3.1.2 Wet gas startup

After performing the tasks in Section 3.1, the wet gas startup can be executed.

WET GAS STARTUP			
Step	Action/Activity	Description	Confirm/check
1	Close V1-007	Manual air supply valve to turbine inlet	Leakages around quick-release connection
2	Close V1-006	Rig air supply valve	-
3	Close V1-012	Rig air supply valve to pipeline	-
4	Close V1-001	Bypasses separator (F-001)	-
5	Close V1-002	Close separator inlet valve (F-001)	-
6	Close V1-003	Close inlet supply to piston compressor (V-001)	-
4	Close V1-005	Close outlet to piston compressor (V-001)	-
5	Close V1-011	Centrifugal compressor (V-002) bypass	-
6	Measure system LVF	Measure LVF for pipeline volume to achieve desired GVF	According to <i>Table 3.1</i>
7	Connect supply to V1-013	Liquid injection hose to the injection port	-

8	Fill liquid	Pour measured liquid into the system	Check for leakage around port
9	Close V1-013	Liquid Injection port valve	-
10	Connect supply to X01	Work shop air supply hose to air supply connection	Leakages around quick-release connection
11	Open V1-006	Rig air supply valve	-
12	Open V1-012	Rig air supply valve to pipeline	MAN02 = 2 barg
13	Close V1-012	Rig air supply valve to pipeline	-
14	Open V1-007	Manual air supply valve to turbine inlet	Leakages around turbine inlet
15	Proceed to Case A-C	-	-

## 4 Laboratory operation (Case A – F)

### 4.1 Wet gas compression cases

<b>Case A: Subsea separation and gas compression (Separator, piston compressor and centrifugal compressor)</b>			
Step	Action/Activity	Description	Check
1	Open VU-001	Supply counter flow cooler (W-002) with water	Leakages around connections
2	Close V1-001	Close separator (F-001) bypass	-
3	Close V1-004	Close piston compressor (V-001) bypass	-
4	Close V1-011	Close bypass valve for centrifugal compressor (V-002)	-
5	Open V1-002	Open separator (F-001) inlet valve	-
6	Open V1-003	Open piston compressor (V-001) inlet	-
7	Open V1-005	Open piston compressor (V-001) outlet	-
8	Open V1-008	Open centrifugal compressor (V-002) inlet	-
9	Open V1-010	Open centrifugal compressor (V-002) outlet	-
10	Switch S3 to ON	Turn on the oil pump, centrifugal compressor cooling	Check green light at PL3
<b>Software steps</b>			
1	Set desired set point for V-002 speed	Done in Labview, global.vi. This will gradually supply the turbine with air to generate torque to the compressor shaft	Leakages around centrifugal compressor
2	Read PT04	Read pressure at V-001 outlet	Verify if reading is below 6 barg
3	Fix speed of V-001	Set to constant speed, check if control algorithm ensures this	-

Case B: Subsea separation and gas compression (Separator and Centrifugal Compressor)			
Step	Action/Activity	Description	Check
1	Open VU-001	Supply counter flow cooler (W-002) with water	Leakages around connections
2	Close V1-001	Close separator (F-001) bypass	-
3	Close V1-003	Close piston compressor (V-001) inlet	-
4	Close V1-005	Close piston compressor (V-001) outlet	-
5	Open V1-002	Open separator (F-001) inlet	-
6	Open V1-004	Bypass piston compressor (V-001)	-
7	Close V1-011	Close centrifugal compressor (V-002) bypass	-
8	Switch S4 to ON	Turn on the oil pump, centrifugal compressor cooling	Check green light at PL3
Software steps			
1	Turn ON the frequency converter	Switch the power supply on to the frequency converter.	-
2	Set desired speed for V-001	In PROGRAM set the VFD frequency to (see documentation for conversion between frequency and speed)	-
3	Read PT05	Read pressure at outlet of V-001	Verify if ok/reached desired
4	Set desired set point for V-002 speed	Done in Labview, global.vi. This will gradually supply the turbine with air to generate torque to the compressor shaft	Leakages around centrifugal compressor
5	Read PT04	Read pressure at V-001 outlet	Verify if reading is below 6 barg
6	Fix speed of V-001	Set to constant speed, check if control algorithm ensures this	-

Case C: Direct inlet wet gas compression (Centrifugal Compressor)			
Step	Action/Activity	Description	Check
1	Open VU-001	Supply counter flow cooler W-002 with water	Leakages around connections
2	Close V1-002	Close separator (F-001) inlet	-
3	Close V1-003	Close piston compressor (V-001) inlet	-
4	Close V1-005	Close piston compressor (V-001) outlet	-
5	Close V1-011	Close centrifugal compressor (V-002) bypass	-



6	Open V1-001	Bypass separator (F-001)	-
7	Open V1-008	Open centrifugal compressor (V-002) inlet	-
8	Open V1-010	Open centrifugal compressor (V-002) outlet	-
9	Switch S4 to ON	Turn on the oil pump, centrifugal compressor cooling	Check green light at PL3
Software steps			
1	Gradually open CV-02	Gradually supply the turbine with air to generate torque to the compressor shaft	Leakages around centrifugal compressor
2	Set desired set point for V-002 speed	Done in Labview, global.vi. This will gradually supply the turbine with air to generate torque to the compressor shaft	Leakages around centrifugal compressor
3	Read PT04	Read pressure at V-001 outlet	Verify if reading is below 6 barg
4	Fix speed of V-001	Set to constant speed, check if control algorithm ensures this	-

## 4.2 Dry gas compression cases

Case D: Dry Gas Compression, piston and centrifugal compressor			
Step	Action/Activity	Description	Check
1	Open VU-001	Supply counter flow cooler (W-002) with water	Leakages around connections
2	Close V1-002	Close separator (F-001) inlet	-
3	Open V1-003	Open piston compressor (V-001) inlet	-
4	Open V1-005	Open piston compressor (V-001) outlet	-
5	Close V1-004	Close piston compressor (V-001) bypass	-
6	Close V1-011	Close centrifugal compressor (V-002) bypass	-
7	Open V1-001	Bypass separator (F-001)	-
8	Open V1-008	Open centrifugal compressor (V-002) inlet	-
9	Open V1-010	Open centrifugal compressor (V-002) outlet	-
10	Switch S4 to ON	Turn on the oil pump, centrifugal compressor cooling	Check green light at PL3
Software steps			
1	Turn ON the frequency converter	Switch the power supply on to the frequency converter.	-
2	Set desired speed for V-001	In PROGRAM set the VFD frequency to (see documentation for conversion between frequency and speed)	-
3	Read PT05	Read pressure at outlet of V-001	Verify if ok/reached desired
4	Set desired set point for V-002 rpm	Done in Labview, global.vi. This will gradually supply the turbine with air to generate torque to the compressor shaft	Leakages around centrifugal compressor
5	Read PT04	Read pressure at V-001 outlet	Verify if reading is below 6 barg
6	Fix speed of V-001	Set to constant speed, check if control algorithm ensures this	-

Case E: Dry Gas Compression, piston compressor			
Step	Action/Activity	Description	Check
1	Open VU-001	Supply counter flow cooler (W-002) with water	Leakages around connections

2	Close V1-002	Close separator (F-001) inlet	-
3	Open V1-001	Open separator (F-001) bypass	-
4	Open V1-003	Open piston compressor (V-001) inlet	-
5	Open V1-005	Open piston compressor (V-001) outlet	-
6	Close V1-004	Close piston compressor (V-001) bypass	-
7	Open V1-011	Open centrifugal compressor (V-002) bypass	-
8	Close V1-008	Close centrifugal compressor (V-002) inlet	-
9	Close V1-010	Close centrifugal compressor (V-002) outlet	-
Software steps			
1	Turn ON the frequency converter	Switch the power supply on to the frequency converter.	-
2	Set desired speed for V-001	In PROGRAM set the VFD frequency to (see documentation for conversion between frequency and speed)	-

Case F: Dry Gas Compression, centrifugal compressor			
Step	Action/Activity	Description	Check
1	Open VU-001	Supply counter flow cooler (W-002) with water	Leakages around connections
2	Close V1-002	Close separator (F-001) inlet	-
3	Open V1-001	Open bypass of separator (F-001)	-
4	Close V1-003	Close piston compressor (V-001) inlet	-
5	Close V1-005	Close piston compressor (V-001) outlet	-
6	Open V1-004	Open bypass of piston compressor (V-001)	-
7	Close V1-011	Close bypass for centrifugal compressor (V-002)	-
8	Open V1-008	Close centrifugal compressor (V-002) inlet	-
9	Open V1-010	Close centrifugal compressor (V-002) outlet	-
10	Switch S4 to ON	Turn on the oil pump, centrifugal compressor cooling	Check green light at PL3
Software steps			
1	Set desired set point for V-002 rpm	Done in Labview, global.vi. This will gradually supply the turbine with air to generate torque to the compressor shaft	Leakages around centrifugal compressor
2	Read PT04	Read pressure at V-001 outlet	Verify if reading is below 6 barg
3	Fix speed of V-001	Set to constant speed, check if control algorithm ensures this	-

## 5 Shut down procedure

The following operation table shows the procedure to perform a shutdown of the laboratory.

Shutdown - Manual instructions			
Step	Action/Activity	Description	Check
1*	Ramp down M-001	Ramp down the speed of the piston compressor to avoid damage to internal crankshaft	Verify that the compressor is not running
2	<b>Go to step 1 in software instructions</b>	-	-
3	Switch S4 to OFF	Shutting off the oil pump for centrifugal compressor cooling	-
4	Close VU-001	Shut off the water supply to counter flow cooler (W-002)	-
5	Open V1-002	Open separator (F-001) inlet	-
6	Close V1-013	Ensure the air supply valve is closed	-
7	Close workshop air supply valve	Close the work shop air supply valve and ensure there are no pressure at rig supply point X01	-
8	Open V1-006	Rig air supply valve	-
9	Open F-001 drainage valve	Locate the drainage hose for F-001 and gradually open to depressurize system	-
10	Close F-001 drainage valve	Ensure that the air is at 0 barg at MAN02, if not = wait with closure of F-001 drainage valve	MAN02 = 0 (1 atm)
11	<b>Go to step 3 in Software instructions</b>	-	-
Shut down - Software / Electrical steps			
1	Set global.vi to <initiate manual shutdown>	Shut down ensures opening of all critical valves to reduce pressure in the system	-
2	<b>Go back to step 3 in manual instructions</b>	-	-
3	Switch S1 to OFF	Shutting off the power supply to M-001 to 3	-
4	Disconnect DAQ from USB	-	-

\* Can be excluded if not operating with piston compressor in test loop

## 6 Troubleshooting

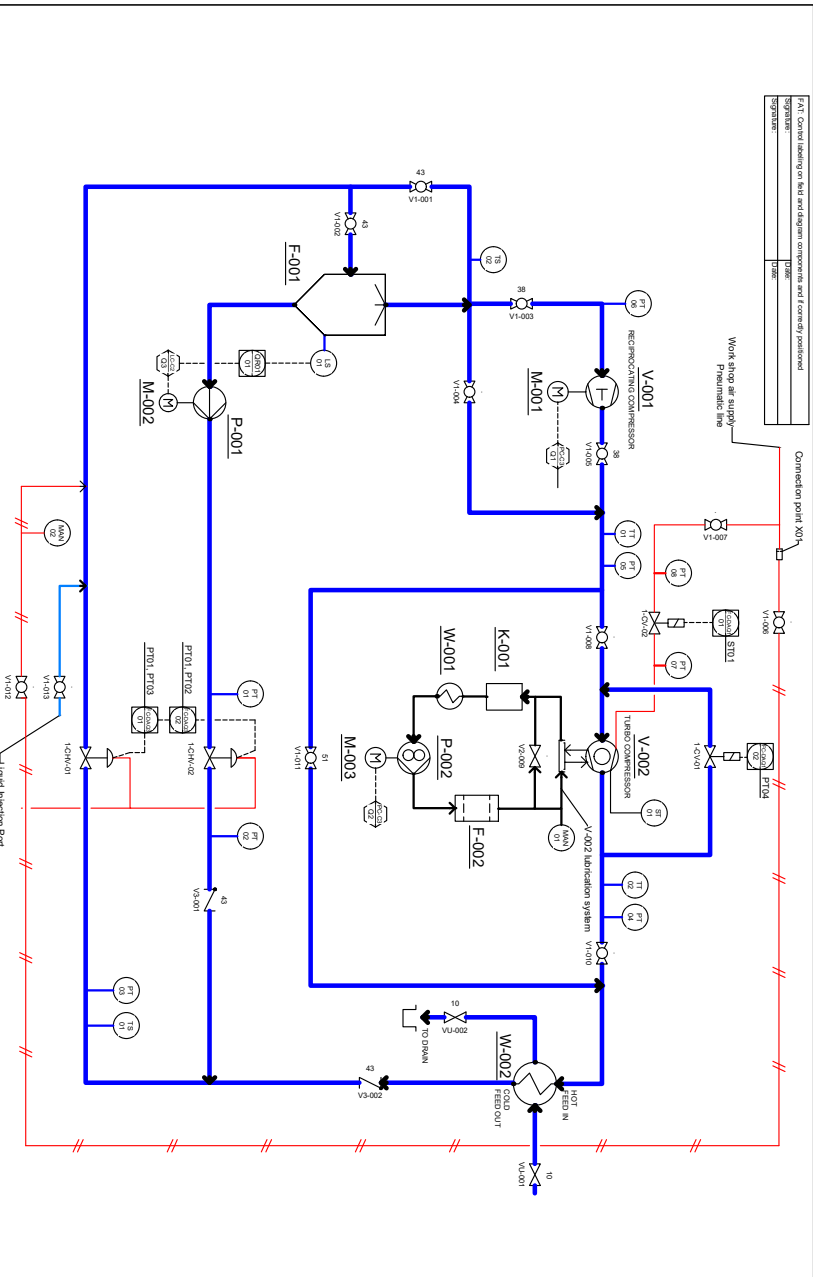
1. No readings from measurement I/O  
Solution proposal: Check USB connection to computer. Restart Labview and locate potential wire breaks to control cabinet.
2. Program goes to SHUTDOWN MODE immediately  
Solution proposal: Check the pressure and temperature readings of the system, and if the values are beyond what is recommended.
3. PL6 light is red, water pump **is not running** or motor protection circuit breaker has tripped  
Solution proposal: Turn of the system equipment. Switch off the power supply (S1) and call certified personnel to inspect the water pump and control cabinet.
4. Cabinet fan is not working  
Solution proposal: Turn of the system equipment. Switch off the power supply (S1) and call certified personnel to inspect the fan circuit inside the control cabinet

Comment to 3: PL6 is wired on the NC pair on the motor protection relay for C2-water pump circuit. This ensures that when the circuit is powered and the water pump is not running, the pilot light glows. This is a design issue, since the motor protection relay does not have a separate contact pair for fuse trip. Therefore, it is wired to the NC pair.

**If non of the above is a solution, please consult laboratory responsible.**

## 7 References

- [1] M. Brænden Bordal, E. Flatlandsmo and J.-H. Krøke Medby, "Subsea Gas Boosting Laboratory: Design and Construction," Department of Production and Quality Engineering, NTNU, Trondheim, 2016.
- [2] D. Nedregård, "Subsea Boosting Lab: Completion of Build," Department of Production and Quality Engineering, NTNU, Trondheim, 2016.



P&ID for process laboratory <b>Wet Gas Compression</b> Designed by: N.T. DN Date: 13/03/2017 Scale: A4, Sheet 1 of 1		Department of Mechanical and Industrial Engineering (MPE) NTNU Subsea Process Control Laboratory	
--	--	---	--

**LEGEND:**  
 W - Heat Exchangers | F - Separator | K - Reservoir | P - Pump | M - Motor drive  
 V1 - Ball valve | V2 - Needle Valve | V3 - Check Valve | VU - Valve Utility | CV - Control Valve | DV - Dose Control Valve  
 LS - Level Sensor | TS - Temperature Sensor | TT - Temperature Transmitter | ST - Speed Transmitter | PT - Pressure Transmitter | MAH - Manometer  
 PC - Pressure Controller | LC - Level Controller | FC - Flow Controller | DAD - Data Acquisition Unit | Measurement and Control I/O

P&ID Control labeling on field and diagram components and geometry positioned  
 SYSTEM: V002  
 OPERATOR: V002